Calhoun: The NPS Institutional Archive

DSpace Repository

Theses and Dissertations | 1. Thesis and Dissertation Collection, all items

2004-12

Multiple satellite trajectory optimization

Mendy, Paul B., Jr.

Monterey California. Naval Postgraduate School

http://hdl.handle.net/10945/1255

This publication is a work of the U.S. Government as defined in Title 17, United States Code, Section 101. Copyright protection is not available for this work in the United States.

Downloaded from NPS Archive: Calhoun

http://www.nps.edu/library

Calhoun is the Naval Postgraduate School's public access digital repository for research materials and institutional publications created by the NPS community. Calhoun is named for Professor of Mathematics Guy K. Calhoun, NPS's first appointed -- and published -- scholarly author.

Dudley Knox Library / Naval Postgraduate School
411 Dyer Road / 1 University Circle
Monterey, California USA 93943

NAVAL POSTGRADUATE SCHOOL

MONTEREY, CALIFORNIA

THESIS

MULTIPLE SATELLITE TRAJECTORY OPTIMIZATION

by

Paul B. Mendy, Jr.

December 2004

Thesis Advisor:	I. Michael Ross
Thesis Co-Advisor:	D. A. Danielson

Approved for public release; distribution is unlimited

THIS PAGE INTENTIONALLY LEFT BLANK

REPORT DOCUMENTATION PAGE			Form Approved OMB No. 0704-0188
Public reporting burden for this collection of information is estimated to average 1 hour per response, including the time for reviewing instruction, searching existing data sources, gathering and maintaining the data needed, and completing and reviewing the collection of information. Send comments regarding this burden estimate or any other aspect of this collection of information, including suggestions for reducing this burden, to Washington headquarters Services, Directorate for Information Operations and Reports, 1215 Jefferson Davis Highway, Suite 1204, Arlington, VA 22202-4302, and to the Office of Management and Budget, Paperwork Reduction Project (0704-0188) Washington DC 20503.			
1. AGENCY USE ONLY ***(Leave blank)***	**2. REPORT DATE** December 2004	**3. REPORT TYPE AND DATES COVERED** Astronautical Engineer's Thesis	
4. TITLE AND SUBTITLE: Multiple Satellite Trajectory Optimization			**5. FUNDING NUMBERS**
6. AUTHOR(S) Paul B. Mendy, Jr.			
7. PERFORMING ORGANIZATION NAME(S) AND ADDRESS(ES) Naval Postgraduate School Monterey, CA 93943-5000			**8. PERFORMING ORGANIZATION REPORT NUMBER**
9. SPONSORING /MONITORING AGENCY NAME(S) AND ADDRESS(ES) N/A			**10. SPONSORING/MONITORING AGENCY REPORT NUMBER**
11. SUPPLEMENTARY NOTES The views expressed in this thesis are those of the author and do not reflect the official policy or position of the Department of Defense or the U.S. Government.			
12a. DISTRIBUTION / AVAILABILITY STATEMENT Approved for public release; distribution is unlimited			**12b. DISTRIBUTION CODE**

13. ABSTRACT (maximum 200 words)

This thesis develops and validates a satellite trajectory optimization model. A summary is given of the general mathematical principles of dynamic optimal control to minimize fuel consumed or transfer time. The dynamic equations of motion for a satellite are based upon equinoctial orbital elements in order to avoid singularities for circular or equatorial orbits. The study is restricted to the two-body problem, with engine thrust as the only possible perturbation. The optimal control problems are solved using the general purpose dynamic optimization software, DIDO. The dynamical model together with the fuel optimal control problem is validated by simulating several well known orbit transfers. By replicating the single satellite model, this thesis shows that a multi-satellite model which optimizes all vehicles concurrently can be easily built. The specific scenario under study involves the injection of multiple satellites from a common launch vehicle; however, the methods and model are applicable to spacecraft formation problems as well.

14. SUBJECT TERMS Satellite Trajectory Control, Multi-Agent Optimization, Optimal Control, DIDO, Dynamic Optimization			**15. NUMBER OF PAGES** 111
			16. PRICE CODE
17. SECURITY CLASSIFICATION OF REPORT Unclassified	**18. SECURITY CLASSIFICATION OF THIS PAGE** Unclassified	**19. SECURITY CLASSIFICATION OF ABSTRACT** Unclassified	**20. LIMITATION OF ABSTRACT** UL

NSN 7540-01-280-5500

Standard Form 298 (Rev. 2-89)
Prescribed by ANSI Std. 239-18

THIS PAGE INTENTIONALLY LEFT BLANK

Approved for public release; distribution is unlimited

MULTIPLE SATELLITE TRAJECTORY OPTIMIZATION

Paul B. Mendy, Jr.
Major, United States Air Force
B.S., Clarkson University, 1991

Submitted in partial fulfillment of the
requirements for the degrees of

MASTER OF SCIENCE IN ASTRONAUTICAL ENGINEERING

AND

ASTRONAUTICAL ENGINEER

from the

NAVAL POSTGRADUATE SCHOOL
December 2004

Author: Paul B. Mendy, Jr.

Approved by: I. Michael Ross
Thesis Advisor

D. A. Danielson
Thesis Co-Advisor

Anthony J. Healey
Chairman, Department of Mechanical and Astronautical Engineering

THIS PAGE INTENTIONALLY LEFT BLANK

ABSTRACT

This thesis develops and validates a satellite trajectory optimization model. A summary is given of the general mathematical principles of dynamic optimal control to minimize fuel consumed or transfer time. The dynamic equations of motion for a satellite are based upon equinoctial orbital elements in order to avoid singularities for circular or equatorial orbits. The study is restricted to the two-body problem, with engine thrust as the only possible perturbation. The optimal control problems are solved using the general purpose dynamic optimization software, DIDO. The dynamical model together with the fuel optimal control problem is validated by simulating several well known orbit transfers. By replicating the single satellite model, this thesis shows that a multi-satellite model which optimizes all vehicles concurrently can be easily built. The specific scenario under study involves the injection of multiple satellites from a common launch vehicle; however, the methods and model are applicable to spacecraft formation problems as well.

THIS PAGE INTENTIONALLY LEFT BLANK

TABLE OF CONTENTS

I. INTRODUCTION....1
A. PROBLEM....1
B. PROPOSED SOLUTION....2
C. DIDO AND THE MULTI-SATELLITE OPTIMIZATION MODEL....3

II. PRINCIPLES OF DYNAMIC OPTIMIZATION....5
A. SOLVING OPTIMAL CONTROL PROBLEMS....5
1. Define the Performance Index, States, and Controls....5
2. Develop the Dynamic Equations....6
3. Develop the Boundary Conditions....7
4. Develop the Path Constraints....7
5. Develop the Hamiltonian....7
6. Develop the Lagrangian of the Hamiltonian....7
7. Apply Karush-Kuhn-Tucker (KKT) Theorem....8
B. OBSERVING NECESSARY CONDITIONS OF OPTIMALITY....8
1. Feasibility....8
2. Behavior of the Hamiltonian....9
3. Minimized Lagrangian of the Hamiltonian with Respect to Controls....11
4. Complementarity Condition....12
5. Others....13
C. SCALING....14
D. CONCLUSIONS....14

III. THE EQUINOCTIAL ELEMENT SET....15
A. DRAWBACKS OF THE ORBITAL ELEMENT SET....15
B. DEFINITION OF THE EQUINOCTIAL ELEMENTS....15
C. FEATURES OF THE EQUINOCTIAL ELEMENT SET....18
1. Elimination of Singularities....18
2. Scaling....19
3. Mathematical Complexity....20
D. TRANSFORMATION OF EQUINOCTIAL ELEMENTS TO POSITION AND VELOCITY....21
E. CONCLUSIONS....22

IV. FORMULATION OF THE PROBLEM....23
A. STATES AND CONTROLS....23
B. COST....24
C. DYNAMIC EQUATIONS OF MOTION....25
D. EVENTS....26
E. STATE AND CONTROL BOUNDS....26
1. State Bounds....27
2. Control Bounds....28

F. PATH CONSTRAINTS 28
G. DEVELOPMENT OF THE HAMILTONIAN 29
H. DEVELOPMENT OF THE LAGRANGIAN OF THE HAMILTONIAN....30
I. COMPLEMENTARITY CONDITION....32
J. CONCLUSIONS 33
V. MODEL VALIDATION 35
A. MODEL NOTES....35
B. HOHMANN TRANSFER SCENARIO 36
1. Hohmann Transfer Input Parameters....37
2. Hohmann Transfer Performance 37
3. Hohmann Transfer Model Optimal Behavior....40
a. Hohmann Transfer Feasibility Analysis....40
b. Hohmann Transfer Hamiltonian Behavior....40
c. Hohmann Transfer Lagrangian Behavior....41
d. Hohmann Transfer KKT Complementarity Condition 42
4. Hohmann Transfer Scenario Conclusions....44
C. INCLINATION CHANGE SCENARIO 44
1. Inclination Change Parameters....44
2. Inclination Change Performance....45
3. Inclination Change Optimal Behavior 47
a. Inclination Change Feasibility....47
b. Inclination Change Hamiltonian Behavior....48
c. Inclination Change Lagrangian Behavior 48
d. Inclination Change KKT Complementarity Condition 49
4. Inclination Change Scenario Conclusions 51
D. SEMIMAJOR AXIS CHANGE SCENARIO 51
1. Semimajor Axis Change Parameters 51
2. Semimajor Axis Change Performance....52
3. Semimajor Axis Change Optimal Behavior 54
a. Semimajor Axis Change Feasibility....54
b. Semimajor Axis Change Hamiltonian Behavior....55
c. Semimajor Axis Change Lagrangian Behavior....56
d. Semimajor Axis Change KKT Complementarity Condition..56
4. Semimajor Axis Change Scenario Conclusions 57
E. MINIMUM TIME TRANSFER SCENARIO....58
1. Minimum Time Transfer Input Parameters....58
2. Minimum Time Transfer Performance 59
3. Minimum Time Transfer Optimal Behavior....61
a. Minimum Time Transfer Feasibility....61
b. Minimum Time Transfer Hamiltonian Behavior....62
c. Minimum Time Transfer Lagrangian Behavior 63
d. Minimum Time Transfer KKT Complementarity Condition....64
4. Minimum Time Transfer Scenario Conclusions....66

F. CONCLUSIONS 68

VI. MULTI-AGENT CONTROL 71
A. MODEL MODIFICATIONS 71
B. TWO-AGENT MODEL 72
1. Two-Agent Input Parameters 73
a. Agent 1 (Positive Inclination Change) *73*
b. Agent 2 (Negative Inclination Change) *73*
2. Two-Agent Model Performance 74
3. Two-Agent Model Optimal Behavior 77
a. Agent 1 Feasibility and Optimality Analysis *77*
b. Agent 2 Feasibility and Optimality Analysis *79*
4. Two-Agent Model Overconstraint Issue 81
5. Two-Agent Model Conclusions 85
C. CONCLUSIONS 86

VII. CONCLUSIONS AND FUTURE WORK 87
A. CONCLUSIONS 87
B. MODEL ISSUES 88
1. Limitation on Number of Variables 88
2. True Retrograde Orbit 89
3. Scaling and Tolerance 90
C. FUTURE WORK 90
1. Extension to *N* Agents 90
2. Scaling Investigation 90
3. Increased Model Fidelity 91
4. Sensitivity Analysis 91
5. Extension to Constellation / Formation Control 91
6. Proportional Fuel Expenditure 92
7. Interface to Graphical Visualizer and GUI Input 92

LIST OF REFERENCES 93

INITIAL DISTRIBUTION LIST 95

THIS PAGE INTENTIONALLY LEFT BLANK

LIST OF FIGURES

Figure 1 Sample graph of solution behavior vs. independent propagation (for six controls) 9
Figure 2 Representative Hamiltonian behavior for optimal solution 11
Figure 3 Representative behavior of the stationary Lagrangian of the Hamiltonian with respect to controls for optimal solution (six controls) 12
Figure 4 Representative optimal control switching behavior (one control) 13
Figure 5 Equinoctial reference frame 16
Figure 6 Equinoctial Orbital Elements 17
Figure 7 Satellite thrust convention diagram. Note, positive normal thrust T_{n1} not shown 24
Figure 8 Hohmann transfer state and control histories 38
Figure 9 Hohmann transfer mass flow 38
Figure 10 Hohmann transfer 39
Figure 11 Plots of Hohmann transfer model performance vs. ODE45 propagation 40
Figure 12 Hohmann transfer Hamiltonian behavior 41
Figure 13 Hohmann transfer minimized Lagrangian behavior 42
Figure 14 Switching structure for Hohmann transfer 43
Figure 15 Detailed switching structure for positive transverse thrust, T_{t1}, including expanded blowup (bottom). Behavior approaches that reported by Lawden. 43
Figure 16 State and control histories for inclination change 46
Figure 17 Mass flow for inclination change 46
Figure 18 Inclination change 47
Figure 19 Plots of inclination change model performance vs. ODE45 propagation 48
Figure 20 Hamiltonian behavior for inclination change 49
Figure 21 Inclination change minimized Lagrangian behavior 49
Figure 22 Switching behavior for inclination change 50
Figure 23 Switching detail for thruster T_{n1}, with blow-up 51
Figure 24 State and control histories for semimajor axis change 53
Figure 25 Mass flow for semimajor axis change 53
Figure 26 Semimajor axis change transfer orbit 54
Figure 27 Plots of semimajor axis change model performance vs. ODE45 propagation 55
Figure 28 Hamiltonian behavior for semimajor axis change 55
Figure 29 Semimajor axis change minimized Lagrangian behavior 56
Figure 30 Switching behavior for semimajor axis change 57
Figure 31 Single burn semimajor axis change maneuver 58
Figure 32 State and control histories for minimum time transfer 60
Figure 33 Minimum time transfer mass flow 60
Figure 34 Minimum time transfer. Note period of zero net thrust 61

Figure 35 Plots of minimum time transfer model performance vs. ODE45 propagation 62
Figure 36 Hamiltonian behavior for minimum time transfer 62
Figure 37 Minimum time transfer minimized Lagrangian behavior 64
Figure 38 Switching structure for minimum time transfer 65
Figure 39 Switching detail for minimum time transfer, T_{t1} and T_{t2} 65
Figure 40 State and control history for minimum time transfer (normal thrusters disabled) 67
Figure 41 Minimum time transfer (normal thrusters disabled) 68
Figure 42 Complex orbit transfer, all classical elements modified 69
Figure 43 Satellite 1 state and control histories 75
Figure 44 Satellite 2 state and control histories 75
Figure 45 Satellite 1 and 2 mass flow 76
Figure 46 Two satellite orbit transfer with inclination change 76
Figure 47 Plots of satellite 1 performance vs. ODE45 propagation 77
Figure 48 Multi-agent Hamiltonian behavior (both satellites) 78
Figure 49 Satellite 1 minimized Lagrangian behavior 78
Figure 50 Switching structure for satellite 1 79
Figure 51 Plots of satellite 2 performance vs. ODE45 propagation 80
Figure 52 Satellite 2 minimized Lagrangian behavior 80
Figure 53 Switching structure for satellite 2 81
Figure 54 Multi-agent maneuver involving time constraint difficulty. Note satellite 1 orbit raise to loiter. 82
Figure 55 Satellite 2 (slave) not provided adequate time to perform Hohmann transfer, resulting in radial thrusting to meet final orbit 84
Figure 56 Satellite 1 (master) given longer execution time to facilitate Hohmann transfer by satellite 2 84
Figure 57 Satellite 1 (master, performing Hohmann transfer) sets constellation execution time, allowing adequate time for transfer and for satellite 2 inclination change. Note: satellite 1&2 designations switched from previous examples 85
Figure 58 Complex two-agent scenario 86

ACKNOWLEDGMENTS

To my wife, best friend, and confidant, Alyshia, for supportively enduring many long days and late nights of study. I Love You, and these academic triumphs pale in comparison to what we have built.

To my children, Chase and Nicole, for continuing to be my greatest and most amazing accomplishment. The quest for knowledge is a lifelong endeavor, and I hope I can be an example that helps fuel this fire in you both.

To my advisor, Mike Ross, for your continued inspiration, tutelage, mentorship, and friendship. I look forward to researching broad-ranging topics over many beers in the future.

THIS PAGE INTENTIONALLY LEFT BLANK

I. INTRODUCTION

A. PROBLEM

In the space business, available fuel can be directly equated to mission life. Depletion of a satellite's fuel and the associated loss of maneuvering capability generally renders useless whatever remaining capabilities a satellite may have. Add to this a tremendous cost of launching satellites, where the mass of the payload needs to be maximized, and careful trades must be made to make sure every ounce of fuel onboard has a purpose. Therefore the task of ensuring efficient maneuvering during the life of the vehicle takes great scrutiny, for every gram of fuel saved early is a gram that can be used later to extend the mission life.

Designing fuel efficient maneuvers for a single vehicle is a time consuming process, involving iterative checks to ensure that the minimum amount of fuel is expended. Attempting to do this concurrently for multiple vehicles is very difficult; instead, a more serial approach from vehicle to vehicle is usually preferred. For some scenarios, the process does not necessarily take into account relationships and interactions between vehicles. In situations where spacecraft are closely spaced, parallel computations are difficult to perform because engineers must understand where the first satellite is and where it will go before they can calculate what the second should do. Therefore, it is a mathematically complex and labor-intensive process, involving numerous semi-automated tools.

These methods are tried and true, and to some degree are considered black art practiced by highly knowledgeable and experienced specialists. The space industry is notorious in its conservatism and caution in moving away from "what works" for promises of improvement that don't always bear fruit, but one can still question whether these methods are the most effective use of time and energy given the advancements in computation and optimization. An automated tool that could handle this process without fail for any circumstance would be ideal; however, this is a highly unrealistic prospect. Perhaps nearer at hand are methods and tools that can quickly provide a starting point to this process, enabling a much shortened timeline to completion. It could also enable

quick calculation of several different possible scenarios to choose from, with a minimal resource impact. The research for this thesis explores these new methods.

B. PROPOSED SOLUTION

Tools have been developed over the past few years at the Naval Postgraduate School that can be used to great effect in almost any imaginable dynamic optimization problem. Specifically, a generic optimization engine, DIDO, has been developed which allows the user to quickly perform dynamic optimization on any problem that can be properly framed in mathematical terms, and this tool has been at the heart of several recent theses and dissertations published at the school [King (2002), Stephens (2002), Josselyn (2003), Shaffer (2004), Fleming (2004)]. The generic capability that DIDO presents is startling, for the only resemblance of these problems (outside of the coincidence of all being aerospace related) is in the underlying DIDO/MATLAB™ toolset.

The primary goal of this research is to show that a DIDO based optimization tool can be developed which can predict fuel optimal control maneuvers for orbital application. Some previous work has been done in this area specific to single satellite models. However, this research aims to extend this work most notably by extending developed ideas and methods to optimal control prediction for multiple satellites simultaneously. Additionally, the model will be constructed so that it is universally applicable to all elliptical orbits, whereas previous models have been narrowly focused on orbital regimes of interest (which allows for equations which exhibit singularities in some cases outside of study). As a fundamental premise of this research, it is believed that a validated single satellite model can be replicated into several nearly identical versions of itself and interconnected in such a way that they can all be run simultaneously. By doing so, it is hoped that multi-agent optimal control can be shown as nothing more than a slight extension of well understood theories, and that, in theory, a large number of agents can be controlled through this process.

C. DIDO AND THE MULTI-SATELLITE OPTIMIZATION MODEL

Although it will be discussed very little through the rest of this thesis, the DIDO optimization tool developed at the Naval Postgraduate School by Dr. I. Michael Ross and Dr. Fariba Fahroo represents the enabling technology which has made this research possible. It is the first and only object-oriented computer program for solving dynamic optimization programs [Ross and Fahroo (2002)], and it uses a Legendre pseudospectral method to perform this task. However, one of the great benefits of this tool is that the computation method is almost completely transparent to the casual user, provided inputs are framed in a structured manner understood by the DIDO interface, as explained in the DIDO User's Manual. Therefore its inner workings are left to be considered a black box for this research, and the curious reader is invited to browse several papers by Ross and Fahroo to discover more about this tool.

All programming for this research was performed in MATLAB™ release 13 (version 6.5) and release 14 (version 7.0). All developed MATLAB™ codes supporting the multi-satellite optimization model (hereafter referred to as "the model") and a common version of the DIDO engine (DIDO 2003) are portable between the two versions with little apparent difference for this application, other than a significant increase in processing speed with the later version. The vast majority of this thesis will focus on more general mathematics upon which the model is built, and will not generally discuss actual code language. However, it is assumed to be understood that the mathematical generalities and specifics discussed throughout this work is fully implemented into an operational MATLAB™ based code structure wrapped around the DIDO optimization tool.

THIS PAGE INTENTIONALLY LEFT BLANK

II. PRINCIPLES OF DYNAMIC OPTIMIZATION

A. SOLVING OPTIMAL CONTROL PROBLEMS

The driving principle used to solve optimal control problems was first formalized by the Soviet mathematician Pontryagin in the 1950s [Kopp (1962)], and is generally known as the Minimum Principle[1]. His work showed conclusively that optimal solutions to all differential equations exhibit several observable characteristics, even though the solutions themselves do not readily announce themselves as optimal. By verifying these observables numerically, we can use engineering judgment to conclude that a given solution is in fact optimal. Stated another way, optimal solutions must meet several necessary conditions as proof of optimality, and by some reverse logic, if we can observe the necessary conditions of optimality, we can with fair confidence conclude that a solution is optimal. In order to determine the optimal controls, several steps must first be taken, as detailed below.[2]

1. Define the Performance Index, States, and Controls

Bryson (1999) defines optimal control as "the process of determining control and state histories for a dynamic system over a finite time period to minimize a performance index." In order to solve for optimality, we must first decide what index we want to minimize (or maximize). The majority of this research has focused on minimizing the amount of fuel that is consumed by the spacecraft in performing their combined maneuvers. This can also be described as maximizing the end mass of the satellite. In truth, maximum and minimum conditions are largely interchangeable and are realizable simply with a change of sign (i.e., a minimized condition can also be considered a negative maximized condition).

Regardless of the performance index chosen, the fundamental problem is based on minimizing (or maximizing) the index (or cost). We can generically state this cost as:

---

[1] In truth, Pontryagin's work was known as the Maximum Principle, but for reasons to be discussed the two titles are largely interchangeable

[2] The following development largely follows the course notes of Dr. I.M. Ross for AA3830 – Spacecraft Guidance and Control

$$J[x(\cdot),u(\cdot),t_f] = E[x(t_f),t_f] + \int_{t_0}^{t_f} F[x(t),u(t),t]dt \qquad \textbf{(2.1)}$$

Here E is the end point (Mayer) cost and F is the running (Lagrange) cost. As we will soon see, the research in this thesis focuses exclusively on Mayer cost indices.

The variables x and u represent state and control vectors. This is the standard notational convention that will be used throughout this document. The state variables are required to completely describe the condition of the system at any point in time, and need to be chosen wisely and in concert with selection of the dynamic equations. Care and consideration should be given in the choices of state and control to most accurately model the system under study as well as to gain whatever residual benefits a particular set of variables has to offer.

2. Develop the Dynamic Equations

The next step in modeling is to develop a set of dynamic equations of motion suitable for the task at hand. These equations are time derivatives of the state variables denoted simply by $\dot{x} = \frac{dx}{dt}$.

A given set of equations is not a silver bullet; any set of equations can be used if they properly mathematically describe the physics of the problem at hand. Our application is orbital, and one could envision using equations based on classical elements, equinoctial elements, Delaunay elements, Poincaré elements [Vallado (2001)], or any number of representations one could imagine. The choice of equations matters only in that they must be completely capable of describing the dynamics of the scenarios under study.

The study at hand is then fundamentally the determination of state and control pairs which minimize the cost index, subject to the dynamic equations:

$$\dot{x}(t) = f[x(t),u(t),t] \qquad \textbf{(2.2)}$$

This determination necessarily involves two boundary values: an initial condition, and an end manifold. For this reason, this system is termed a two point boundary value problem.

3. Develop the Boundary Conditions

A set of starting values for the state variables, $x(t_0) = x_0$, must be created to provide initial conditions for the dynamic differential equations. A set of end conditions, $x(t_f) = x_f$, must also be created to provide an end manifold and to complete the two point boundary value problem. Simply stated, these conditions determine the state that the model starts from, and the state in which we desire the model to end.

4. Develop the Path Constraints

A set of path constraints, *g*, must be developed to constrain the problem solution to some less-than-infinite set for computational purposes. This set of path constraints can be a family of possible variables which includes constraints on the controls, which will be our primary concern. Upper and lower path constraints must be set, where $g_l \le g(x,u,t) \le g_u$. These path constraints determine the maximum and minimum values that the variables can achieve, and effectively bound the solution space of the problem.

5. Develop the Hamiltonian

The first real step in checking optimality involves development of the Hamiltonian function, *H*:

$$H(x,u,t,\lambda) = F(x,u,t) + \lambda(t)^T f(x,u,t) \qquad \textbf{(2.3)}$$

Here $\lambda(t)$ generically represents Lagrangian multipliers associated with the dynamic constraint equations (our equations of motion), also known as costates.

6. Develop the Lagrangian of the Hamiltonian

In order to find the optimal control for this problem, at each instant in time we must minimize the Hamiltonian with respect to the control vector (***u***). In order to do this, we next need to form the Lagrangian of the Hamiltonian:

$$\bar{H}(x,u,t,\lambda,\phi) = H(x,u,t,\lambda) + \phi(t)^T g(x,u,t) \qquad \textbf{(2.4)}$$

Here $\phi(t)$ generically represents Lagrange multipliers associated with the path constraints (including control duals, as we will later see)

7. Apply Karush-Kuhn-Tucker (KKT) Theorem

By applying KKT theorem to the above developed forms, we can observe the following conditions necessary for optimality:

$$\frac{\partial \bar{H}}{\partial u} = 0 \qquad \textbf{(2.5)}$$

$$\phi = \begin{cases} \leq 0 & \\ \geq 0 & \\ = 0 & \\ unrestricted & \end{cases} \quad if \quad \begin{matrix} g_l = g(x,u,t) \\ g(x,u,t) = g_u \\ g_l < g(x,u,t) < g_u \\ g_l = g_u \end{matrix} \qquad \textbf{(2.6)}$$

Here g_l represents the lower bound on the path constraint (e.g., a minimum control value), and g_u represents the upper bound.

The Minimum Principle states that an optimal solution *must* meet these three conditions, which are necessary but not sufficient in proving optimality. In observing the above necessary conditions then, we can use reverse logic and engineering judgment to conclude with reasonable certainty that a particular solution meeting these conditions is optimal. This is the primary method of proof of optimality used in this research, and will be a recurring theme throughout the remainder of this thesis.

B. OBSERVING NECESSARY CONDITIONS OF OPTIMALITY

As mentioned above, an optimal solution must meet several necessary conditions according to the Minimum Principle. The following discussion will focus on the methods with which numerical observations were performed using the previously described tools.

1. Feasibility

Although this condition does not prove optimality per se, it is first necessary to show that a given solution is feasible as a potential optimal solution. If the solution does not meet the feasibility test, there is little point in carrying through the rest of the necessary calculations to determine optimality. Because the equations of motion used in this thesis are ordinary differential equations, the easiest way of showing feasibility is to

independently propagate a solution from initial conditions to see how closely the solution matches model results. Since MATLAB™ provides the processing engine around which our model is wrapped, the on-board differential equation solvers generally known as the ODE toolset provide a natural choice for this task. Although there are a number of these tools for various conditions using different methods, it was found that ODE_45 works sufficiently well for this application. By graphing the performance of the model against an independently propagated solution, it could be very quickly determined visually whether or not a solution provided a feasible answer. A representative example of this graphical technique is shown as Figure 1 in order to begin familiarizing the reader with the process to be used later in the document.

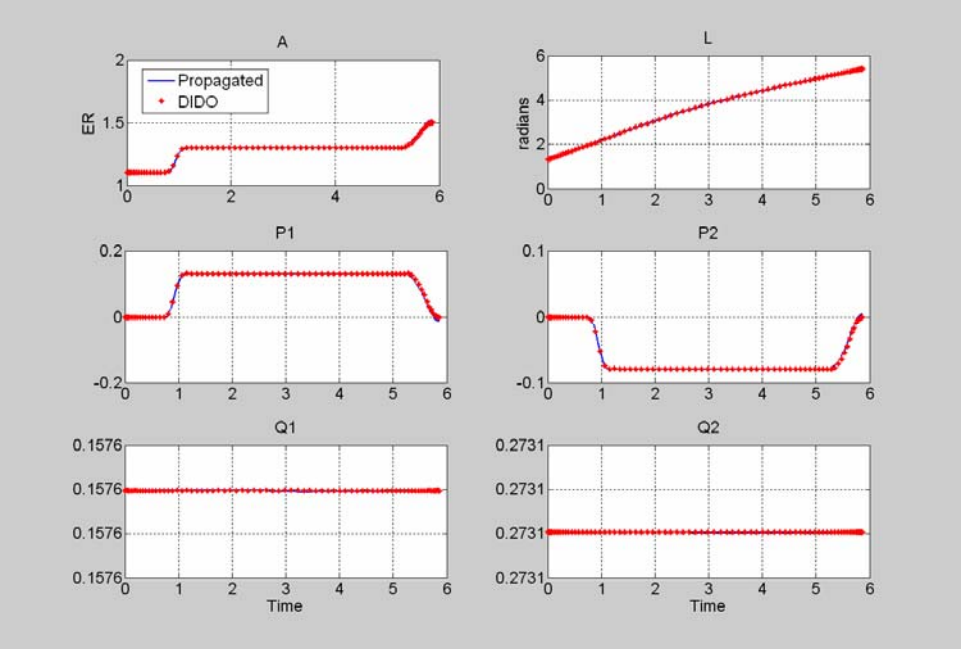

Figure 1 Sample graph of solution behavior vs. independent propagation (for six controls)

2. Behavior of the Hamiltonian

For optimal control problems, the Hamiltonian follows a simple rule as dictated by the Hamiltonian Evolution Equation, where:

$$\frac{dH}{dt} = \frac{\partial H}{\partial t} \tag{2.7}$$

For the types of problem under consideration this value generally is equal to zero, indicating that the Hamiltonian maintains a constant value over the optimal time span (since $\frac{dH}{dt} = 0$). This development will be shown once specifics for this family of problems are discussed.

The actual value of the constant value Hamiltonian depends on the type of problem solved. The value is dependent on a terminal transversality condition called the Hamiltonian Value Condition, which can be stated as:

$$H(t_f) = -\frac{\partial \bar{E}}{\partial t_f} \qquad \textbf{(2.8)}$$

Here, E is the end-point Mayer cost, and $\bar{E}$ is developed as follows:

$$\bar{E} = E + \sum_{i=1}^{N_e} \nu_i e_i$$

where

$N_e =$ number of equations defining the endpoint manifold

$e_i = x_i(t_f) - x_i$

$\nu_i =$ end state Lagrange multiplier **(2.9)**

As we will see in a later chapter, the value of the Hamiltonian is generally zero for minimum fuel problems. Using this fact coupled with the Hamiltonian Evolution equation, it can be concluded that the Hamiltonian will remain zero over the optimal control period. For minimum time problems, this constant value is -1. As with the feasibility analysis, a quick graphical method will be used to verify compliance with this condition, and a representative graph sample is shown as Figure 2.

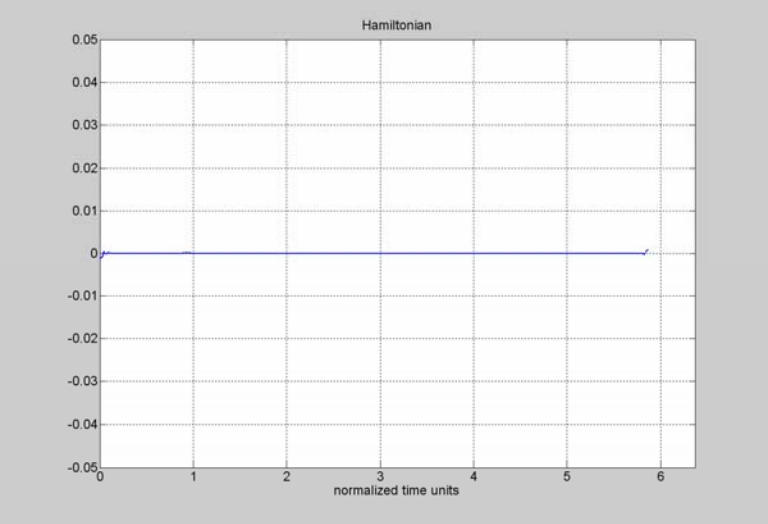

Figure 2 Representative Hamiltonian behavior for optimal solution

3. Minimized Lagrangian of the Hamiltonian with Respect to Controls

As discussed earlier, it is necessary that KKT equation (2.5) must be equal to zero for optimality. This equation represents the stationary Lagrangian of the Hamiltonian with respect to control (for sake of simplicity, this will be alternately referred to for the rest of this thesis as the stationary Lagrangian). This equation must hold true for each control, and therefore the number of equations implied is equal to the number of controls used. By representing this condition graphically for each of the controls under consideration, we can quickly get a feeling for whether or not the condition meets our optimality test, namely that a constant zero should be maintained throughout the time span. A representative example of this graphical technique is shown in Figure 3.

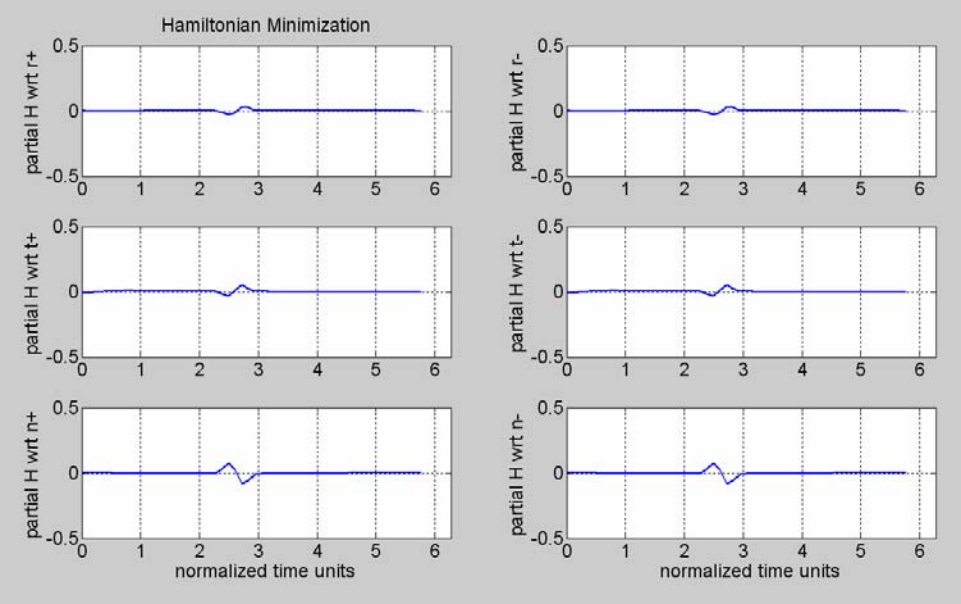

Figure 3 Representative behavior of the stationary Lagrangian of the Hamiltonian with respect to controls for optimal solution (six controls)

4. Complementarity Condition

As described by equation (2.6), a relationship exists between the Lagrange multipliers and the controls under observation. By graphically representing these together, a definite pattern of switching should occur. For example, when the control multiplier is less than zero, its associated control should be at its minimum value. Similarly, when the multiplier is greater than zero, the control should be at its maximum. When the multiplier crosses through zero, the control should demonstrate a switch from one condition to the other, consistent with the direction of the crossing. Again, a graphical technique will be used for compliance, and a representative example is shown as Figure 4.

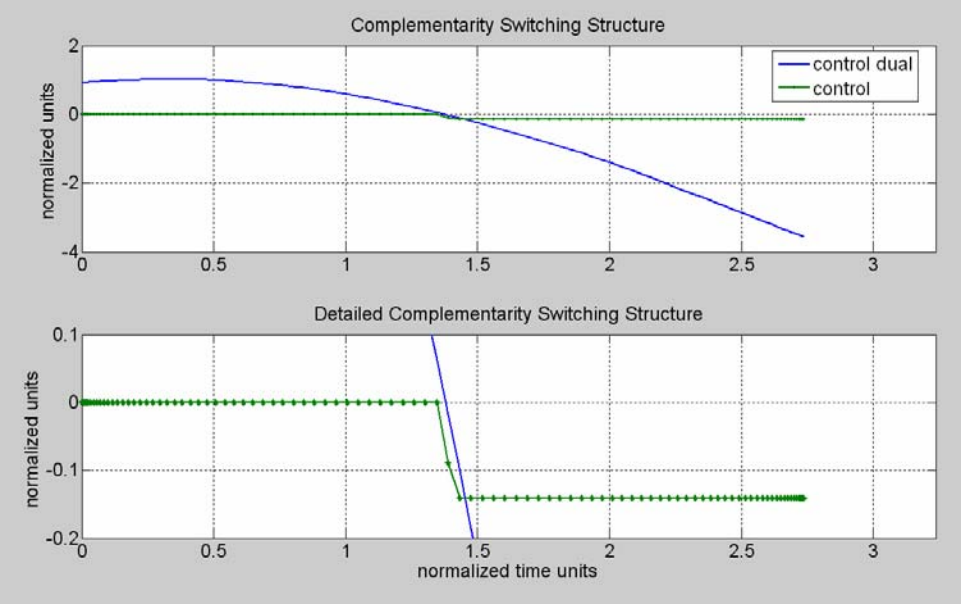

Figure 4 Representative optimal control switching behavior (one control)

Some further explanation of control switching behavior and model behavior is warranted here. One of the input parameters used with the model is the number of discrete time nodes to be used for a given scenario run. This can be roughly equated as a measure of resolution with which the discrete solution can approximate a continuous time result. For the sake of processing speed, the number of nodes can be set low. When observing the switching behavior, this can sometimes have the adverse effect of making the control appear as if it is not achieving maximum or minimum (bang-bang) control, but that the control is throttling in some manner. When the number of nodes for a given scenario is increased, bang-bang control is more evidently displayed.

Generally, the nodal number for the scenarios studied is set at what is to be considered mid-range. In some cases, bang-bang control is not immediately evident, however, when the number of nodes is increased, bang-bang control can generally be observed.

5. Others

Although the above mentioned conditions were primarily used as verification of optimality for modeling, there are other conditions which were deemed overly complex

to prove for little residual return for the already complicated equations of motion under consideration in this research. These conditions include development of adjoint equations and determination of further terminal transversality conditions, which can be reviewed in greater depth in the text by Bryson and Ho (1975).

C. SCALING

One of the peculiarities of working with optimal control codes is that they perform best when the inputs are well scaled relative to one another [Ross and Fahroo, (2002)]. The inputs used should be numerically close to each other in an attempt to avoid calculations involving vastly different number ranges which might throw answers outside the bounds of computational precision. By scaling inputs prior to computation, we can avoid these problems entirely as long as we maintain the understanding that outputs of the system will also be in scaled variables. This can be easily rectified by reversing the scaling process at the end of the computation to achieve results in the same units as the original inputs.

The choice of a particular set of state variables can go a long way in assisting with this scaling problem. If the elements of the state vector are naturally well scaled, matters are simplified somewhat, as will be demonstrated in the following chapter.

D. CONCLUSIONS

The basic theory of the Minimum Principle has been summarized, and the following chapters will show how this theory will be applied to the specific topic of this research. The tenets of the Minimum Principle will be used throughout this thesis, and form the basis for all verifications of optimality that will be discussed.

III. THE EQUINOCTIAL ELEMENT SET

In order to build a model which is universally applicable to any orbit transfer problem, we need to define equations of motion which can be applied to all potential conditions. These equations can be defined in any way that ultimately describes orbital motion of a body around a central gravitational force; however, we want to simplify this as much as possible so that no "special cases" exist that fall outside the chosen equations and complicate the algorithms.

A. DRAWBACKS OF THE ORBITAL ELEMENT SET

One of the most commonly used element sets in orbital mechanics is the classical orbital element (COE) set. Although this set is fairly easily understood, it has well known cases for which it exhibits singularities [Vallado (2001)]. In particular, certain elements become undefined in either perfectly circular orbits or equatorial orbits. For zero eccentricity orbits, the argument of periapsis has no meaning. For zero inclination orbits, the right ascension does not exist. Substitutions for these "special cases" must be accounted for in order to have a universally applicable tool. Although scaled to canonical values, Delaunay elements exhibit similar difficulties with these special cases. While the difficulties are not large enough to discount these element sets from use (workarounds can be coded into the model), these reasons as well as a new challenge drove the early decision to research the use of an alternate element set which did not pose these problems, namely the equinoctial orbital element (EOE) set.

B. DEFINITION OF THE EQUINOCTIAL ELEMENTS

An overview of the equinoctial elements, widely credited to Broucke and Cefola (1972) for initial exploration, is provided in this section. Although several conventions have been used in various published discussions of these elements, the convention used by Battin (1999) has been adopted, and a more detailed derivation of these elements exists there. Although these elements can be applied to parabolic and hyperbolic orbits

with some variation [Coverstone and Prussing (2003)], this version of the model has been limited to elliptical orbits (including circular orbits) only.

To begin describing the equinoctial element set, the reference frame will first be defined. The equinoctial elements are best defined within the *fgw* equinoctial frame as illustrated in Figure 5. This frame can be described as a three rotation sequence from the *xyz* frame: a positive ***Ω*** rotation about $\hat{z}$, a positive ***i*** rotation about $\hat{f}$, and a negative ***Ω*** rotation about $\hat{w}$.

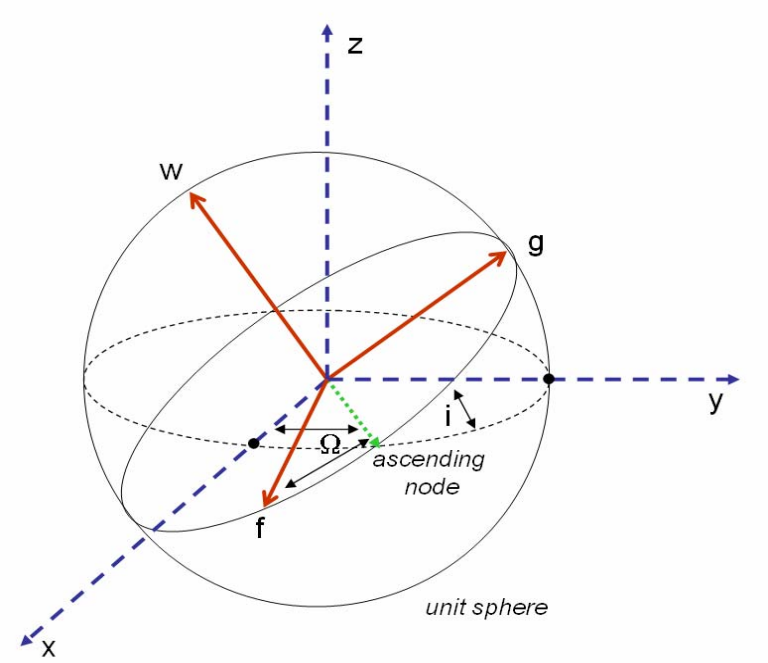

Figure 5 Equinoctial reference frame

There are six elements in the equinoctial element set, listed below and depicted in Figure 6:

- a = semimajor axis
- P_1 = g-component of the eccentricity vector
- P_2 = f-component of the eccentricity vector
- Q_1 = g-component of the ascending node vector
- Q_2 = f-component of the ascending node vector

- L = true longitude

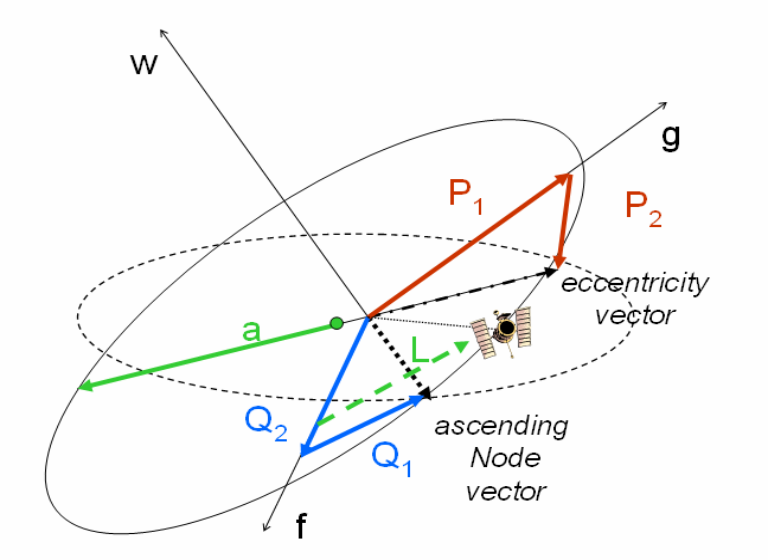

Figure 6 Equinoctial Orbital Elements

In order to help understanding, we can define these elements as they relate to the classical elements: semimajor axis, eccentricity, inclination, right ascension of ascending node, argument of perigee, and true anomaly ($a, e, i, \Omega, \omega, \nu$), as discussed by Danielson et al (1995).

The semimajor axis for the EOE set is the same as that of the COE set, in line with standard conic geometry, and will be assumed to require no further explanation.

The P_1 and P_2 elements together have a magnitude equal to the eccentricity of the orbit and form a vector that points to periapsis from the gravitational center, where:

$$P_1 = e\sin(\omega + I\Omega) \qquad \textbf{(3.1)}$$

$$P_2 = e\cos(\omega + I\Omega) \qquad \textbf{(3.2)}$$

The variable *I* as used here is a retrograde factor, which is +1 for direct orbits and -1 for retrograde orbits. However, this is ignored by many texts since the -1 factor is only required for true retrograde orbits (i.e. – exhibiting 180° inclination), which are very rarely used.

The Q_1 and Q_2 elements together have a magnitude dependent on the inclination and form a vector that points to the ascending node from the gravitational center, where:

$$Q_1 = \tan\left(\frac{i}{2}\right)^I \sin\Omega \qquad \textbf{(3.3)}$$

$$Q_2 = \tan\left(\frac{i}{2}\right)^I \cos\Omega \qquad \textbf{(3.4)}$$

The L element defines position of the satellite in the orbit, and is considered the only rapidly changing variable in this element set. It is related to the classical true anomaly, right ascension, and argument of perigee by the following:

$$L = \omega + \nu + I\Omega \qquad \textbf{(3.5)}$$

C. FEATURES OF THE EQUINOCTIAL ELEMENT SET

Equinoctial elements are a very good candidate for this thesis for reasons discussed below. Unfortunately, they can be mathematically challenging to use in practice, and this perhaps remains their principal drawback. However, through careful and thorough coding, this problem can be overcome.

1. Elimination of Singularities

The primary reason EOEs were chosen for the model is that they do not suffer the singularity problems exhibited by the COE set and others in dealing with circular and equatorial orbits. Since (ideally) equatorial orbits and (ideally) circular orbits play such a prominent role in the satellite systems that we use, it was desired to model using a system which could easily handle these cases. In fact, the only orbit for which the principal equinoctial elements exhibit a singularity is direct retrograde (i.e., – exhibiting 180° inclination), and this can be rectified by using a retrograde factor as discussed previously[3].

[3] Similarly, using the retrograde factor at -1, the only orbit where the retrograde elements exhibit singularity is for inclination of 0°.

2. Scaling

As discussed previously, scaling is a major consideration when performing optimal control computations, and using naturally well scaled state variables has instant benefit. Equinoctial orbital elements are such variables, and with the possible exception of the semimajor axis, the rest of the variables are already well scaled. Several constants that are used globally within the modeling code also need to be scaled in order to ensure efficient computation. The following is a discussion of how scaling is performed for the model used in this research.

First, four primary constants are defined which seed the scaling process. Although these values remain constant for a given run of the model, these values are modeled as variables for ease of modification for different runs. The constants used are thruster exit velocity ($v_e=I_{sp}*g_0$; where specific impulse (I_{sp}) and Earth's gravitational acceleration ($g_0=9.81*10^{-3}$ km/sec) are inputs not used beyond this calculation), max thrust (T_{max}), the gravitational constant for an Earth centered system ($\mu_0=398600.4415$ km^3/s^2), and the initial mass of the satellite (M_0). These constants serve as the basis for further scaling, and are used in scaled form globally within the model.

Next, generic scaling factors are developed to convert physical units to scaled units. The five principal scaling factors are:

- Du (Distance Unit) = Radius of the Earth, 6378.1363 km
- Mu (Mass Unit) = M_0
- Tu (Time Unit) = $\sqrt{\frac{DU^3}{\mu_0}}$
- Fu (Force Unit) = $\frac{Mu * Du}{Tu^2}$
- Vu (Velocity Unit) = $\frac{Du}{Tu}$

Using these factors, scaled versions of the principal constants are developed for further use throughout the model code:

$$\textbf{Scaled } v_e = \frac{v_e}{Vu} \tag{3.6}$$

$$\textbf{Scaled } T_{max} = \frac{T_{max}}{Fu} \tag{3.7}$$

$$\textbf{Scaled } \mu_0 = \mu_0 \frac{Tu^2}{Du^3} \tag{3.8}$$

$$\textbf{Scaled } M_0 = \frac{M_0}{Mu} \tag{3.9}$$

As mentioned above, the equinoctial orbit elements are naturally suited to scaling. With the exception of the semimajor axis, which when provided in kilometers must be divided by the Du scale factor to normalize, the remainder of the elements are well scaled. The P_1 and P_2 variables are converted from COEs using sin and cos functions and therefore fall between 0 and 1 automatically. The Q_1 and Q_2 variables are converted using a tan function, and although they are well behaved for most values, they exhibit difficulty as inclination approaches 180˚ (when I = 1) and must be limited by enforcing bounds, as will be discussed in the following chapter. The true longitude is measured in radians in orbit and therefore increases slowly enough (2π per orbit) not to be an issue over relatively short periods.

3. Mathematical Complexity

Unfortunately, the benefits of EOEs do not come without a price. Working with the elements can quickly become very complicated mathematically, as evidenced in the works of Betts (2001), Kechichian (1990, 1991), and others. Although these sources provide excellent treatments of the complicated matrix mathematics required for classical application, the use of the tools involved in this research have made replication of most of this work unnecessary outside of a formulation of the equations of motion. This in itself has proven to be one of the major benefits of this research, and will be covered in more detail in the following chapter.

D. TRANSFORMATION OF EQUINOCTIAL ELEMENTS TO POSITION AND VELOCITY

Transformations of equinoctial elements to classical elements can be accomplished simply by reversing the equations provided earlier in this chapter. However, for some applications, transformation directly to position and velocity vectors is preferred. The following equations [Battin, (1999)] provide the means of this transformation.

$$\mathbf{r} = r\begin{bmatrix}\cos L\\ \sin L\\ 0\end{bmatrix} \tag{3.10}$$

$$\mathbf{v} = \frac{h}{p}\begin{bmatrix}-P_1 - \sin L\\ P_2 + \cos L\\ 0\end{bmatrix} \tag{3.11}$$

where:

h = angular momentum = $\sqrt{\mu_0 a(1-P_1^2-P_2^2)}$

r = radius from gravitational center = $\dfrac{a(1-P_1^2-P_2^2)}{1+P_1\sin(L)+P_2\cos(L)}$

p = semiparameter = $a(1-P_1^2-P_2^2)$

μ_0 = gravitational constant

A rotation matrix must be used to transform these resultant vectors from fgw coordinates to xyz coordinates:

$$\mathbf{R} = \frac{1}{1+Q_1^2+Q_2^2}\begin{bmatrix}1-Q_1^2+Q_2^2 & 2Q_1Q_2 & 2Q_1\\ 2Q_1Q_2 & 1+Q_1^2-Q_2^2 & -2Q_2\\ -2Q_1 & 2Q_2 & 1-Q_1^2-Q_2^2\end{bmatrix} \tag{3.12}$$

Using these together:

$$\begin{aligned}\mathbf{r}_{\{\text{xyz frame}\}} &= \mathbf{R} * \mathbf{r}_{\{\text{fgw frame}\}}\\ \mathbf{v}_{\{\text{xyz frame}\}} &= \mathbf{R} * \mathbf{v}_{\{\text{fgw frame}\}}\end{aligned} \tag{3.13}$$

E. CONCLUSIONS

The judicious selection of state variables can provide much benefit to a particular problem. For this research, equinoctical orbit elements have been chosen due to favorable scaling properties and lack of singularities for all orbits. The following chapter will describe how these states will be employed into dynamic equations completely describing orbital motion, and form the foundation for all of the research that follows.

IV. FORMULATION OF THE PROBLEM

In order to move away from the broad theory that has been discussed thus far and work into the specific applications for the problem under study, a specific optimal control problem used throughout this research will be formulated. The following development will be performed for a single agent; however as will be later shown, the desired multi-satellite problem is a relatively simple extension of this basic problem.

A. STATES AND CONTROLS

As discussed earlier, the states are the equinoctial orbital elements. The state vector is symbolically expressed as follows:

$$x = \begin{Bmatrix} a \\ P_1 \\ P_2 \\ Q_1 \\ Q_2 \\ L \\ M \end{Bmatrix} \qquad \textbf{\textit{(4.1)}}$$

Mass is required to represent changes as fuel is consumed by the satellite's thrusters.

The control variables for this problem were decided to be six body-fixed thrusters: one for each direction in the +/- XYZ scheme. This decision was in part based on considerations of using the L^1 control norm for mass flow calculation, and follows discussion by Ross (2004) regarding minimum fuel controllers. Thus, the controls used for this problem are:

$$u = \begin{Bmatrix} T_{r1} \\ T_{t1} \\ T_{n1} \\ T_{r2} \\ T_{t2} \\ T_{n2} \end{Bmatrix} \tag{4.2}$$

Here T represents thrust, r, t, and n represent radial, transverse, and normal directions, and the *1* and *2* subscripts represent positive and negative directions respectively. Thus, $T_{r1}, T_{t1}, T_{n1} \geq 0$ while $T_{r2}, T_{t2}, T_{n2} \leq 0$. A diagram of this convention is shown in Figure 7.

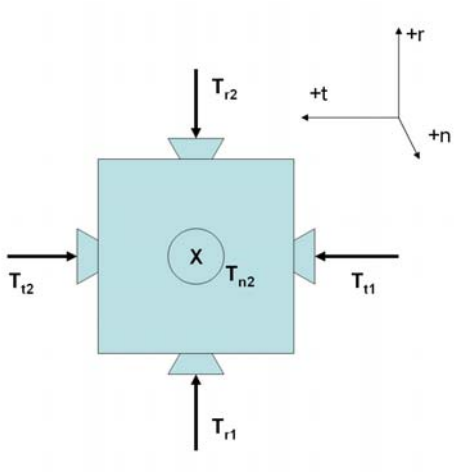

Figure 7 Satellite thrust convention diagram. Note, positive normal thrust T_{n1} not shown

B. COST

The main goal of this research is to minimize the amount of fuel consumed during commanded maneuvers. As discussed previously, this can also be stated as maximizing the final mass of the vehicle. If we consider the Bolza cost functional, then only the end-point Mayer cost E needs to be considered, so that:

$$J = E(x(t_f), t_f) = -M_f \tag{4.3}$$

Here the state variable M is the mass of the satellite at any point in time, and M_f is the final mass of the vehicle, the variable to be maximized.

C. DYNAMIC EQUATIONS OF MOTION

The maximization of the performance index M_f must be accomplished subject to dynamic equations governing orbital motion. These equations are based on the derivatives of the state variables, and can be represented simply as:

$$\dot{x} = \begin{Bmatrix} \dot{a} \\ \dot{P}_1 \\ \dot{P}_2 \\ \dot{Q}_1 \\ \dot{Q}_2 \\ \dot{L} \\ \dot{M} \end{Bmatrix} = f(x,u) \tag{4.4}$$

The right hand sides of seven the differential equations, f(x,u), are intricately coupled. As stated previously, the derivation of the full equations is based on Battin's text (1999) coupled with the chosen controls. The full equations of motion can be written as follows:

$$\dot{a} = 2\left(\frac{a^2}{\mathrm{h}}\right)(P_2\sin(L) - P_1\cos(L))\left(\frac{T_{r1}+T_{r2}}{M}\right) + \left(\frac{p}{r}\right)\left(\frac{T_{t1}+T_{t2}}{M}\right) \tag{4.5}$$

$$\begin{aligned}\dot{P}_1 = {} & \left(\frac{r}{h}\right)\left(\left(-\frac{p}{r}\right)\cos(L)\left(\frac{T_{r1}+T_{r2}}{M}\right) + \left(P_1 + \left(1+\left(\frac{p}{r}\right)\right)\sin(L)\right)\left(\frac{T_{t1}+T_{t2}}{M}\right)\right) \\ & -\left(\frac{r}{h}\right)\left(P_2(Q_1\cos(L) - Q_2\sin(L))\left(\frac{T_{n1}+T_{n2}}{M}\right)\right)\end{aligned} \tag{4.6}$$

$$\begin{aligned}\dot{P}_2 = {} & \left(\frac{r}{h}\right)\left(\left(\frac{p}{r}\right)\sin(L)\left(\frac{T_{r1}+T_{r2}}{M}\right) + \left(P_2 + \left(1+\left(\frac{p}{r}\right)\right)\cos(L)\right)\left(\frac{T_{t1}+T_{t2}}{M}\right)\right) \\ & +\left(\frac{r}{h}\right)\left(P_1(Q_1\cos(L) - Q_2\sin(L))\left(\frac{T_{n1}+T_{n2}}{M}\right)\right)\end{aligned} \tag{4.7}$$

$$\dot{Q}_1 = \left(\frac{r}{2h}\right)(1+Q_1^2+Q_2^2)\sin(L)\left(\frac{T_{n1}+T_{n2}}{M}\right) \tag{4.8}$$

$$\dot{Q}_2 = \left(\frac{r}{2h}\right)(1+Q_1^2+Q_2^2)\cos(L)\left(\frac{T_{n1}+T_{n2}}{M}\right) \tag{4.9}$$

$$\dot{L}=\left(\frac{h}{r^2}\right)+\left(\frac{rh}{p\mu_0}\right)\left(Q_2\sin(L)-Q_1\cos(L)\right)\left(\frac{T_{n1}+T_{n2}}{M}\right) \qquad \textbf{(4.10)}$$

$$\dot{M}=-\frac{(T_{r1}-T_{r2})+(T_{t1}-T_{t2})+(T_{n1}-T_{n2})}{v_e} \qquad \textbf{(4.11)}$$

where:

h = angular momentum = $\sqrt{\mu_0 a(1-P_1^2-P_2^2)}$

r = radius from gravitational center = $\dfrac{a(1-P_1^2-P_2^2)}{1+P_1\sin(L)+P_2\cos(L)}$

p = semiparameter = $a(1-P_1^2-P_2^2)$

μ_0 = gravitational constant

v_e = exit velocity of thruster

D. EVENTS

Since this is a two point boundary value problem, the only events required are the initial and final boundary conditions for the state variables. Further, since we are looking to maximize final mass, M_f can be left undefined. Thus, our relevant boundary events are:

$$\begin{aligned} a(t_0)&=a_i & a(t_f)&=a_f\\ P_1(t_0)&=P_{1i} & P_1(t_f)&=P_{1f}\\ P_2(t_0)&=P_{2i} & P_2(t_f)&=P_{2f}\\ Q_1(t_0)&=Q_{1i} & Q_1(t_f)&=Q_{1f}\\ Q_2(t_0)&=Q_{2i} & Q_2(t_f)&=Q_{2f}\\ L(t_0)&=L_i & L(t_f)&=L_f\\ M(t_0)&=M_i \end{aligned}$$

Outside of some path constraints and defining constants, these are the only inputs required by the model to determine optimal control.

E. STATE AND CONTROL BOUNDS

Some boundaries need to be enforced on states and controls in order to define a subset of possible solutions inside of which we will find a locally optimum one. This

helps to constrain a potentially mathematically infinite range of possible solutions to some reasonable (but not overconstrained) subset. Each of the set boundaries bears some discussion, but state bounds have been set as follows. Note that all values shown are scaled as previously discussed.

1. State Bounds

The bounds on semiparameter are straightforward, and are simply 1 Earth radius as the lower bound (to avoid "Earth intercept" orbits), and an arbitrarily large number (not infinity for computational reasons) as the upper bound.

$$1 \le a \le 10000 \qquad \textbf{(4.12)}$$

The bounds on P_1 and P_2 are set in order to constrain the possible set to elliptical orbits only, since the two parameters are based upon the orbit's eccentricity $\left(e = \sqrt{P_1^2 + P_2^2}\right)$. This relationship is also defined as a path constraint in order to maintain ellipticity within the transfer (i.e., $0 \le e < 1$). In reality, both P_1 and P_2 can not be at the maximum (or minimum) value at the same time; however, the bound is set at less than 1 so that a parabolic orbit (i.e., where e=1) is not achieved if one value equals 1 while the other is 0.

$$\begin{aligned} -.999 \le P_1 \le .999 \\ -.999 \le P_2 \le .999 \end{aligned} \qquad \textbf{(4.13)}$$

The bounds on Q_1 and Q_2 are again simply set arbitrarily high. Since the conversion to the Q variables is reliant on a function involving *tan(i/2)*, most values are within reasonable scaled ranges. However, as ***i*** approaches 180°, these values begin to grow towards infinity, so must be given room to run.

$$\begin{aligned} -10000 \le Q_1 \le 10000 \\ -10000 \le Q_2 \le 10000 \end{aligned} \qquad \textbf{(4.14)}$$

The bounds on true longitude are set between zero and an arbitrarily high upper value which is set as a constant within the model code.

$$0 \le L \le 10000 \tag{4.15}$$

The bounds on mass are set between an arbitrary non-zero minimum, with the initial mass of the satellite used for the upper bound. The minimum can be set as a way of defining the usuable propellant portion of the satellite mass and must be greater than zero (since equations (4.5) - (4.10) are singular for M=0).

$$M_{f\min} \le M \le M_i \tag{4.16}$$

2. Control Bounds

The bounds levied on the control variables are fairly straightforward. A maximum thrust is defined as a constant based on the individual thruster being modeled. The positive and negative directions for each dimension are then just set by convention as being between 0 and the max thrust for that direction. The upper and lower bounds are determined by which direction that thruster operates, as follows:

$$\begin{aligned} 0 \le T_{r1} \le T_{\max} \\ 0 \le T_{t1} \le T_{\max} \\ 0 \le T_{n1} \le T_{\max} \\ -T_{\max} \le T_{r2} \le 0 \\ -T_{\max} \le T_{t2} \le 0 \\ -T_{\max} \le T_{n2} \le 0 \end{aligned} \tag{4.17}$$

F. PATH CONSTRAINTS

For the single agent model, only one path constraint has been levied on the system. As has been previously mentioned, a path constraint was created in order to ensure that orbits remained elliptical at all times, including transfer. This was done to keep parabolic and hyperbolic trajectories from being considered during transfer, and to assist computational efficiency. Since this model was built to only consider the mathematics of elliptical orbits, this constraint serves to keep solutions within an

understood regime and avoid wandering into territory for which the system has not been suitably tested[4]. The path constraint simply stated is:

$$0 \le \sqrt{P_1^2 + P_2^2} < 1 \qquad \textbf{(4.18)}$$

As we will show later, additional path constraints must be added once we consider multi-agent models in order to ensure that collision avoidance between agents can be maintained, as well as to provide relational operating windows between agents.

G. DEVELOPMENT OF THE HAMILTONIAN

The Hamiltonian of the subject system of equations can be represented in a fairly straightforward manner (avoiding full expansion for the time being):

$$H = -M_f + \lambda_a(\dot{a}) + \lambda_{P_1}(\dot{P}_1) + \lambda_{P_2}(\dot{P}_2) + \lambda_{Q_1}(\dot{Q}_1) + \lambda_{Q_2}(\dot{Q}_2) + \lambda_L(\dot{L}) + \lambda_M(\dot{M}) \qquad \textbf{(4.19)}$$

Here λ represents Lagrangian multipliers of the state variables, as previously discussed. Since none of the dynamic equations are explicitly dependent on time, and following the previously discussed Hamiltonian Evolution equation (2.7), we find:

$$\frac{dH}{dt} = \frac{\partial H}{\partial t} = 0 \qquad \textbf{(4.20)}$$

The natural conclusion to this statement is that the Hamiltonian must exhibit constant behavior at all points in time during the optimal span, since $\dot{H} = 0$. Further, following the discussion of the Hamiltonian Value condition (2.8), we find:

[4] However, by altering the semimajor axis state to semiparameter ($p=a(1-e^2)$), it is believed that this model can be developed to work with hyperbolic orbits as well

$$
\begin{aligned}
&H(t_f) = -\frac{\partial \bar{E}}{\partial t_f} \\
&\bar{E} = E + \nu_i e_i = -M_f + \nu_a e_a + \nu_{P_1} e_{P_1} + \nu_{P_2} e_{P_2} + \nu_{Q_1} e_{Q_1} + \nu_{Q_2} e_{Q_2} + \nu_L e_L + \nu_M e_M \\
&e_a = a(t_f) - a \\
&e_{P_1} = P_1(t_f) - P_1 \\
&e_{P_2} = P_2(t_f) - P_2 \\
&e_{Q_1} = Q_1(t_f) - Q_1 \\
&e_{Q_2} = Q_2(t_f) - Q_2 \\
&e_L = L(t_f) \\
&e_M = M(t_f) \\
&\quad So: \\
&H(t_f) = -\frac{\partial \bar{E}}{\partial t_f} = 0
\end{aligned}
\qquad \textbf{(4.21)}
$$

Since the Hamiltonian is zero at the end state, and we have shown that the Hamiltonian must remain constant throughout the optimal control span, we must conclude that a constant zero must be maintained throughout the control span for a given solution to this problem to be considered optimal.

H. DEVELOPMENT OF THE LAGRANGIAN OF THE HAMILTONIAN

Using the above results, we can now express the Lagrangian of the Hamiltonian as follows:

$$
\begin{aligned}
\bar{H} = &-M_f + \lambda_a(\dot{a}) + \lambda_{P_1}(\dot{P}_1) + \lambda_{P_2}(\dot{P}_2) + \lambda_{Q_1}(\dot{Q}_1) + \lambda_{Q_2}(\dot{Q}_2) + \lambda_L(\dot{L}) + \lambda_M(\dot{M}) \\
&+ \mu_{T_{r1}} T_{r1} + \mu_{T_{t1}} T_{t1} + \mu_{T_{n1}} T_{n1} + \mu_{T_{r2}} T_{r2} + \mu_{T_{t2}} T_{t2} + \mu_{T_{n2}} T_{n2}
\end{aligned}
\qquad \textbf{(4.22)}
$$

Here μ represents Lagrangian multipliers on the control variables, as previously discussed. According to KKT theory, the Lagrangian of the Hamiltonian is stationary with respect to the optimal control at all points in time over the optimized interval, as previously shown in equation (2.5) , so that:

$$
\frac{\partial \bar{H}}{\partial u} = 0 \qquad \textbf{(2.5)}
$$

If we expand this relationship to its full glory, we get the following set of equations which represent the stationarity of the Lagrangian of the Hamiltonian with respect to the controls, and which will be used for further proof of optimality:

$$\frac{\partial \bar{H}}{\partial T_{r1}} = \frac{\lambda_a}{M}\left[\frac{2a^2}{h}(P_2 \sin L - P_1 \cos L)\right] - \frac{\lambda_{P_1}}{M}\left[\frac{p}{h}\cos L\right] + \frac{\lambda_{P_2}}{M}\left[\frac{p}{h}\sin L\right] - \frac{\lambda_M}{\mathrm{v}_e} + \mu_{T_{r1}} = 0 \tag{4.23}$$

$$\frac{\partial \bar{H}}{\partial T_{r2}} = \frac{\lambda_a}{M}\left[\frac{2a^2}{h}(P_2 \sin L - P_1 \cos L)\right] - \frac{\lambda_{P_1}}{M}\left[\frac{p}{h}\cos L\right] + \frac{\lambda_{P_2}}{M}\left[\frac{p}{h}\sin L\right] + \frac{\lambda_M}{\mathrm{v}_e} + \mu_{T_{r2}} = 0 \tag{4.24}$$

$$\frac{\partial \bar{H}}{\partial T_{t1}} = \frac{\lambda_a}{M}\left[\frac{2a^2}{h}\left(\frac{p}{r}\right)\right] + \frac{\lambda_{P_1}}{M}\left[\frac{r}{h}\left(P_1 + \left(1+\frac{p}{r}\right)\sin L\right)\right] + \frac{\lambda_{P_2}}{M}\left[\frac{r}{h}\left(P_2 + \left(1+\frac{p}{r}\right)\cos L\right)\right] - \frac{\lambda_M}{\mathrm{v}_e} + \mu_{T_{t1}} = 0 \tag{4.25}$$

$$\frac{\partial \bar{H}}{\partial T_{t2}} = \frac{\lambda_a}{M}\left[\frac{2a^2}{h}\left(\frac{p}{r}\right)\right] + \frac{\lambda_{P_1}}{M}\left[\frac{r}{h}\left(P_1 + \left(1+\frac{p}{r}\right)\sin L\right)\right] + \frac{\lambda_{P_2}}{M}\left[\frac{r}{h}\left(P_2 + \left(1+\frac{p}{r}\right)\cos L\right)\right] + \frac{\lambda_M}{\mathrm{v}_e} + \mu_{T_{t2}} = 0 \tag{4.26}$$

$$\frac{\partial \bar{H}}{\partial T_{n1}} = -\frac{\lambda_{P_1}}{M}\left[\frac{r}{h}\left(P_2 + \left(Q_1 \cos L - Q_2 \sin L\right)\right)\right] + \frac{\lambda_{P_2}}{M}\left[\frac{r}{h}\left(P_1 + \left(Q_1 \cos L - Q_2 \sin L\right)\right)\right] + \frac{\lambda_{Q_1}}{M}\left[\frac{r}{2h}\left(1+Q_1^{\,2}+Q_2^{\,2}\right)\sin L\right] + \frac{\lambda_{Q2}}{M}\left[\frac{r}{2h}\left(1+Q_1^{\,2}+Q_2^{\,2}\right)\cos L\right] + \frac{\lambda_L}{M}\left[\frac{rh}{p\mu_0}\left(Q_2 \sin L - Q_1 \cos L\right)\right] - \frac{\lambda_M}{\mathrm{v}_e} + \mu_{T_{n1}} = 0 \tag{4.27}$$

$$\frac{\partial \bar{H}}{\partial T_{n2}} = -\frac{\lambda_{P_1}}{M}\left[\frac{r}{h}\left(P_2 + \left(Q_1 \cos L - Q_2 \sin L\right)\right)\right] + \frac{\lambda_{P_2}}{M}\left[\frac{r}{h}\left(P_1 + \left(Q_1 \cos L - Q_2 \sin L\right)\right)\right] + \frac{\lambda_{Q_1}}{M}\left[\frac{r}{2h}\left(1+Q_1^{\,2}+Q_2^{\,2}\right)\sin L\right] + \frac{\lambda_{Q2}}{M}\left[\frac{r}{2h}\left(1+Q_1^{\,2}+Q_2^{\,2}\right)\cos L\right] + \frac{\lambda_L}{M}\left[\frac{rh}{p\mu_0}\left(Q_2 \sin L - Q_1 \cos L\right)\right] + \frac{\lambda_M}{\mathrm{v}_e} + \mu_{T_{n2}} = 0 \tag{4.28}$$

again where:

h = angular momentum = $\sqrt{\mu_0 a(1-P_1^2-P_2^2)}$

r = radius from gravitational center = $\dfrac{a(1-P_1^2-P_2^2)}{1+P_1\sin(L)+P_2\cos(L)}$

p = semiparameter = $a(1-P_1^2-P_2^2)$

μ_0 = gravitational constant

v_e = exit velocity of thruster

It should be noted that these equations look almost identical for any given +/- thruster pair, the only differences being the sign on the $\dfrac{\lambda_M}{v_e}$ term, as well as the differing values of the individual Lagrangian control multipliers.

I. COMPLEMENTARITY CONDITION

At each instant of time, the multiplier-control pair must satisfy the KKT complementarity condition, which defines the switching structure of the optimal control:

$$\mu_i = \begin{cases} \leq 0 & u_i = u_{il} \\ \geq 0 & u_i = u_{iu} \\ = 0 & u_{il} < u < u_{iu} \\ unrestricted & u_{il} = u_{iu} \end{cases} \quad if \qquad \textbf{(4.29)}$$

As an example of this, and using previously discussed values for one of the controls (T_{r1}), we can observe:

$$\mu_{T_{r1}} = \begin{cases} \leq 0 & T_{r1} = 0 \\ \geq 0 & T_{r1} = T_{\max} \\ = 0 & 0 < T_{r1} < T_{\max} \\ unrestricted & 0 = T_{\max} \end{cases} \quad if \qquad \textbf{(4.30)}$$

By observing behavior following this discussion, we can use this as a third data point in validating optimal control.

J. CONCLUSIONS

Having now developed the specific equations, conditions, and tools for achieving and proving optimal control, we can now focus on validating that these building blocks and the model built upon them works according to the Minimum Principle.

THIS PAGE INTENTIONALLY LEFT BLANK

V. MODEL VALIDATION

Having established the basic methods and processes of solving optimal control problems, this section will demonstrate how the formulations work as expected.

Once coded, the model was validated by running well documented simple optimal control scenarios and observing the results for agreement. The rest of this chapter discusses the efforts performed and their results in confirming optimal control behavior by the model.

A. MODEL NOTES

As has been alluded to previously, the MATLAB™ based model accepts inputs in the form of Keplerian orbital elements, then automatically performs the conversion to equinoctial elements, including automatic scaling for computational efficiency. This was deemed the most appropriate and easily understood method of input, since classical elements are considered somewhat of a basic standard among astrodynamicists. However, once the conversion is made to equinoctial elements by the model, all internal calculations are in scaled equinoctial variables for purposes of singularity avoidance.

For the purposes of all of the scenarios run used in this thesis, a uniform set of constants was used, and they are:

$$\begin{aligned} &I_{sp} = 320 \text{ s} \\ &g_0 = 0.00981 \text{ km/s}^2 \\ &\mathrm{v}_e = I_{sp} * g_0 = 3.1392 \text{ km/s} \\ &\mathrm{T}_{\max} = 10 \text{ N} \\ &\mu_0 = 398600.4415 \text{ km}^3 / s^2 \\ &M_0 = 3000 \text{ kg} \end{aligned} \qquad \textit{(5.1)}$$

During the following scenarios, no judgment was made as to how much fuel was consumed by the spacecraft, only proving that it was the optimal amount required for the requested transfer. This is to say there was no constraint placed on using for example 90% of a vehicle's mass in fuel to perform a given transfer. For the purposes of this

research, this type of constraint was not imposed, but would be the job of mission planners to determine reasonable fuel-to-payload ratios.

Scenario run speed was not a major focus of this effort, outside of the desire to generally speed up and automate the process of determining fuel optimal maneuvers. This is not considered an issue, since current execution times on the order of man-days are practiced, and this research has produced run times of minutes or less. Approximate times that individual runs have taken will be noted in the following sections. However, these times are to be taken with some suspicion since they are platform and software version specific, and some overhead variance is incurred by running on a network based Windows operating system. For purposes of general discussion, all scenario runs were performed on a 3Ghz Intel® Pentium® 4 notebook computer using MATLAB™ 7.0 running DIDO.

B. HOHMANN TRANSFER SCENARIO

For the first validation scenario, a classic Hohmann transfer was performed. First suggested by Walter Hohmann in 1925, the Hohmann maneuver is mathematically accepted as the most fuel efficient transfer between two circular coplanar orbits, involving two tangential impulsive burns to start and stop the transfer, and is well documented by Vallado (1999), Chobotov (2002), Bate, Mueller, and White (1971) and most introductory texts on orbital dynamics. Although Hohmann's work only considered circular orbits, further work by Lawden (1952) validated that tangential burns are also optimal for some elliptic scenarios.

This orbital transfer was chosen as a classic example of a known two-dimensional orbit transfer with a known optimal result. Performance compliant with this known behavior will serve to validate this model for a two-dimensional coplanar transfer, the first step in validating an overall three-dimensional model.

It should be noted that true Hohmann behavior is not expected from the simulation since the Hohmann transfer involves impulsive burns at the tangent points. Since this model involves discrete finite burns, a similar behavior is expected, however identical performance is not.

1. Hohmann Transfer Input Parameters

The following Keplerian inputs were provided to the model for evaluation:

$$
\begin{aligned}
a_i &= 7015 \text{ km} & a_f &= 9567 \text{ km} \\
e_i &= 0.0 & e_f &= 0.0 \\
i_i &= 35 * \frac{\pi}{180} \text{ rad} & i_f &= 35 * \frac{\pi}{180} \text{ rad} \\
\Omega_{\mathrm{i}} &= 30 * \frac{\pi}{180} \text{ rad} & \Omega_{\mathrm{f}} &= 30 * \frac{\pi}{180} \text{ rad} \\
\omega_{\mathrm{i}} &= 45 * \frac{\pi}{180} \text{ rad} & \omega_{\mathrm{f}} &= 45 * \frac{\pi}{180} \text{ rad} \\
\nu_{\mathrm{i}} &= 0 * \frac{\pi}{180} \text{ rad} & \nu_{\mathrm{f}} &= 235 * \frac{\pi}{180} \text{ rad}
\end{aligned}
\qquad \textit{(5.2)}
$$

The number N of discrete nodes used by the model for this scenario is 80. This number is considered to be reasonably high, and impacts the computational run speed of the scenario. However it offers the benefit of increased resolution for illustrative purposes. Computationally speaking, the model independently solves equations involving the number of state plus control variables times the number of nodes across the optimal time span:

$$\#\ \text{variables} = (x + u) * N \qquad \textit{(5.3)}$$

For this example, this equates to a (7+6)*80=1040 variable problem being optimized for each instant of time.

2. Hohmann Transfer Performance

Given only the above end point conditions, and subject to the cost and dynamic equations discussed earlier, the following performance was recorded. Graphical representations of the state and control histories are shown as Figure 8. Mass flow rate is shown as Figure 9. A pictorial plot of orbital performance is shown as Figure 10. It should be noted that thrusts occur only in the positive transverse thruster, as expected, and that the thrust points all fall in the vicinity of the nominal tangent points for this maneuver. An 80 node run took approximately 124 seconds to execute.

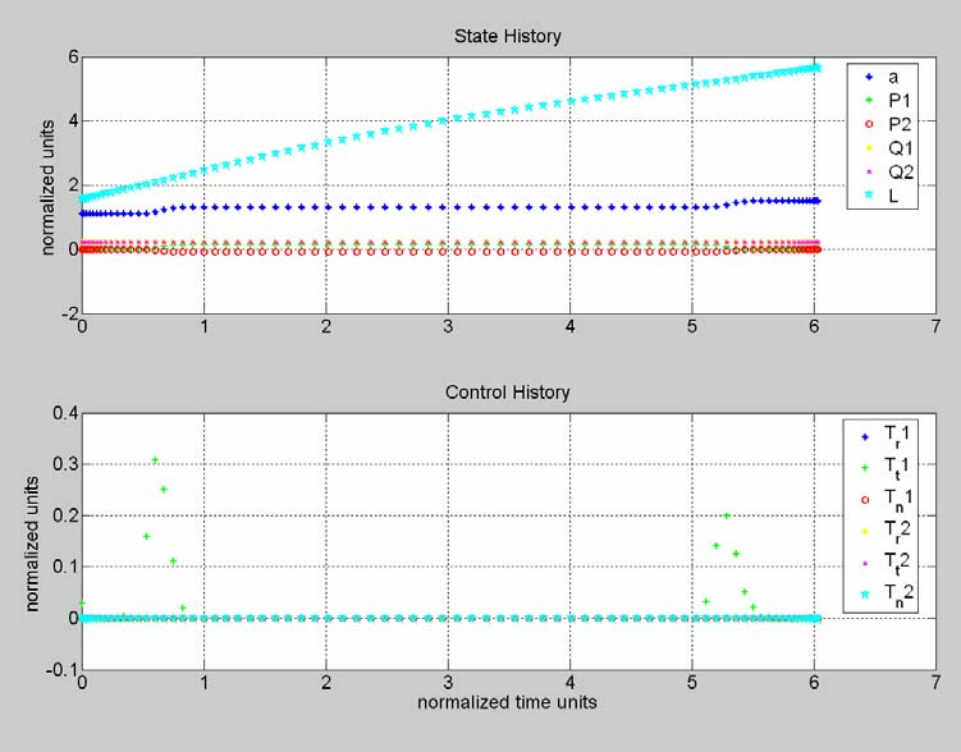

Figure 8 Hohmann transfer state and control histories

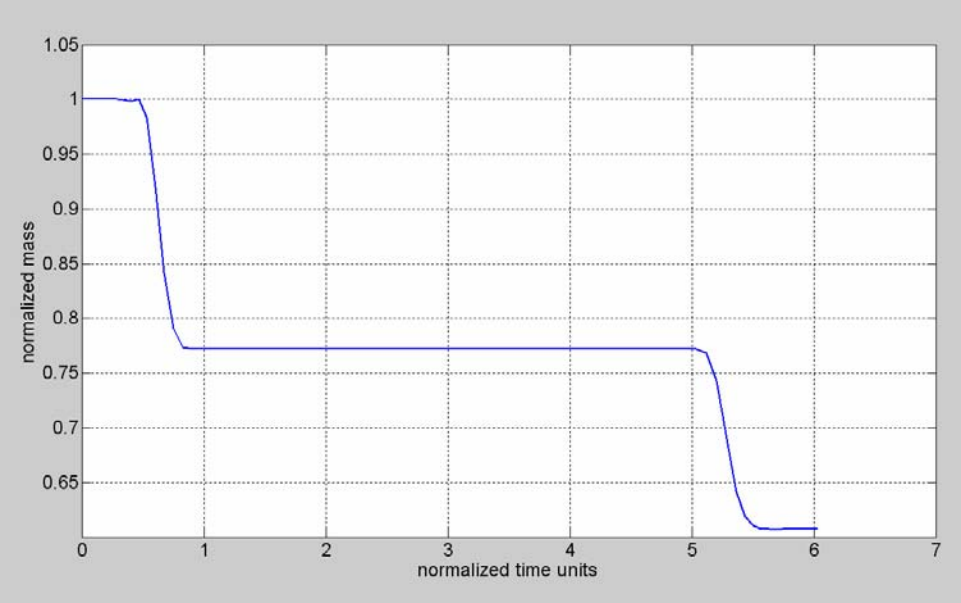

Figure 9 Hohmann transfer mass flow

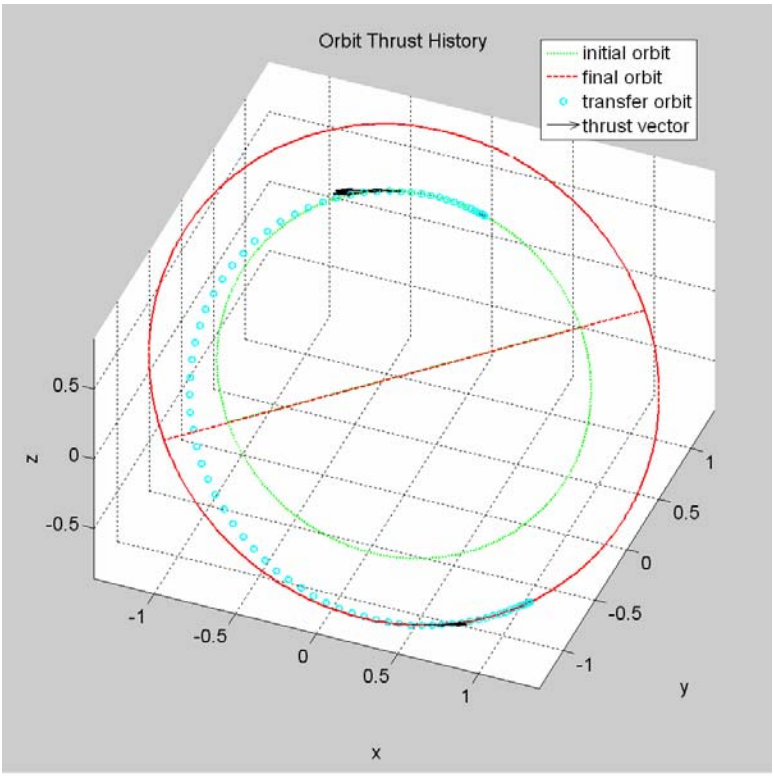

Figure 10 Hohmann transfer.

It is obvious by observation that this performance does not appear to be a strict two burn impulsive maneuver, but as expected, a finite burn over several discrete points closely simulating this behavior. Since limits have been placed on the maximum amount of thrust available within the model representative of a reasonably sized chemical thruster, the thruster is never allowed to reach the force required to accelerate the vehicle by the amount needed for an impulsive maneuver. These differences between theory and a more realistic model are accentuated by the fact that the model used is based upon discrete time points rather than a time continuum, which tends to magnify differences in the thrusting behavior, particularly at low discrete nodal resolution. As the number of nodes is increased, the behavior becomes more like the theoretical solution. This seeming discrepancy is one of the sacrifices made for computational efficiency in the Legendre pseudospectral method, but classical behavior can be extrapolated from these approximations, and indeed recognized as the number of nodes increases. This will be seen as a continuous theme through the performance of the scenario runs through this research, but is no cause for alarm.

3. Hohmann Transfer Model Optimal Behavior

a. Hohmann Transfer Feasibility Analysis

Feasibility was shown by independently propagating the initial conditions through the equations of motion using interpolated controls. A graphical representation of the result is shown as Figure 11, and shows very good behavior. Note that the propagated solution perfectly overlays the model solution. It can be concluded that the result is within the feasible set of optimal solutions.

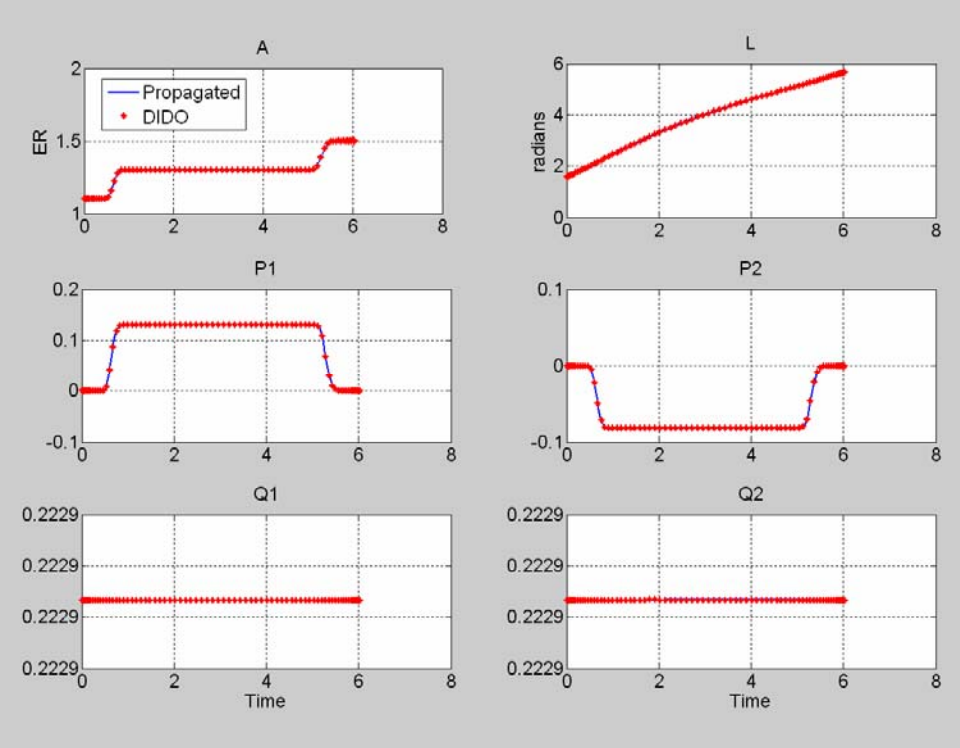

Figure 11 Plots of Hohmann transfer model performance vs. ODE45 propagation

b. Hohmann Transfer Hamiltonian Behavior

Graphical representation of the Hamiltonian during the performance period is shown as Figure 12. In line with our previous discussion, it can be observed that the Hamiltonian exhibits a near constant zero value for the majority of the run. By this test condition, it can be concluded that optimal control is being performed.

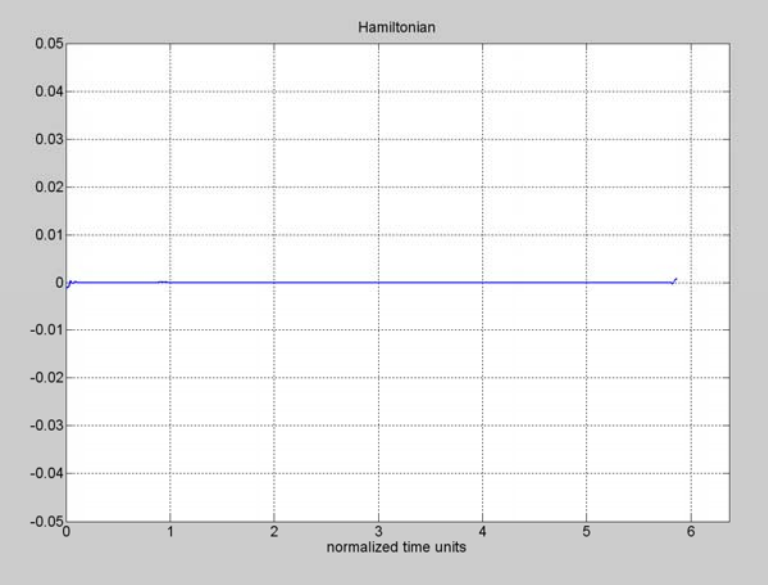

Figure 12 Hohmann transfer Hamiltonian behavior

c. Hohmann Transfer Lagrangian Behavior

Graphical representation of the stationarity of the Lagrangian of the Hamiltonian (with respect to controls) during the performance period is shown as Figure 13 for all six controls. In line with our previous discussion, it can be observed that the Lagrangian exhibits a near zero value for the majority of the run. By this test condition, it can be concluded that optimal control is being performed.

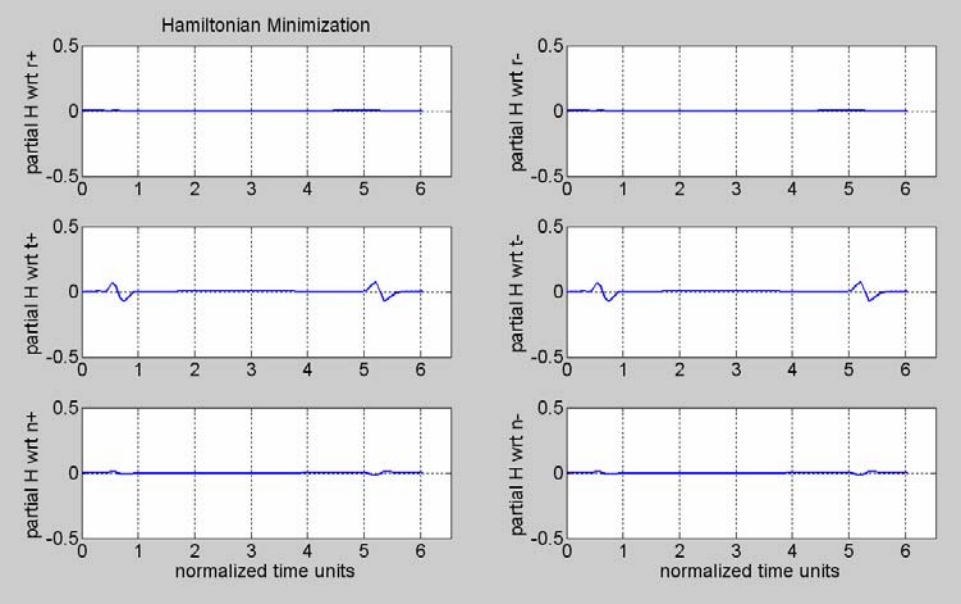

Figure 13 Hohmann transfer minimized Lagrangian behavior

d. Hohmann Transfer KKT Complementarity Condition

Graphical representation of the switching structure for each of the control/dual pairs is shown as Figure 14, with greater detail visible in Figure 15. This switching generally follows the criteria described by equation (4.29), and therefore the conclusion can be made that optimal control is being performed.

Note in Figure 15 that the switch seems to be commanded before the control dual crosses zero. It is also observed that the value of the costate remains very close to zero during the thrusting period. This close zero approach by the costate begins to very closely resemble control/dual behavior reported by Lawden (1963) for an impulsive maneuver, particularly since a prolonged period of maximum thrust is not observed. In these plots, the control does not appear to reach maximum value at the second peak as might be expected; however the control dual is effectively zero at this point so KKT theorem still holds. It is believed that this behavior is due to internal tolerance settings perhaps coupled with some scaling issues, which is not a cause for immediate concern but which will be addressed further in a later section on future work.

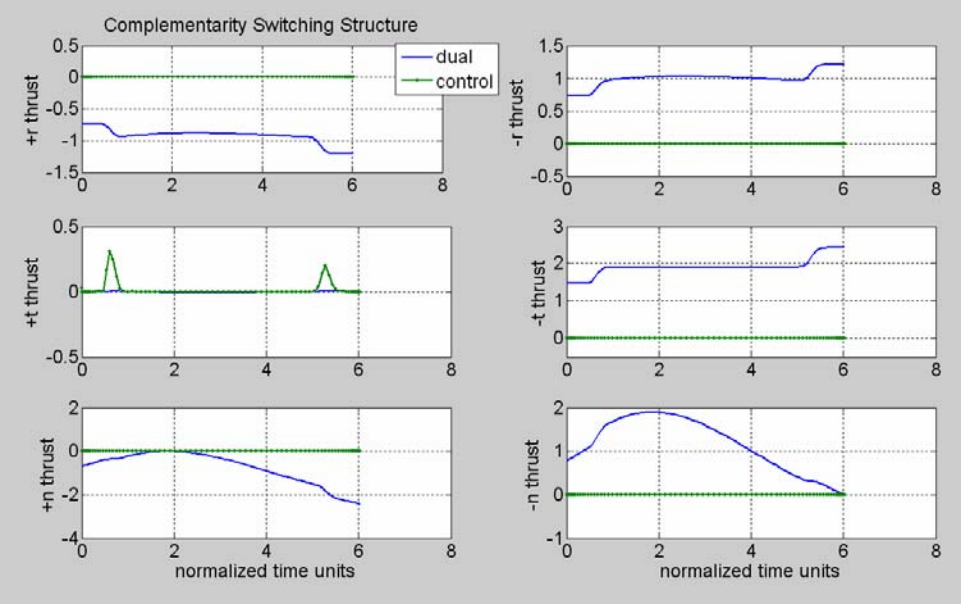

Figure 14 Switching structure for Hohmann transfer

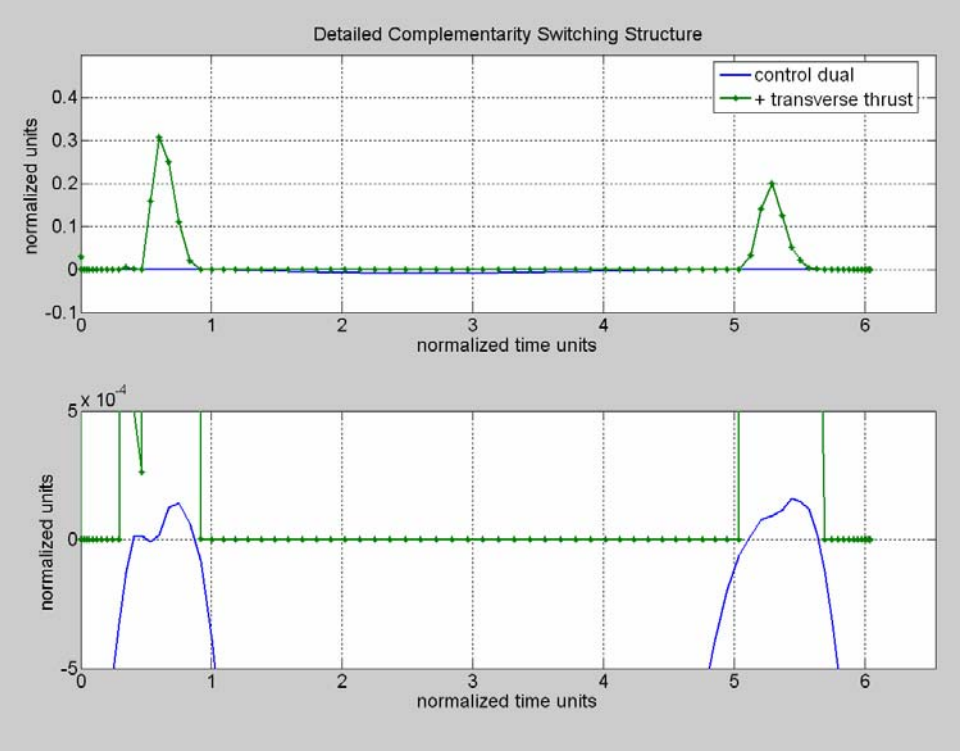

Figure 15 Detailed switching structure for positive transverse thrust, T_{tl}, including expanded blowup (bottom). Behavior approaches that reported by Lawden.

4. Hohmann Transfer Scenario Conclusions

Based on the performance of the model and our observed compliance with several of the necessary conditions of optimality, we can reasonably conclude that the model exhibits optimal control for a two-dimensional (i.e.- coplanar) orbit transfer. As a non-numerical check, the performance of the model also meets our expectations on how we believe a Hohmann transfer should be performed. As an added benefit, this scenario has verified that circular orbits (i.e. – zero eccentricity orbits) do not pose a singularity problem to the model. This is the first step in validating overall three-dimensional compliance with the mathematics and physics involved in Keplerian orbits. It also validates that our derived equinoctial based equations of motion appear to be working as expected. However, we must perform further validation to ensure the system works for a three-dimensional case.

C. INCLINATION CHANGE SCENARIO

Since the model has been validated for a two dimensional scenario, the next step is to prove that it works for a three dimensional scenario. For this reason, a simple inclination change was chosen to be modeled, since we know that the mathematically optimal control solution occurs at the ascending and/or descending nodes. Additionally, an eccentricity was added for the initial and final orbits to introduce a new element into the puzzle. The presentation of this scenario will follow much like the presentation of the previous scenario, so some of the explanatory details of the methodology will be omitted as they should now be familiar to the reader.

1. Inclination Change Parameters

The following COE inputs were provided to the model for evaluation:

$$
\begin{aligned}
a_i &= 9567 \text{ km} & a_f &= 9567 \text{ km} \\
e_i &= 0.5 & e_f &= 0.5 \\
i_i &= 35 * \frac{\pi}{180} \text{ rad} & i_f &= 45 * \frac{\pi}{180} \text{ rad} \\
\Omega_{\mathrm{i}} &= 10 * \frac{\pi}{180} \text{ rad} & \Omega_{\mathrm{f}} &= 10 * \frac{\pi}{180} \text{ rad} \\
\omega_{\mathrm{i}} &= 225 * \frac{\pi}{180} \text{ rad} & \omega_{\mathrm{f}} &= 225 * \frac{\pi}{180} \text{ rad} \\
\nu_{\mathrm{i}} &= 0 * \frac{\pi}{180} \text{ rad} & \nu_{\mathrm{f}} &= 359 * \frac{\pi}{180} \text{ rad}
\end{aligned}
\qquad \textit{(5.4)}
$$

Again, an 80 node solution was requested.

2. Inclination Change Performance

Given only the above end point conditions, and subject to the cost and dynamic equations, the following performance was recorded. Graphical representations of the state and control histories are shown as Figure 16. Mass flow rate is shown as Figure 17. A pictorial plot of orbital performance is shown as Figure 18. It should be noted that thrusts occur only in the normal direction in the vicinity of the ascending node, as expected. An 80 node run took approximately 271 seconds.

Again, it can be observed that this scenario does not behave in impulsive burns at the nodes as predicted by theory, but rather finite burn limitations still hold true for the model. The locations of the burns as expected by optimal behavior is unmistakable, and the previous discussion of bang-bang control is still valid, indicating a period of maximum thrust at the nodal point results in optimal control.

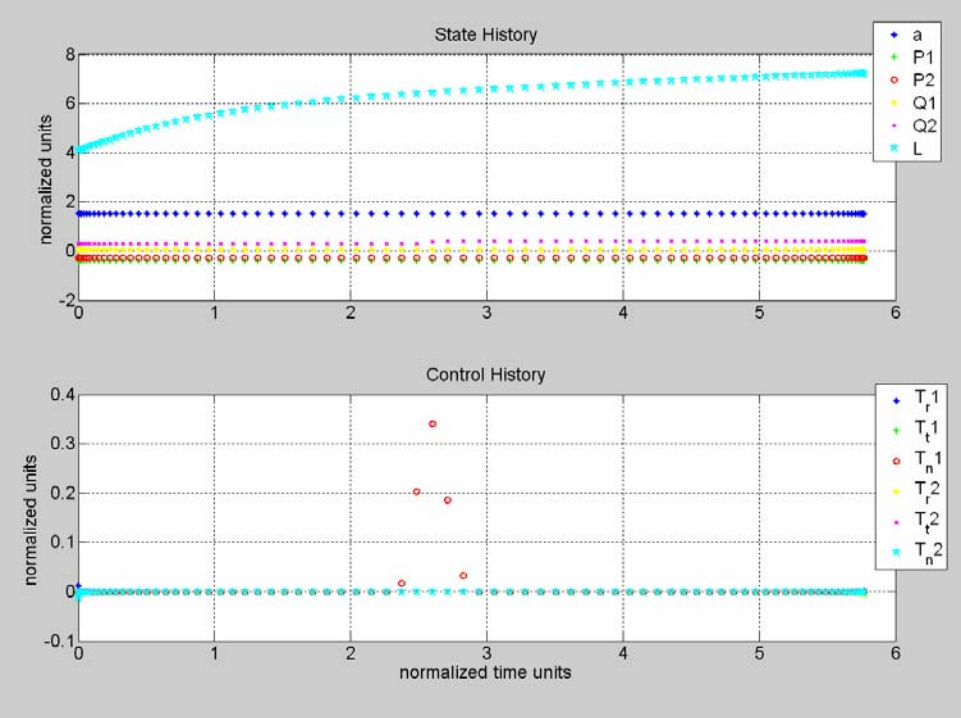

Figure 16 State and control histories for inclination change

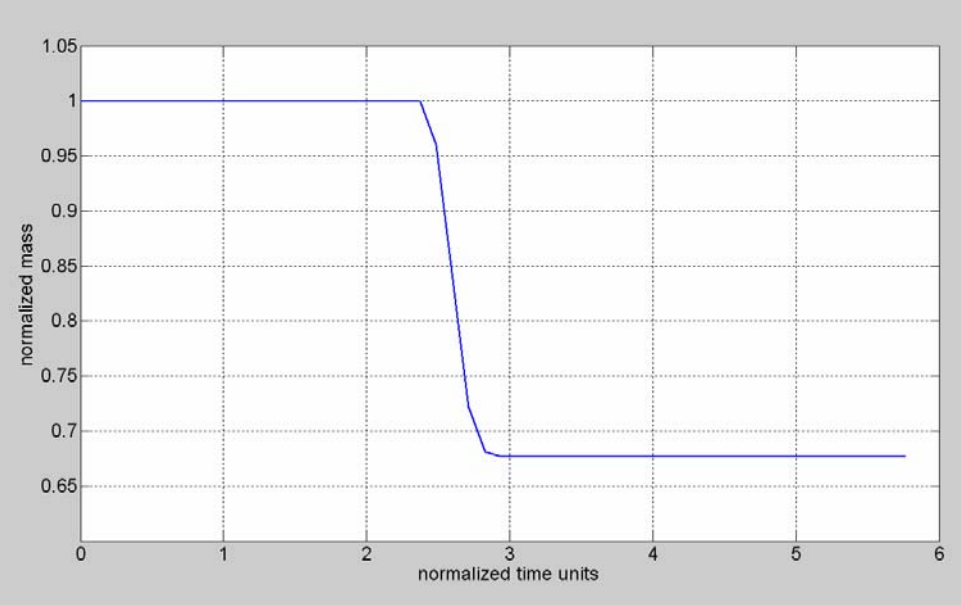

Figure 17 Mass flow for inclination change

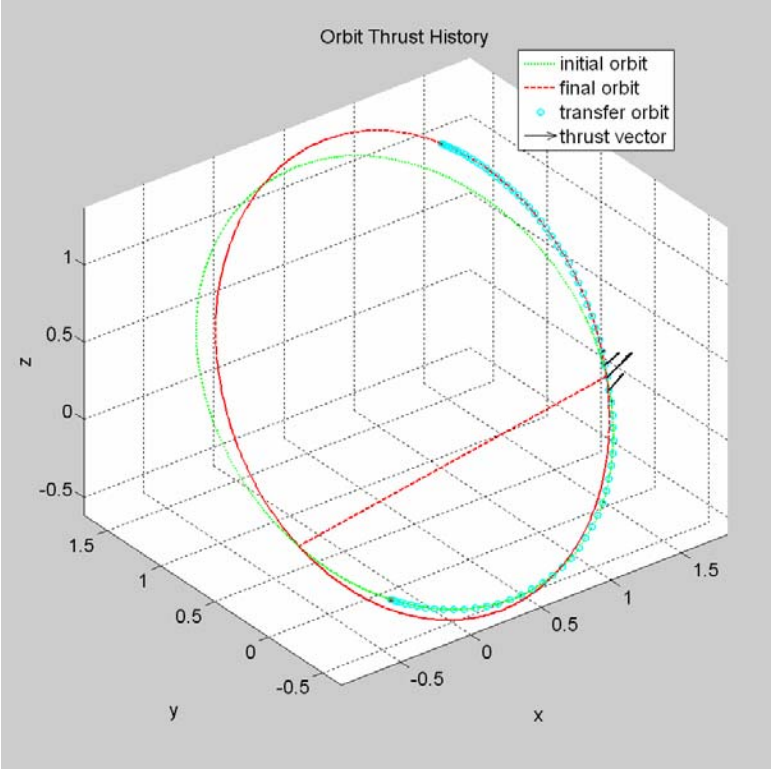

Figure 18 Inclination change

3. Inclination Change Optimal Behavior

a. Inclination Change Feasibility

Feasibility was again shown by independently propagating the initial conditions through the equations of motion using interpolated controls. A graphical representation of the result is shown as Figure 19 and shows very good behavior. We can conclude that the result is within the feasible set of solutions.

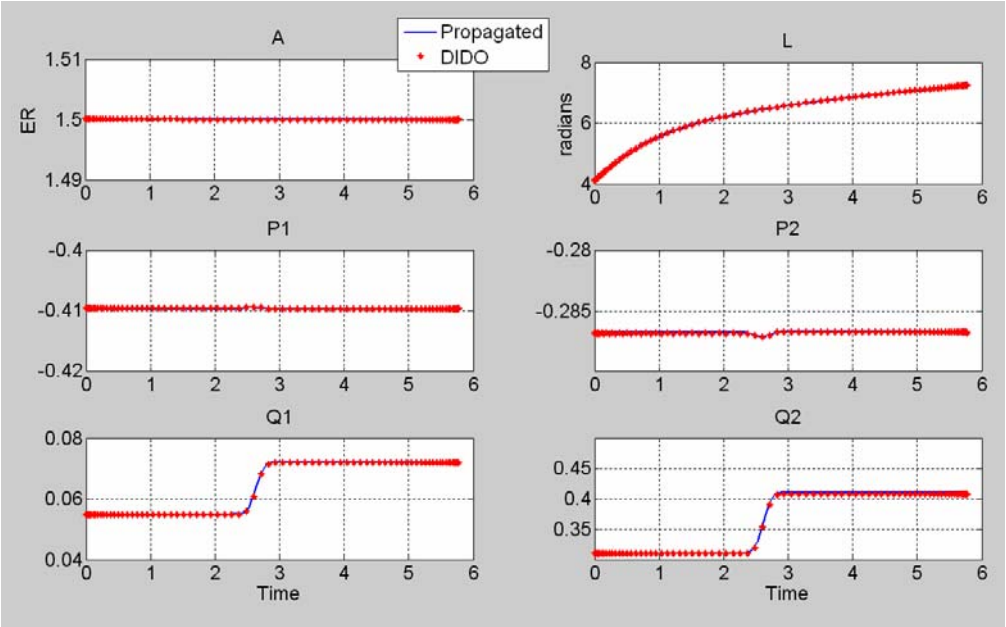

Figure 19 Plots of inclination change model performance vs. ODE45 propagation

b. Inclination Change Hamiltonian Behavior

Graphical representation of the Hamiltonian during the performance period is shown as Figure 20. In line with our previous discussion, we observe that the Hamiltonian exhibits a near constant zero value for the majority of the run. By this test condition, we can conclude that optimal control is being performed.

c. Inclination Change Lagrangian Behavior

Graphical representation of the stationary Lagrangian during the performance period is shown as Figure 21 for all six controls. In line with our previous discussion, we observe that the stationary Lagrangian exhibits a near zero value for the majority of the run. By this test condition, we can conclude that optimal control is being performed.

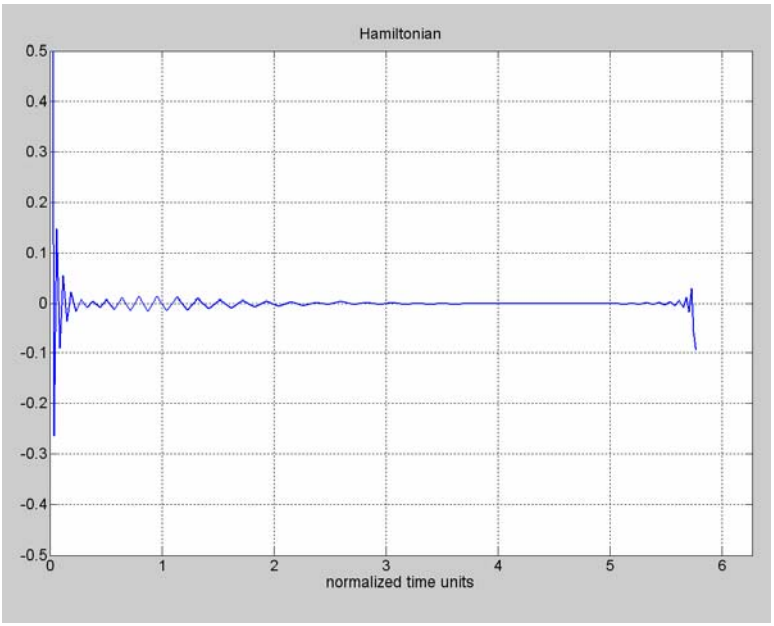

Figure 20 Hamiltonian behavior for inclination change

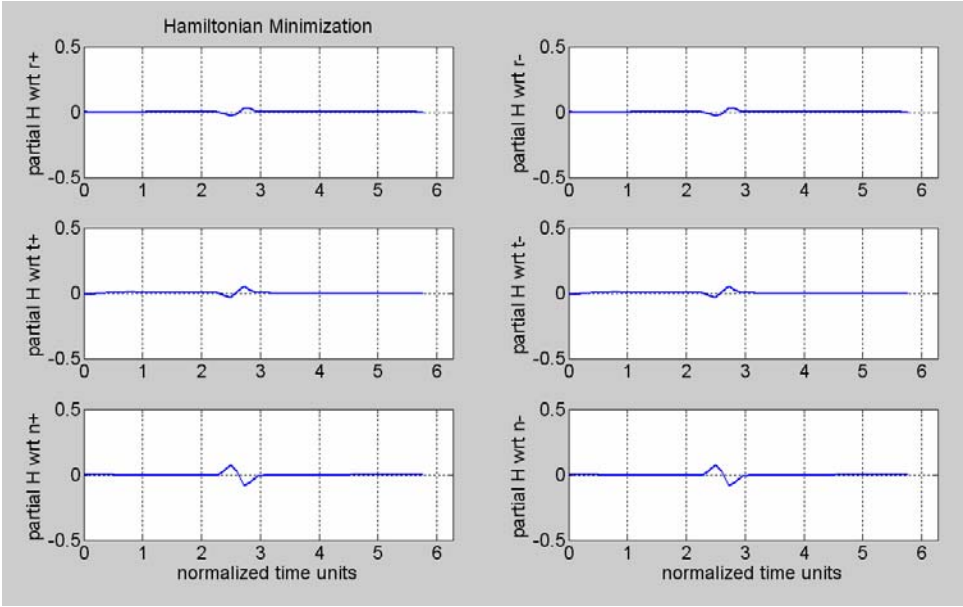

Figure 21 Inclination change minimized Lagrangian behavior

d. Inclination Change KKT Complementarity Condition

Graphical representation of the switching structure for each of the control/dual pairs is shown as Figure 22 and detailed in Figure 23. This switching follows the criteria described by equation (4.29), and therefore we can conclude that

optimal control is being performed. It can be observed that the only control being exercised is by the –n thruster, T_{n2}. It can also be observed in Figure 23 that this behavior again appears to very closely approach Lawden's (1963) dual/control behavior for an impulsive burn. Again, manifestations of the scaling/tolerance behavior observed in the Hohmann scenario can be noted, although in this scenario we do observe the occurrence of maximum thrust (0.34 scaled units).

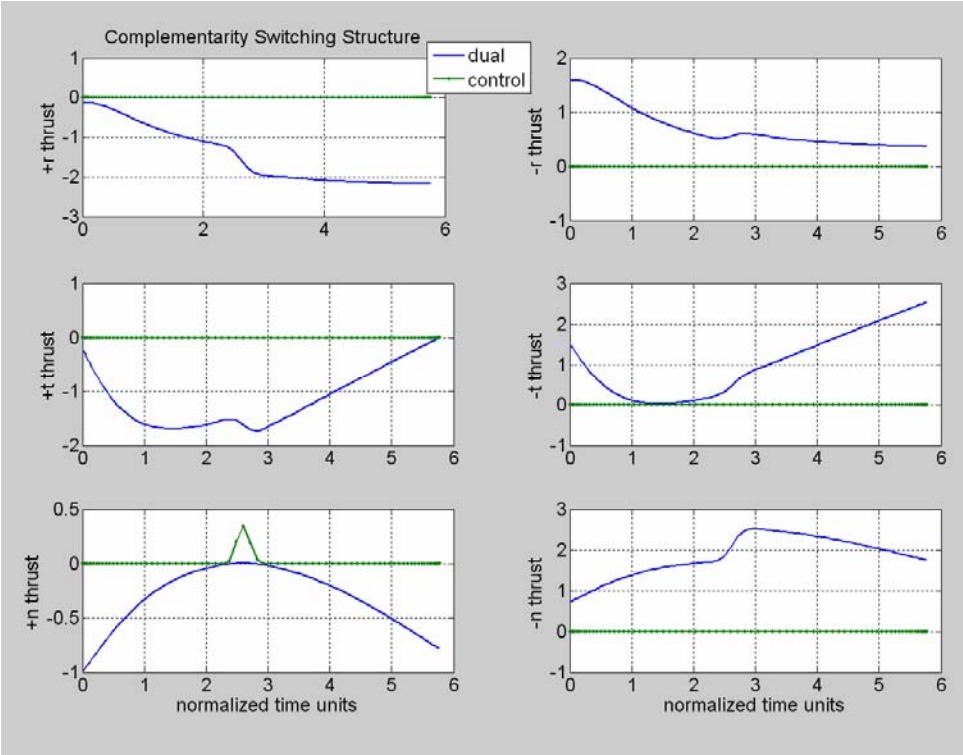

Figure 22 Switching behavior for inclination change

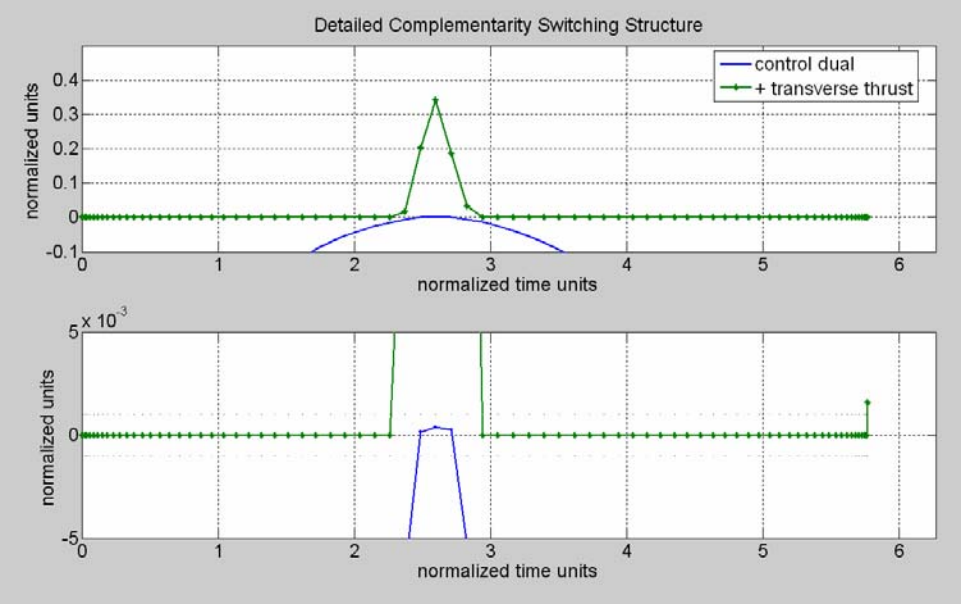

Figure 23 Switching detail for thruster T_{n1}, with blow-up

4. Inclination Change Scenario Conclusions

Based on the performance of the model and our observed compliance with several of the necessary conditions of optimality, we can reasonably conclude that the model exhibits optimal control for a three-dimensional orbit transfer. As a non-numerical check, the performance of the model also meets our expectations on how we believe an optimal inclination change should be performed. At first blush, this seems to validate that our derived equinoctial based equations of motion appear to be working as expected. However, we researched further scenarios to try to get a better feeling that this was in fact the case.

D. SEMIMAJOR AXIS CHANGE SCENARIO

Although two- and three-dimensional model behavior had been proven, the next step was to get further data points on model performance in known optimal problems. A semimajor axis change maneuver was attempted, as first proposed by Lawden (1962).

1. Semimajor Axis Change Parameters

The following COE inputs were provided to the model for evaluation:

$$
\begin{aligned}
a_i &= 9567 \text{ km} & a_f &= 9567 \text{ km} \\
e_i &= 0.5 & e_f &= 0.5 \\
i_i &= 35 * \frac{\pi}{180} \text{ rad} & i_f &= 35 * \frac{\pi}{180} \text{ rad} \\
\Omega_{\mathrm{i}} &= 10 * \frac{\pi}{180} \text{ rad} & \Omega_{\mathrm{f}} &= 10 * \frac{\pi}{180} \text{ rad} \\
\omega_{\mathrm{i}} &= 225 * \frac{\pi}{180} \text{ rad} & \omega_{\mathrm{f}} &= 315 * \frac{\pi}{180} \text{ rad} \\
\nu_{\mathrm{i}} &= 0 * \frac{\pi}{180} \text{ rad} & \nu_{\mathrm{f}} &= 359 * \frac{\pi}{180} \text{ rad}
\end{aligned}
\qquad \textit{(5.5)}
$$

2. Semimajor Axis Change Performance

Given only the above end point conditions, and subject to the cost and dynamic equations, the following performance was recorded. Graphical representations of the state and control histories are shown as Figure 24. Mass flow rate is shown as Figure 25. A pictorial plot of orbital performance is shown as Figure 26. A 100 node run took approximately 368 seconds. It should be noted that the optimal controls for the two burn maneuver occur as predicted by Lawden. Again as discussed previously, differences between these results and true impulsive behavior can be explained by the discrete time nature of this modeling.

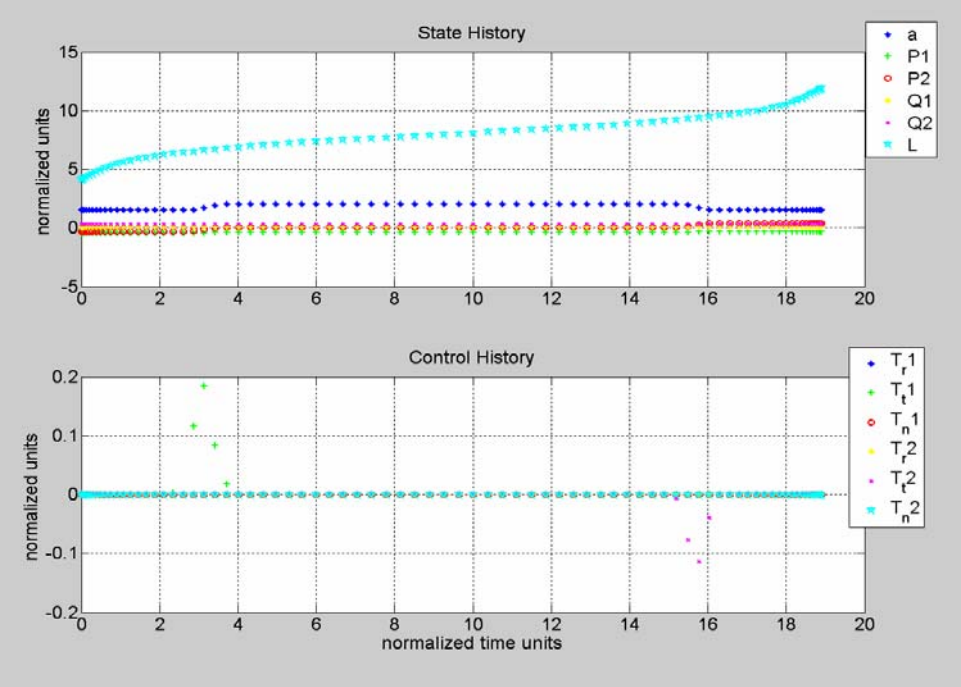

Figure 24 State and control histories for semimajor axis change

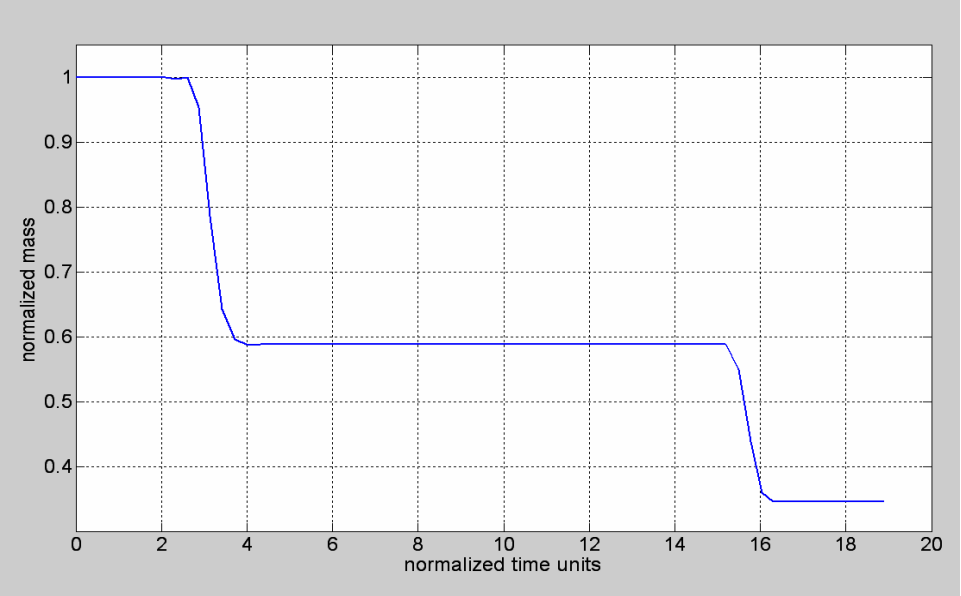

Figure 25 Mass flow for semimajor axis change

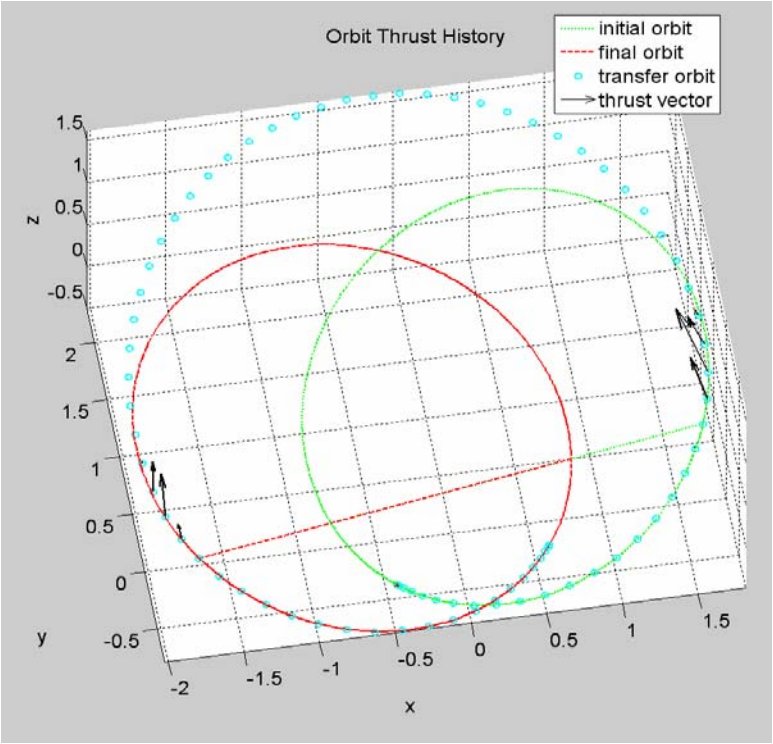

Figure 26 Semimajor axis change transfer orbit

3. Semimajor Axis Change Optimal Behavior

a. Semimajor Axis Change Feasibility

Feasibility was once again shown by independently propagating the initial conditions through the equations of motion using interpolated controls. A graphical representation of the result is shown as Figure 27. We can conclude that the result is within the feasible set of solutions.

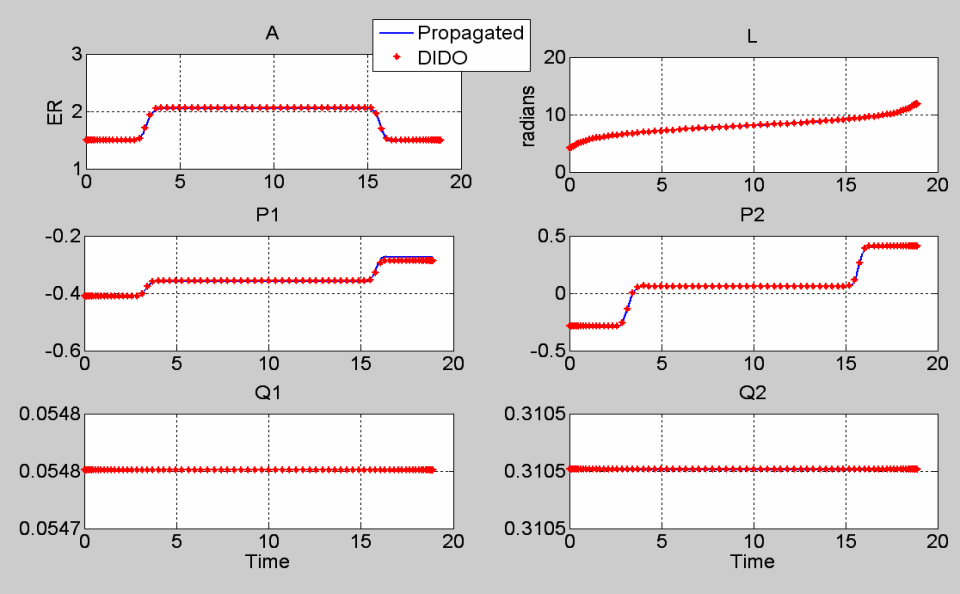

Figure 27 Plots of semimajor axis change model performance vs. ODE45 propagation

b. Semimajor Axis Change Hamiltonian Behavior

Graphical representation of the Hamiltonian during the performance period is shown as Figure 28. It can be noted that the Hamiltonian exhibits a near constant zero value for the majority of the run. By this test condition, we can conclude that optimal control is being performed.

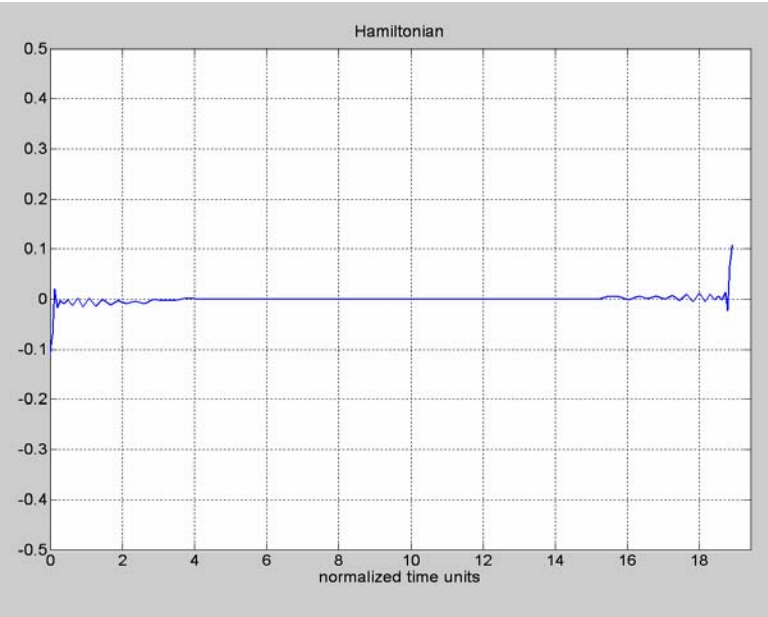

Figure 28 Hamiltonian behavior for semimajor axis change

c. Semimajor Axis Change Lagrangian Behavior

Graphical representation of the stationary Lagrangian during the performance period is shown as Figure 29 for all six controls. We again observe that the minimized Lagrangian exhibits a near zero value for the majority of the run. By this test condition, we can conclude that optimal control is being performed.

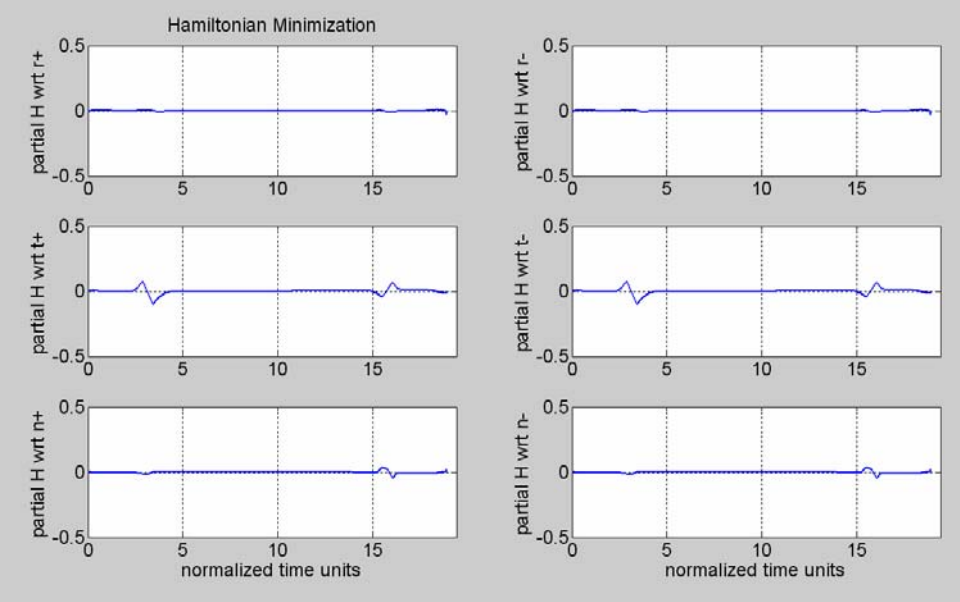

Figure 29 Semimajor axis change minimized Lagrangian behavior

d. Semimajor Axis Change KKT Complementarity Condition

Graphical representation of the switching structure for each of the control/dual pairs is shown as Figure 30. This switching generally follows the criteria described by equation (4.29), and therefore we can conclude that optimal control is being performed. It can be observed that the only controls being exercised are by the + and - t thrusters, T_{t1} and T_{t2}. Although not shown again, expansion of these plots again illustrates scaling and tolerance issues noted previously.

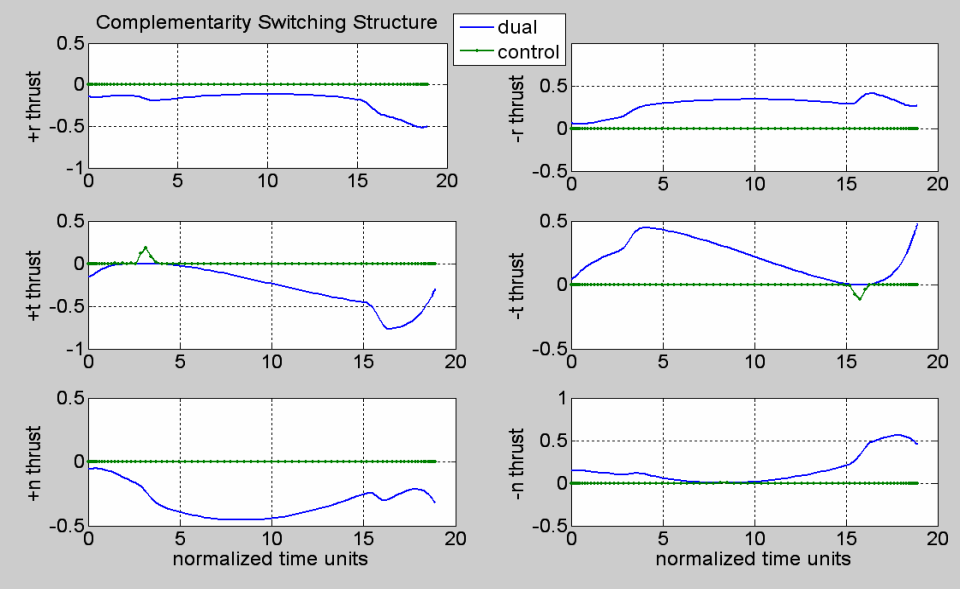

Figure 30 Switching behavior for semimajor axis change

4. Semimajor Axis Change Scenario Conclusions

Based on the results of this scenario, we can again conclude that optimal control is being performed. Although we have already shown this for a coplanar transfer through the Hohmann scenario, this scenario added complexities in non-zero eccentric orbits, and provided additional "feel good" data for the model against a known result.

The semimajor axis change actually has two known optimal solutions [Chobotov (2002)], one involving two burns as has been shown, and one involving a single impulsive burn at either the upper or lower intersection points of the initial and terminal orbits. It should be noted that given the right conditions, the model can also approximate the single burn maneuver. This solution is shown as Figure 31, and it meets all tests for feasibility and optimality. Again, it does not exactly match the classical impulsive maneuver, but resemblance to this maneuver is beginning to be achieved, and differences can be attributed to the particular constraints imposed.

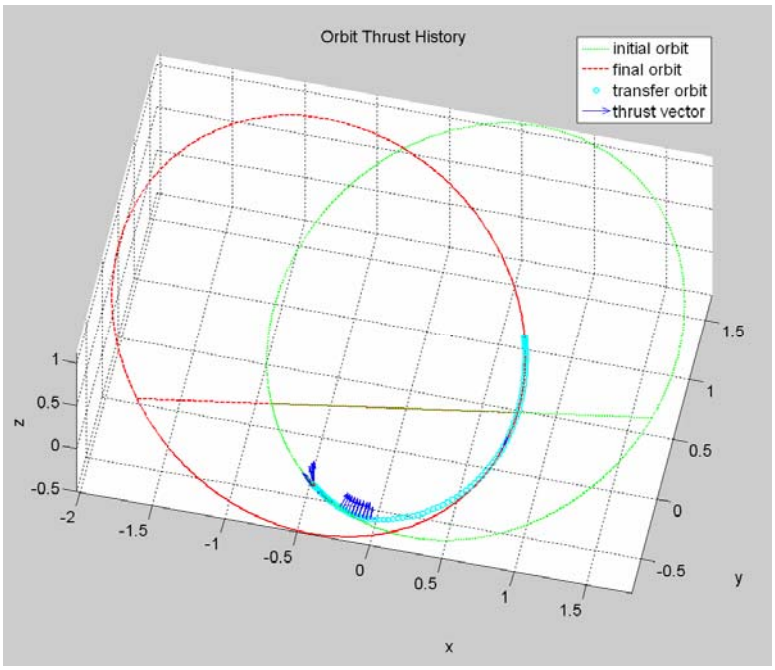

Figure 31 Single burn semimajor axis change maneuver

E. MINIMUM TIME TRANSFER SCENARIO

For the final validation, we decided to use the model to perform optimal controls for a minimum time problem. This involved some additional changes to the model parameters, since the other problems (and the ultimate aim of the research) all involve minimizing fuel. However, by using the model in a slightly different context, it was hoped that final validation of the equations of motion could be achieved independent of the type of application.

This problem was modeled to replicate a minimum time problem as reproduced in the text by Bryson (1999), but first documented by Moyer and Pinkham (1964).

1. Minimum Time Transfer Input Parameters

The first major change relative to previous validations was a difference in the cost functional. Since the goal of the minimum time problem is obviously to execute a maneuver in the minimum amount of time possible, fuel consumption was no longer to be considered an issue. The cost index was changed to reflect this, from final mass to final time.

The input parameters for this problem are based upon Bryson's textbook formulation (pp. 126-128). The unusual values of the numbers are to simulate the geometry of an Earth to Mars transfer as closely as possible, and therefore the initial constant values for the model as used previously were modified to simulate Bryson's numerical solution. The constant I_{sp} was changed to 492.4567 seconds to match Bryson's conditions for this problem. All other constants were left the same. It should be noted, since the problem as calculated is scaled to make the gravitational constant equal to 1.0, it is not necessary to change gravity to a sun centered system for this validation.

The Keplerian inputs, per Bryson, were provided as follows:

$$
\begin{aligned}
a_i &= 6378.1 \text{ km} & a_f &= 9718.2 \text{ km} \\
e_i &= 0.0 & e_f &= 0.0 \\
i_i &= 35 * \frac{\pi}{180} \text{ rad} & i_f &= 35 * \frac{\pi}{180} \text{ rad} \\
\Omega_{\mathrm{i}} &= 45 * \frac{\pi}{180} \text{ rad} & \Omega_{\mathrm{f}} &= 45 * \frac{\pi}{180} \text{ rad} \\
\omega_{\mathrm{i}} &= 45 * \frac{\pi}{180} \text{ rad} & \omega_{\mathrm{f}} &= 45 * \frac{\pi}{180} \text{ rad} \\
\nu_{\mathrm{i}} &= 0 * \frac{\pi}{180} \text{ rad} & \nu_{\mathrm{f}} &= 235 * \frac{\pi}{180} \text{ rad}
\end{aligned}
\qquad \textit{(5.6)}
$$

2. Minimum Time Transfer Performance

Given only the above end point conditions, and subject to the cost and dynamic equations, the following performance was recorded. Graphical representations of the state and control histories are shown as Figure 32. Mass flow rate is shown as Figure 33. A pictorial plot of orbital performance is shown as Figure 34. A 100 node run took approximately 122 seconds.

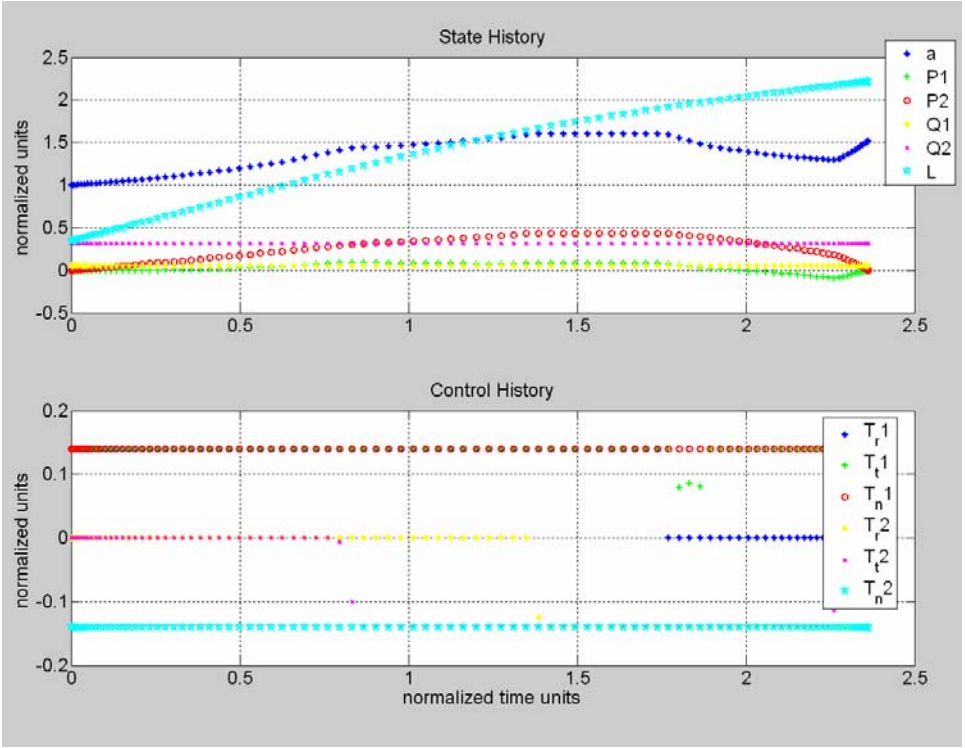

Figure 32 State and control histories for minimum time transfer

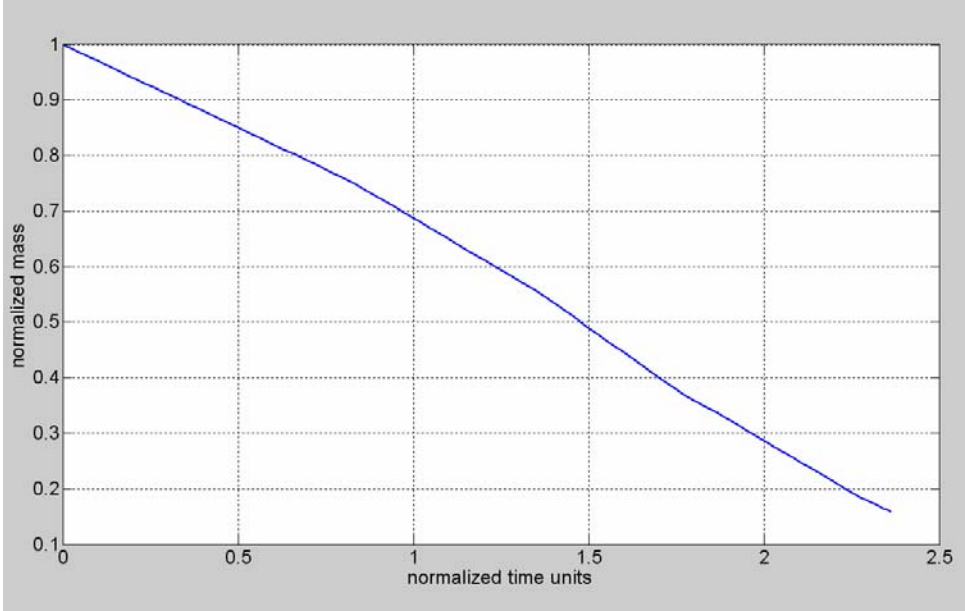

Figure 33 Minimum time transfer mass flow

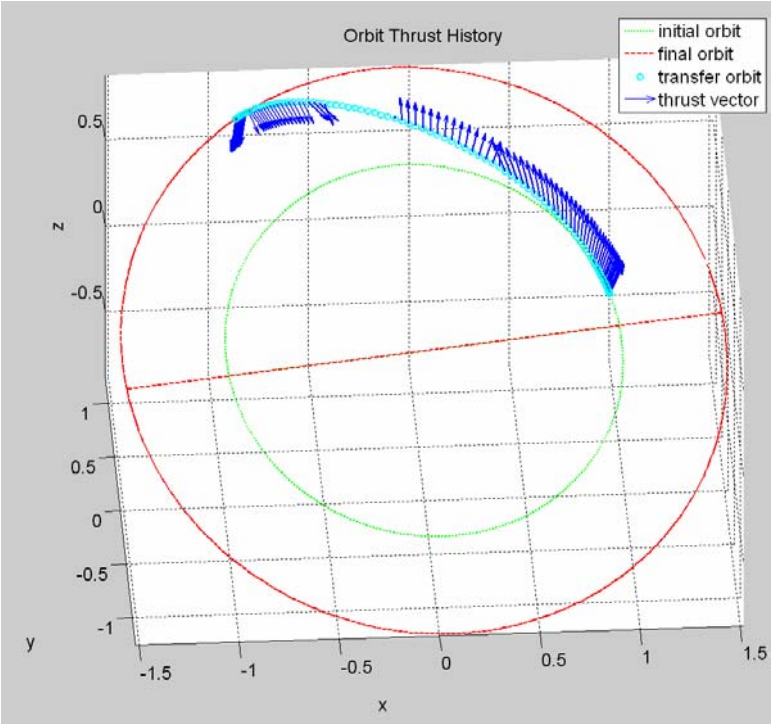

Figure 34 Minimum time transfer. Note period of zero net thrust

An important revelation was made through this performance. It can be readily observed that this behavior is similar in some respects to that documented by Bryson, but it can not be considered an extrapolated result as could the other validation scenarios. Although the thrusting profile appears to spiral similar to what is predicted by Bryson's work (Figure 34), a significant portion of the orbit transfer undergoes an unexpected period of zero net thrust. This is due a major difference between Bryson's model and ours, namely his model's use of a single gimbaled thruster with constant thrust vs. our six fixed thruster model. Still, intuition would have us believe that a constant thrusting profile would be necessary for a minimum time maneuver. This apparently troublesome point will turn out to be very significant, and will be discussed later in the section.

3. Minimum Time Transfer Optimal Behavior

a. Minimum Time Transfer Feasibility

Feasibility was once again shown by independently propagating the initial conditions through the equations of motion using interpolated controls. A graphical

representation of the result is shown as Figure 35. From this, we can conclude that the result is within the feasible set of optimal solutions.

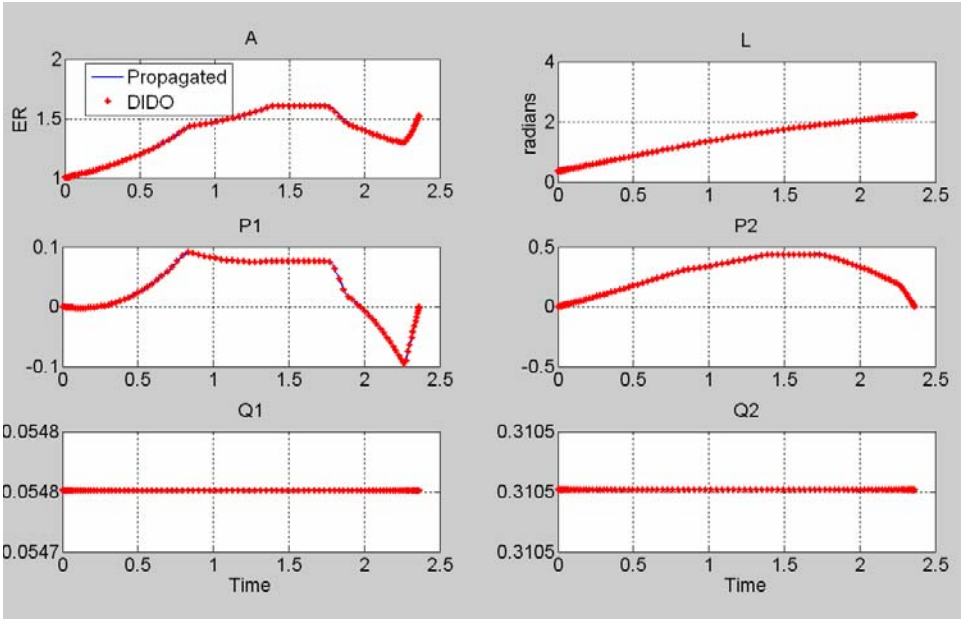

Figure 35 Plots of minimum time transfer model performance vs. ODE45 propagation

b. Minimum Time Transfer Hamiltonian Behavior

Graphical representation of the Hamiltonian during the performance period is shown as Figure 36. It can be noted that the Hamiltonian exhibits a near constant value for the majority of the run.

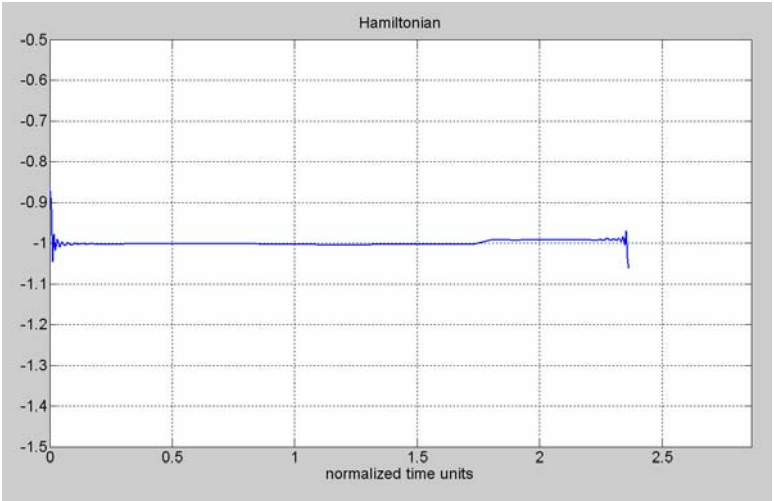

Figure 36 Hamiltonian behavior for minimum time transfer

It is observed that the constant value of the Hamiltonian for this case is -1 vs. the zero value observed for the minimum fuel scenarios. This can be expected by revisiting the Hamiltonian evolution and value condition, similar to the development carried out in equations (4.19) through (4.21). For the minimum time case, the Hamiltonian can be written as:

$$H = t_f + \lambda_a(\dot{a}) + \lambda_{P_1}(\dot{P}_1) + \lambda_{P_2}(\dot{P}_2) + \lambda_{Q_1}(\dot{Q}_1) + \lambda_{Q_2}(\dot{Q}_2) + \lambda_L(\dot{L}) + \lambda_M(\dot{M}) \qquad \textbf{(5.7)}$$

The Hamiltonian Evolution then indicates that a constant value must be maintained for optimality, because:

$$\frac{dH}{dt} = \frac{\partial H}{\partial t} = 0 \qquad \textbf{(5.8)}$$

The Hamiltonian Value condition can then be derived as:

$$H(t_f) = -\frac{\partial \overline{E}}{\partial t_f}$$
$$\overline{E} = E + \nu_i e_i = t_f + \nu_a e_a + \nu_{P_1} e_{P_1} + \nu_{P_2} e_{P_2} + \nu_{Q_1} e_{Q_1} + \nu_{Q_2} e_{Q_2} + \nu_L e_L + \nu_M e_M \qquad \textbf{(5.9)}$$
$$So:$$
$$H(t_f) = -\frac{\partial \overline{E}}{\partial t_f} = -1$$

Combining the Hamiltonian Value with the Hamiltonian Evolution indicates that a value of -1 must be maintained by the Hamiltonian during the optimal control span. By this test condition and our observations then, we can conclude that optimal control is being performed during this scenario.

c. Minimum Time Transfer Lagrangian Behavior

Graphical representation of the stationary Lagrangian during the performance period is shown as Figure 37 for all six controls. We again observe that the stationary Lagrangian exhibits a near zero value for the majority of the run. This particular scenario appears to exhibit some difficulty maintaining optimal control at

periods in the vicinity of the large spiral direction shift where thrust is momentarily directed in a non-optimal manner, however optimality is quickly regained. By this test condition, we can conclude that optimal control is being performed for the majority of the run.

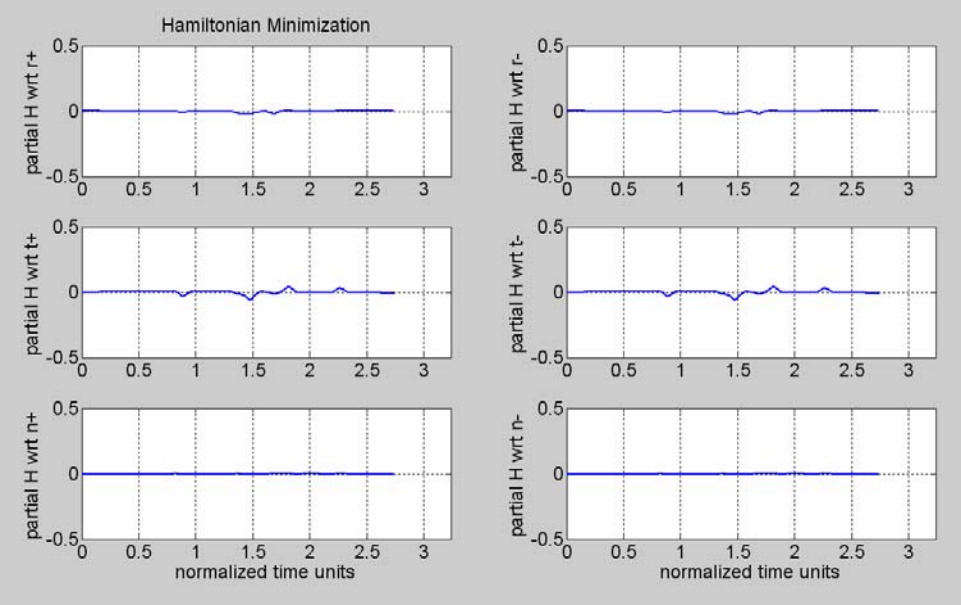

Figure 37 Minimum time transfer minimized Lagrangian behavior

d. Minimum Time Transfer KKT Complementarity Condition

Graphical representation of the switching structure for each of the control/dual pairs is shown as Figure 38. This switching follows the criteria described by equation (4.29), and therefore we can conclude that optimal control is being performed. A detailed view of this switching on a tighter scale for two of the controls (Figure 39) indicates that bang-bang control is clearly achieved. This is the type of result sought but not observed earlier in the minimum fuel scenarios. We can note in this case that the costate does not remain near zero, but instead passes cleanly and quickly through the zero crossing, offering some credence to the scaling and tolerance issues noted earlier.

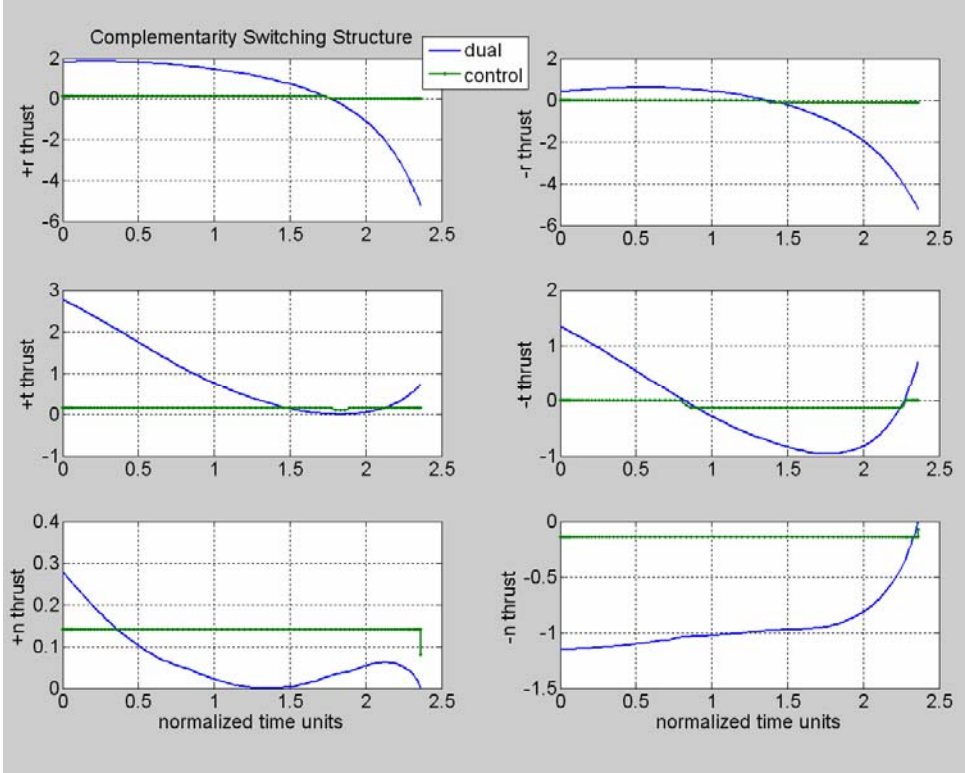

Figure 38 Switching structure for minimum time transfer

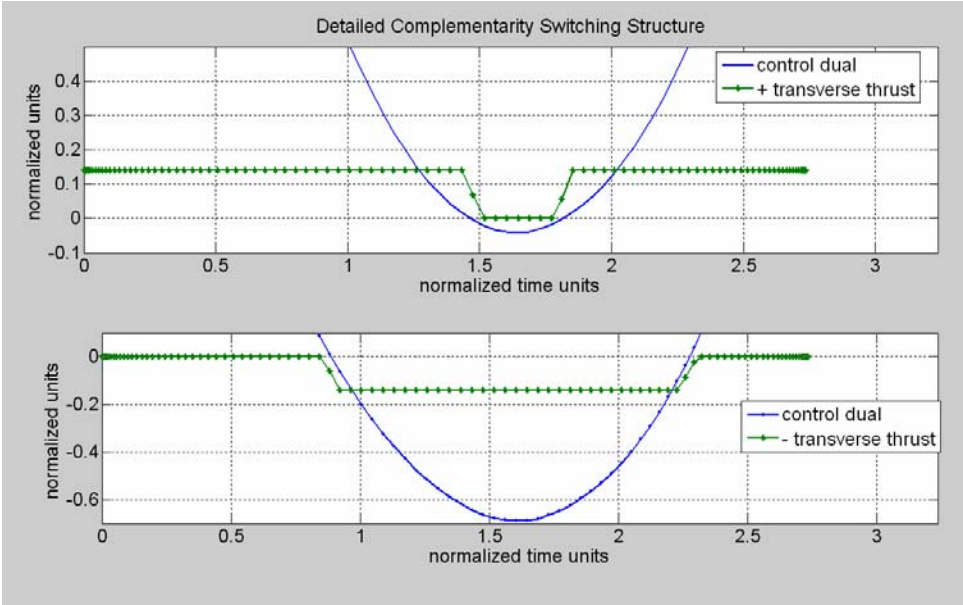

Figure 39 Switching detail for minimum time transfer, T_{t1} and T_{t2}

4. Minimum Time Transfer Scenario Conclusions

From the observations of the preceding sections, we can again conclude that optimal control is being performed. However, as we have noted previously, the thrusting profile of the maneuver does not instantly meet our intuitive expectations. Despite this initial observation, upon closer inspection and analysis we find that the model is actually performing remarkably.

We have already drawn attention to the period of zero net thrust observed in the plot shown in Figure 34. This was unexpected based on what we were predisposed to look for based on Bryson's work. However, the difference between six thrusters and one (as modeled in Bryson's text) turns out to be more surprising than we would believe. If we look closer at the control history shown in Figure 32, we now note two subtle characteristics. First, the positive and negative normal thrusters are firing at maximum capacity, equal in magnitude and opposite in direction, for the duration of the scenario. The net effect of these firings is zero net thrust out of the orbital plane. Second, during a short period of time during the scenario (approximately TU 1.4 – 1.7), all thrusters are firing at maximum capacity, with each pair equal in magnitude and opposite in direction, resulting in zero net thrust during that short period.

The reason for this behavior is explained simply: the model is predicting that optimal control to achieve a minimum time maneuver given the provided end point conditions (including the initial fuel load) is to spend energy on zero net thrust maneuvers in order to *dump fuel*. By doing so, the satellite lightens its mass in order to achieve the maximum acceleration possible, an obvious tactic for any maximum speed maneuver. The model calculates how much fuel it needs to perform the maneuver, and offloads the rest in order to speed up execution.

We can challenge this assertion by commanding the normal thrusters off for the duration of the scenario, leaving all other conditions the same (note: this scenario meets all feasibility and optimality tests as provided previously, but are not shown here for brevity). By doing this, we can observe in Figure 40 that the transfer takes more time to execute (2.739 TU vs. 2.365 with normal thrusters on). This result validates that fuel dumping provides for a faster time solution. It is also observed that the system is firing in

plane throughout the profile, and does not go through a period of full fuel dump (Figure 41), more consistent with Bryson's result[5]. The time of the switch from positive radial to negative radial still does not quite match the Bryson profile (which occurs symmetrically at the transfer halfway point), offering further insight into the differences between one thruster and effectively four for this case. This appears to be a manifestation of the difference between an l^2 norm based model and our l^1 norm based model in associated mass flow rate characteristics [see Ross (2004)].

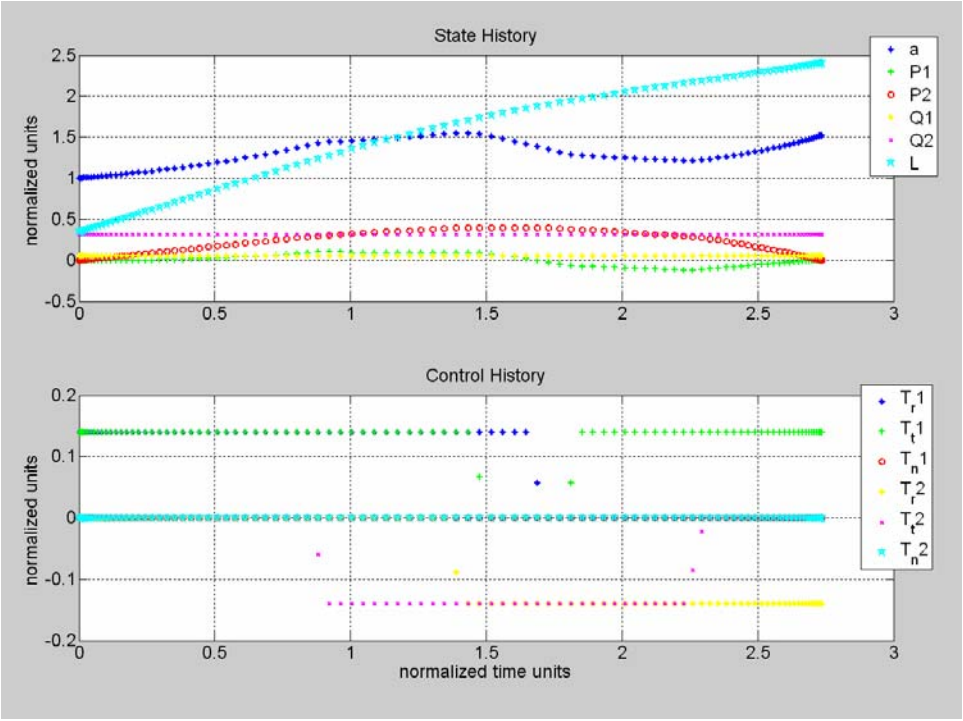

Figure 40 State and control history for minimum time transfer (normal thrusters disabled)

[5] However, if we increase the starting mass of the vehicle, fuel dumping again occurs. The lack of fuel dumping in this case is most likely due to the use of input values scaled from the numerical results reported by Bryson.

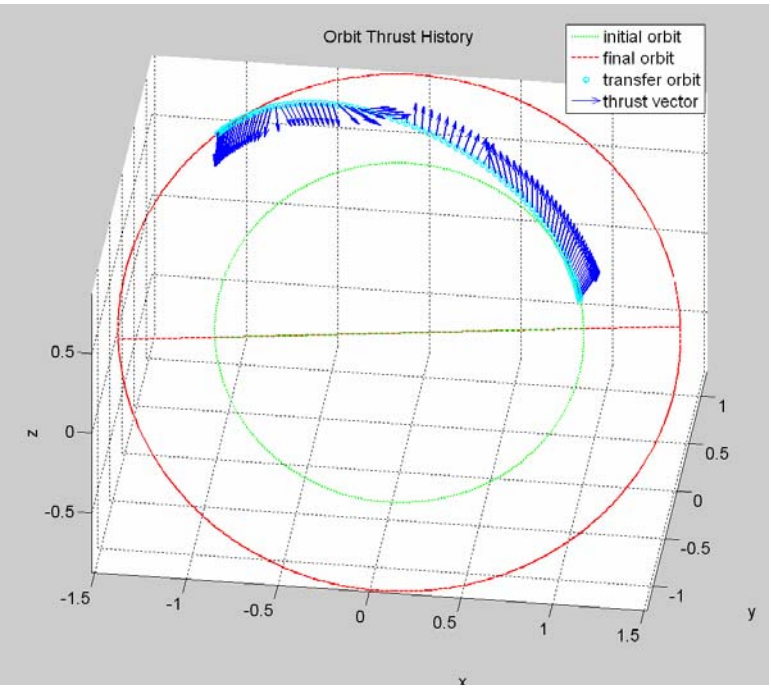

Figure 41 Minimum time transfer (normal thrusters disabled)

Overall, minimum time performance and its unexpected controlled fuel burn is the final validation of the equations of motion and of the coding of the model. The observed behavior transcends the theoretical mathematics of the model formulations and crosses into predictable physics behavior. For this reason, it is believed this scenario provides final proof that the model is working as it should, and we are ready to move on to proving our initial goal: a multi-agent system.

F. CONCLUSIONS

Through the scenarios shown in this section, it is believed that the dynamic equations of motion used and the coding of the MATLAB™ model have been validated. The model is ready to perform complex three dimensional maneuvers which can be trusted as accurate, and optimal behavior can be demonstrated by observing and following the tenets of the Minimum Principle. Complex control scenarios can be input and results observed following the documented methods, and optimal control predictions can be made within the range of feasible solutions for any desired transfer. A representative complex control result is shown as Figure 42, with changes made to all six Keplerian elements between the initial and final conditions. This scenario as run again

meets all feasibility and optimality tests, although the details are not shown for sake of brevity. By using this methodology as a baseline, it is hoped that multiple simultaneous scenarios can be run and predicted for optimal control.

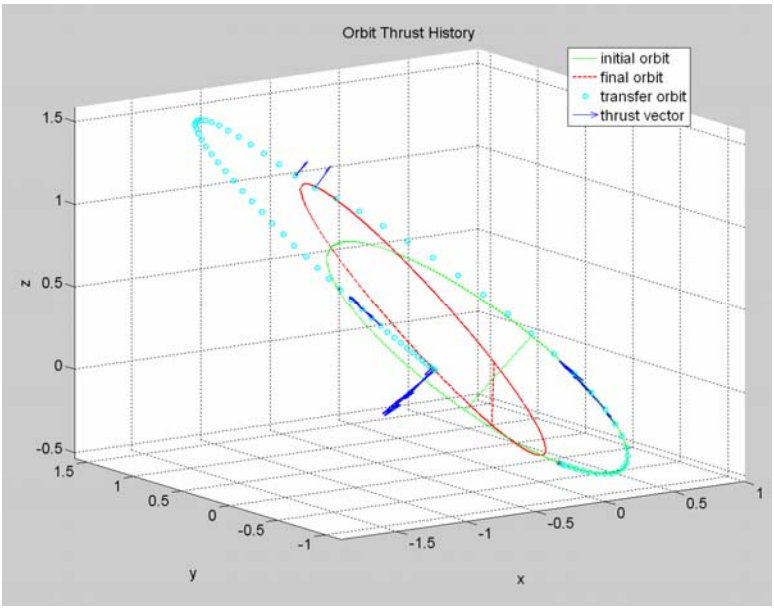

Figure 42 Complex orbit transfer, all classical elements modified

THIS PAGE INTENTIONALLY LEFT BLANK

VI. MULTI-AGENT CONTROL

Having validated behavior of the orbital model for three dimensional motion, the next step is to modify it for processing multiple agents. The primary goal of this research was to prove that this could be done by effectively replicating a validated single satellite problem so that multiple agents could be solved simultaneously. The simultaneous distinction is important, since relationships can exist between satellites which complicate matters tremendously if performed in a serial and iterative fashion.

The term "agent" is used generically to refer to the body being optimized. For this research, an agent can be considered synonymous with a satellite, and the terms will be used interchangeably within this context.

A. MODEL MODIFICATIONS

In order to modify the model to process multiple simultaneous satellites, a careful act of replication had to be carried out. Far from a simple copy and paste exercise, great care was maintained in instilling multiple sets of similar variables into the new version. Certain variables, constants, and subroutines were used universally for all agents, while others were maintained as agent specific. However, once this process was carried out, it turned out to be the most difficult part of the leap from single agent to multi agent problems.

A new consideration in multi-agent problems is establishing relationships between agents. This is necessary to define certain conditions which the user would like to maintain. Foremost is collision avoidance: by establishing a minimum safe distance between satellites, the model can programmed so that two bodies cannot occupy the same space at the same time. Similarly, a maximum distance can be established. By using the two together, a relative operating window can be created for the purpose of establishing formation patterns.

Another new consideration for multi-agent problems is establishing a new performance index which considers all satellites. Again, for this research minimum fuel

is the driving consideration, and the new Bolza cost used is the simple combined maximized final masses of the agents (that is, $J = - M_{1f} - M_{2f}$).

A third consideration for multi-agent problems is that care must be taken not to overconstrain the solution. This will be discussed in greater detail following initial demonstration of the model, which will help understanding of the issue at hand.

B. TWO-AGENT MODEL

To demonstrate proof of the multi-agent concept, the validated single-agent model was replicated and coded to create a two-agent version. This section documents the performance of that model following the same development and proof used in the validation chapter.

The demonstration of this model will be carried out using a previously discussed validation case using all three dimensions. The two satellites modeled will be assumed to be launched on a common launch vehicle, then undergo equal and opposite orbit raise and inclination change. Because the model must consider safe separation distance between vehicles, the starting separation distance for the two vehicles will be considered shortly after tipoff from the final launch stage.

Initial constants for the model will also be maintained as before, with the exception that they now need to be replicated for each vehicle. That is to say:

$$\begin{aligned} &I_{sp1} = I_{sp2} = 220 \text{ s} \\ &g_{01} = g_{02} = 0.00981 \text{ km/s}^2 \\ &v_{e1} = v_{e2} = I_{sp(1/2)} * g_{0(1/2)} = 3.1392 \text{ km/s} \\ &T_{max1} = T_{max2} = 10 \text{ N} \\ &\mu_{01} = \mu_{02} = 398600.4415 \text{ km}^3 / s^2 \\ &M_{01} = M_{02} = 3000 \text{ kg} \end{aligned} \qquad \textit{(6.1)}$$

It is important to note that generally speaking these values do not all have to be equal for both vehicles. The gravitational acceleration constant will always be 9.81 m/s^2 for all vehicles since that is a propulsion system related constant that is based on Earthbound testing and definition of the thrusters [Sutton and Biblarz (2001)], and therefore will never vary regardless of the system under consideration (provided , of

course, that these thrusters are manufactured on the Earth). The gravitational parameter μ is not required to be equal for all agents; however, it will in all likelihood be equal for most practical applications. All other constants can vary between vehicles, and the model has capacity for these situations[6].

1. Two-Agent Input Parameters

For the two-agent model, two sets of initial and final conditions must be considered. Following the verification cases in chapter V, these parameters are as follows:

a. Agent 1 (Positive Inclination Change)

The maneuver by satellite 1 can be considered much like a combination between a Hohmann transfer and an inclination change. The initial and final boundary condition inputs to the model are as follows:

$$
\begin{aligned}
a_{i1} &= 9567.2 \text{ km} & a_{f1} &= 9567.2 \text{ km} \\
e_{i1} &= 0.0 & e_{f1} &= 0.0 \\
i_{i1} &= 35 * \frac{\pi}{180} \text{ rad} & i_{f1} &= 55 * \frac{\pi}{180} \text{ rad} \\
\Omega_{i1} &= 10 * \frac{\pi}{180} \text{ rad} & \Omega_{f1} &= 10 * \frac{\pi}{180} \text{ rad} \\
\omega_{i1} &= 225 * \frac{\pi}{180} \text{ rad} & \omega_{f1} &= 225 * \frac{\pi}{180} \text{ rad} \\
\nu_{i1} &= 0 * \frac{\pi}{180} \text{ rad} & \nu_{f1} &= 200 * \frac{\pi}{180} \text{ rad}
\end{aligned}
\qquad \textbf{(6.2)}
$$

b. Agent 2 (Negative Inclination Change)

The second agent inputs are identical to the equations in (6.2), with the exception that the final inclination changes -20˚ rather than +20˚. Additionally, the initial

[6] Further, the model has some limited capacity to deal with differences in thrust between thrusters on the same vehicle, coded as an efficiency factor constant that can be independently set for each thruster. For this thesis, however, the efficiency setting will be left at 100% of the maximum available thrust.

true anomaly is slightly different that for satellite 1 for the purpose starting at a safe keepaway distance for collision avoidance.

$$
\begin{aligned}
a_{i1} &= 9567.20445 \text{ km} = 1.5 \text{ RE} & a_{f1} &= 9567.20445 \text{ km} = 2.0 \text{ RE} \\
e_{i1} &= 0.0 & e_{f1} &= 0.0 \\
i_{i1} &= 35 * \frac{\pi}{180} \text{ rad} & i_{f1} &= 15 * \frac{\pi}{180} \text{ rad} \\
\Omega_{i1} &= 10 * \frac{\pi}{180} \text{ rad} & \Omega_{f1} &= 10 * \frac{\pi}{180} \text{ rad} \\
\omega_{i1} &= 225 * \frac{\pi}{180} \text{ rad} & \omega_{f1} &= 225 * \frac{\pi}{180} \text{ rad} \\
\nu_{i1} &= .1 * \frac{\pi}{180} \text{ rad} & \nu_{f1} &= 200 * \frac{\pi}{180} \text{ rad}
\end{aligned}
\qquad \textit{(6.3)}
$$

2. Two-Agent Model Performance

State and control history for satellite 1 (performing the positive inclination change) is shown in Figure 43. History for satellite 2 (performing the negative inclination change) is shown in Figure 44. Mass flow for both satellites is shown in Figure 45. Orbital performance for both vehicles is shown in Figure 46.

It can be observed that the two independent satellites closely follow results demonstrated during the model validation for a Hohmann transfer combined with an out of plane inclination change maneuver. The individual maneuvers are performed as we would expect from previous maneuvers, with thruster firings occurring at perigee and apogee tangent points, as well as at the nodal line for inclination change.

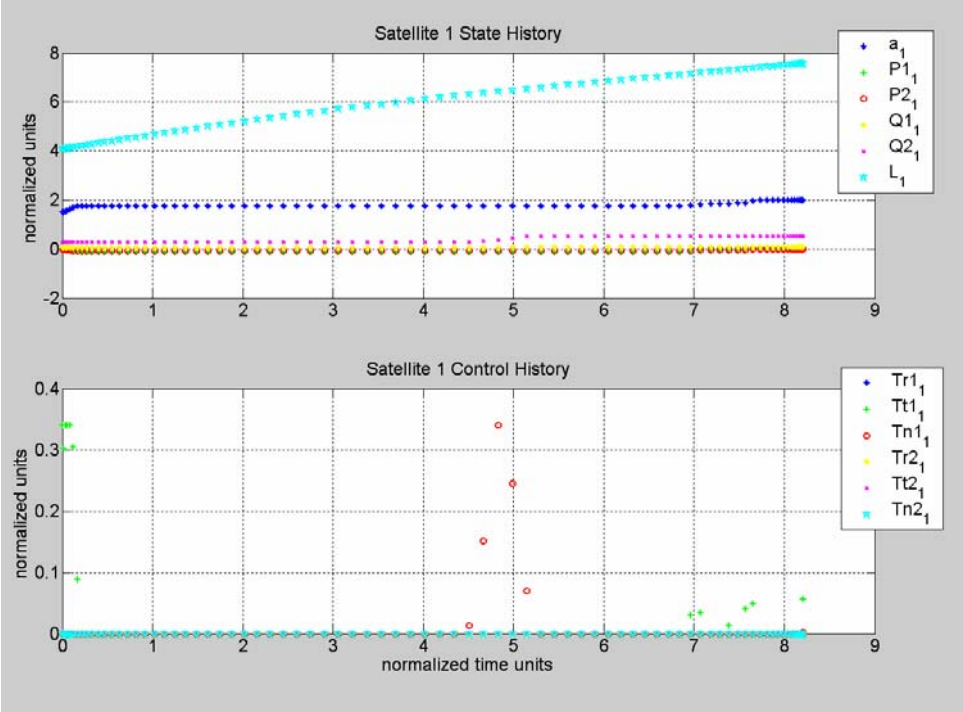

Figure 43 Satellite 1 state and control histories

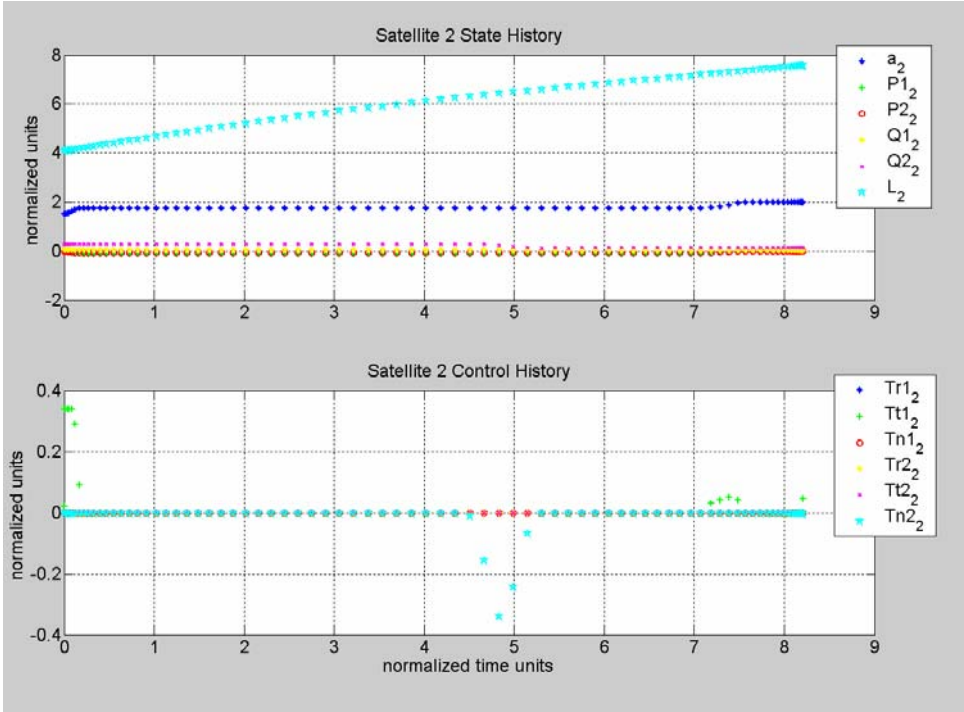

Figure 44 Satellite 2 state and control histories

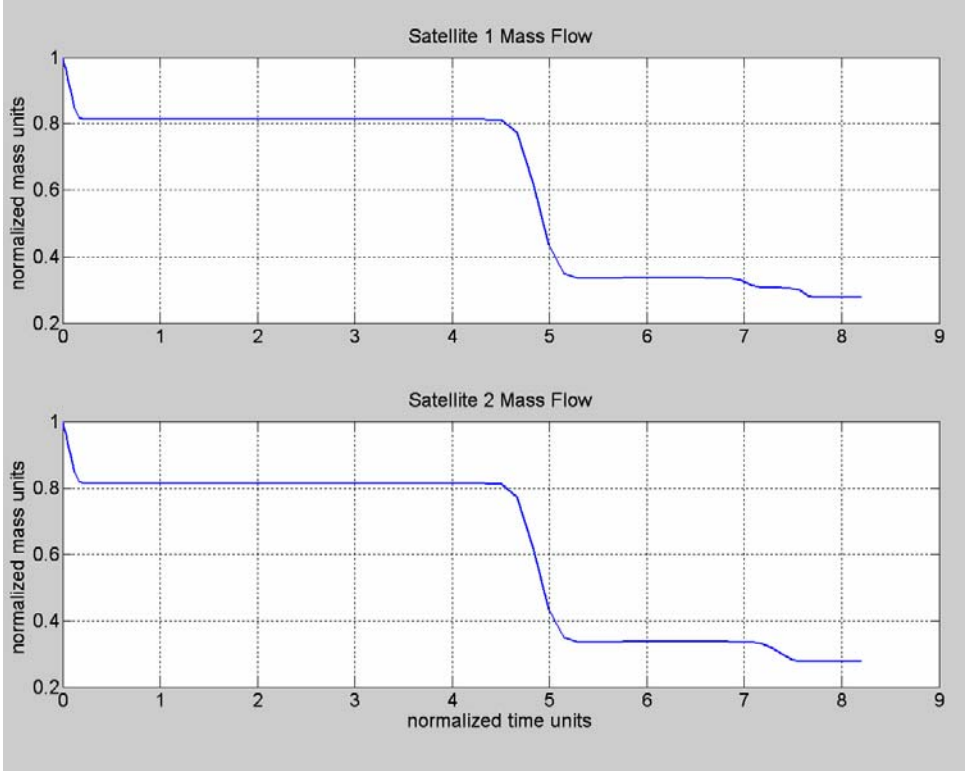

Figure 45 Satellite 1 and 2 mass flow

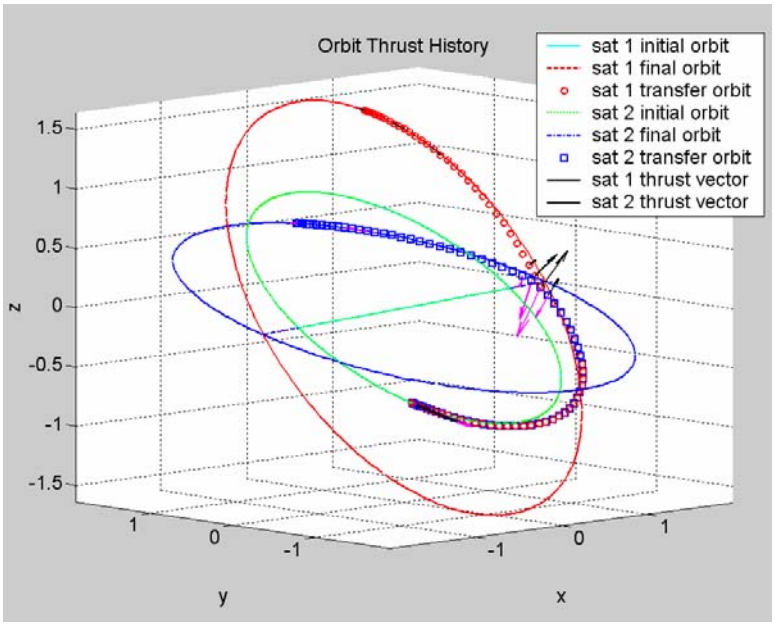

Figure 46 Two satellite orbit transfer with inclination change

3. Two-Agent Model Optimal Behavior

a. Agent 1 Feasibility and Optimality Analysis

Similar to the methods shown during validation, feasibility and optimality for satellite 1 are shown below. Feasibility is shown by Figure 47. Hamiltonian behavior is shown in Figure 48. The minimized Hamiltonian with respect to controls is shown as Figure 49. Switching behavior for satellite 1 is shown as Figure 50 (note tolerance issues once again). Observing this data and using the same logic provided during validation, it can be concluded that satellite 1 is demonstrating optimal control.

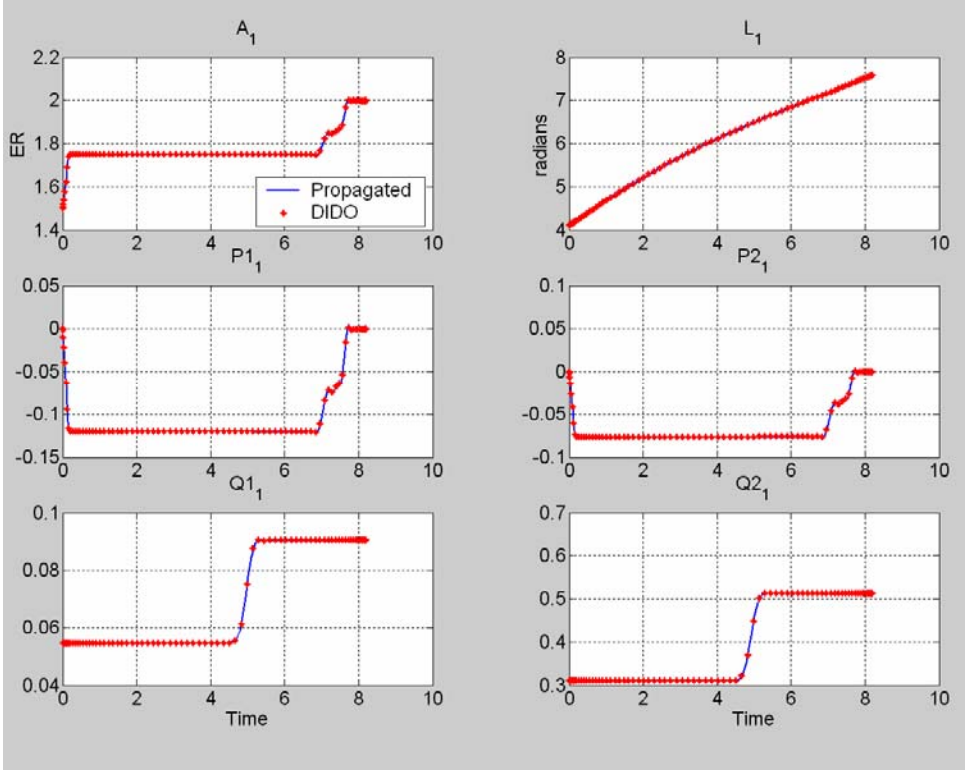

Figure 47 Plots of satellite 1 performance vs. ODE45 propagation

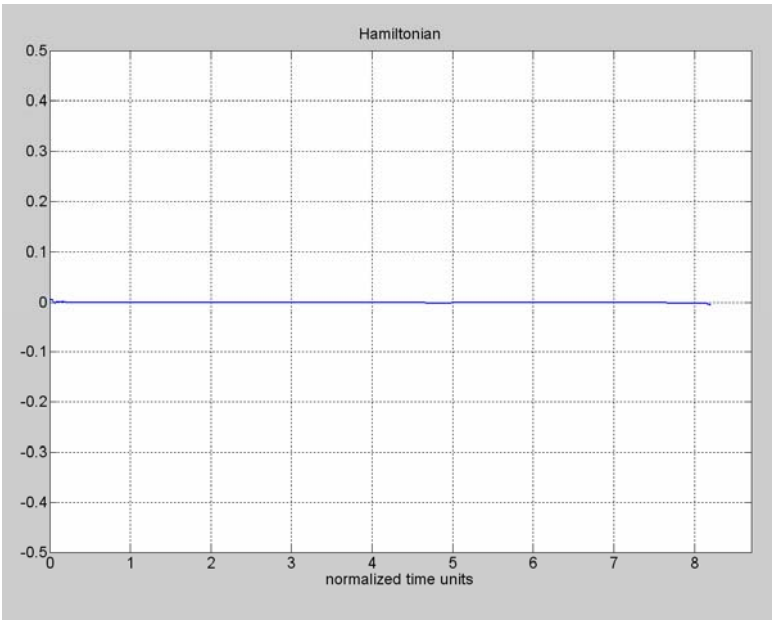

Figure 48 Multi-agent Hamiltonian behavior (both satellites)

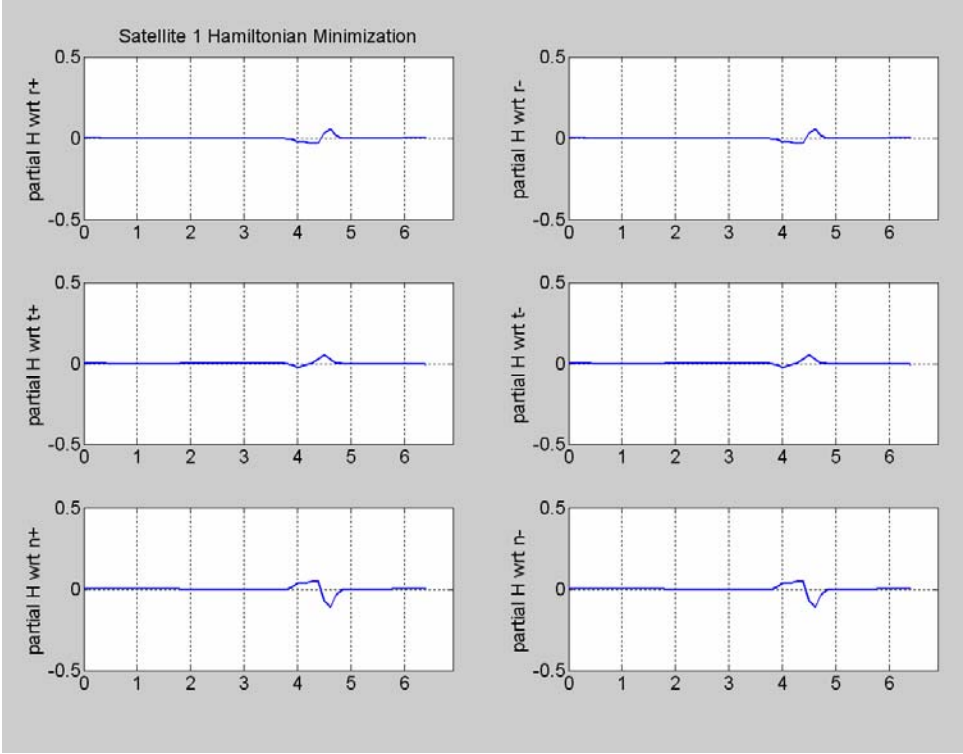

Figure 49 Satellite 1 minimized Lagrangian behavior

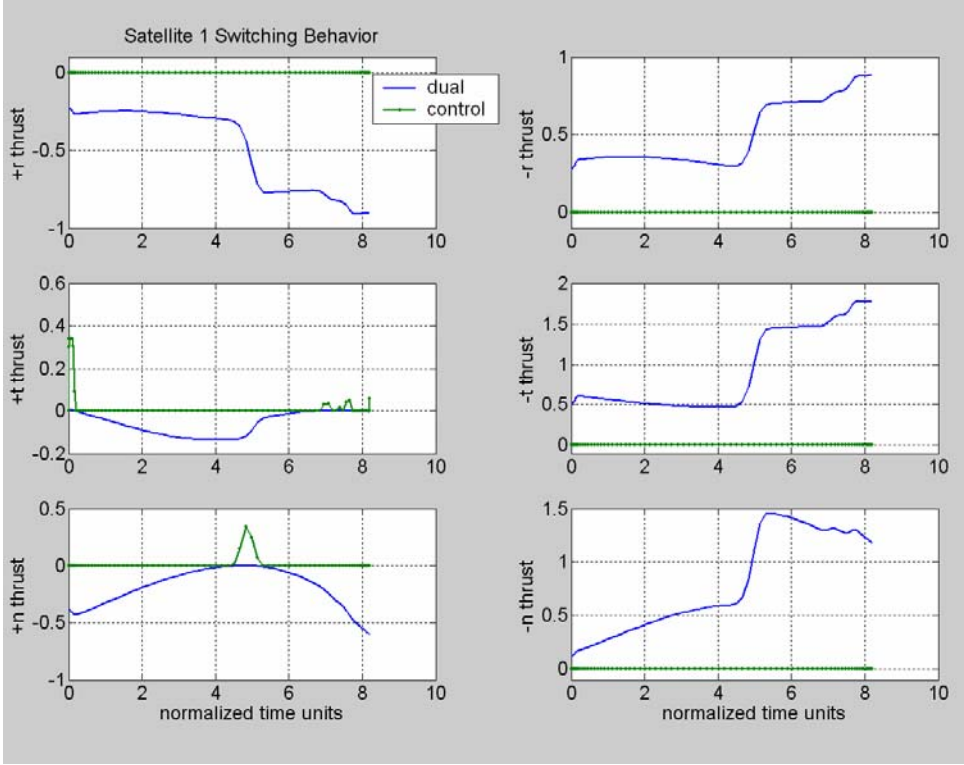

Figure 50 Switching structure for satellite 1

b. Agent 2 Feasibility and Optimality Analysis

Similar to satellite 1, feasibility and optimality for satellite 2 are shown below. Feasibility is shown by Figure 51. Hamiltonian behavior is shown in Figure 48. This is the same plot as for satellite 1, since a single Hamiltonian represents the entire multi-agent problem. The minimized Hamiltonian with respect to controls is shown as Figure 52. Switching behavior for satellite 1 is shown as Figure 53 (again observing scaling and tolerance). Observing this data and using the same logic provided during validation, it can be concluded that satellite 2 is demonstrating optimal control.

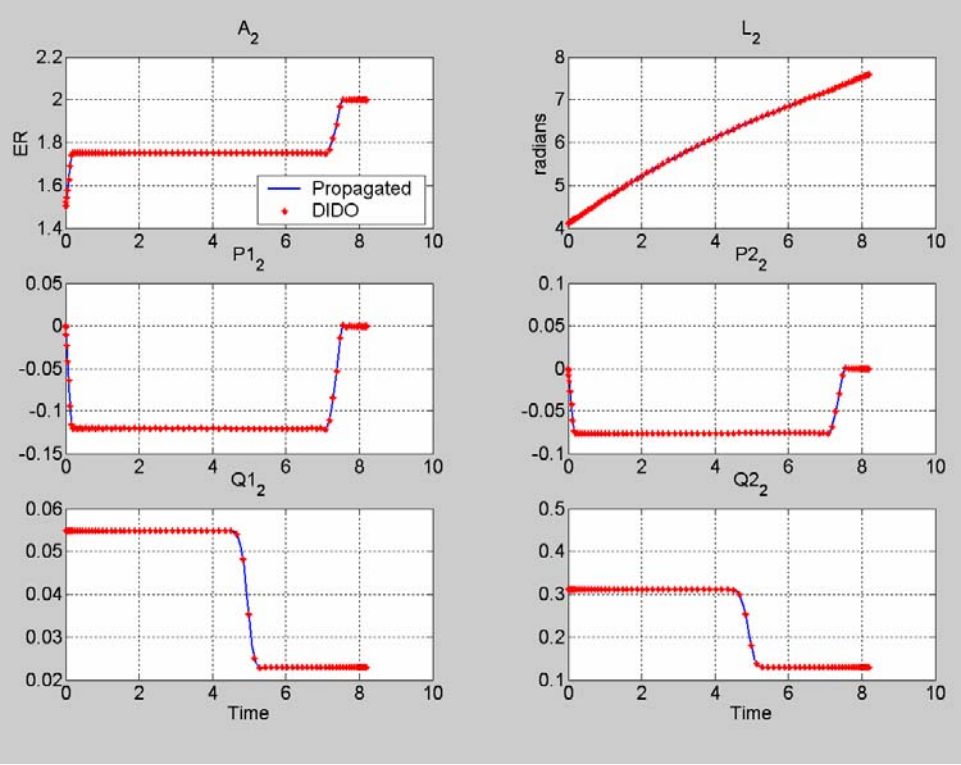

Figure 51 Plots of satellite 2 performance vs. ODE45 propagation

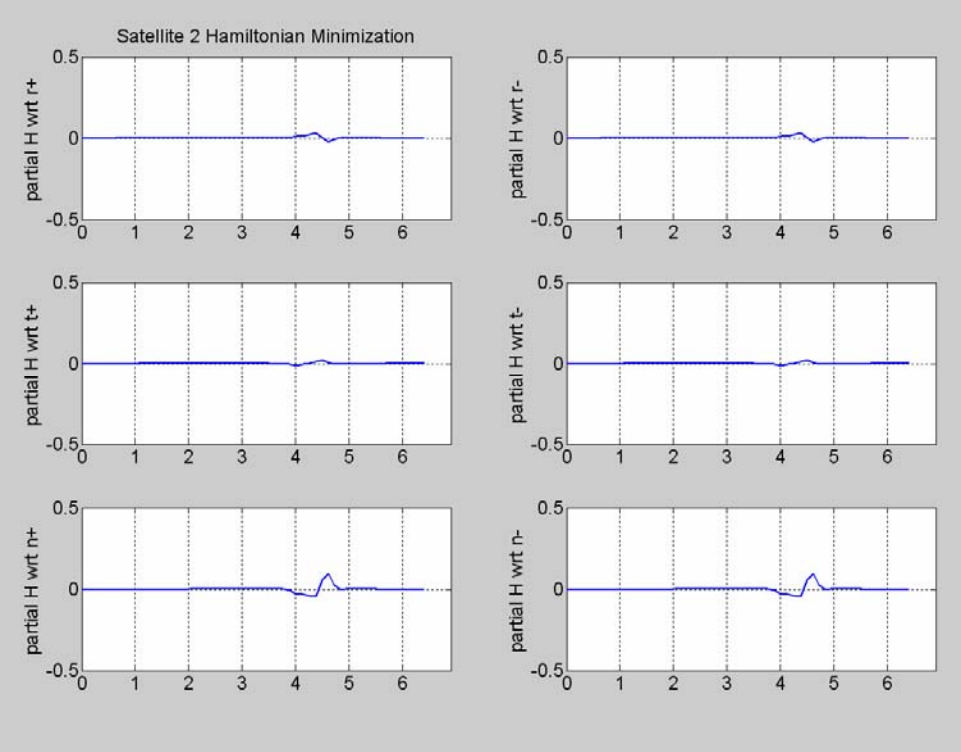
Satellite 2 Hamiltonian Minimization
partial H wrt r+
partial H wrt r-
partial H wrt t+
partial H wrt t-
partial H wrt n+
partial H wrt n-

Figure 52 Satellite 2 minimized Lagrangian behavior

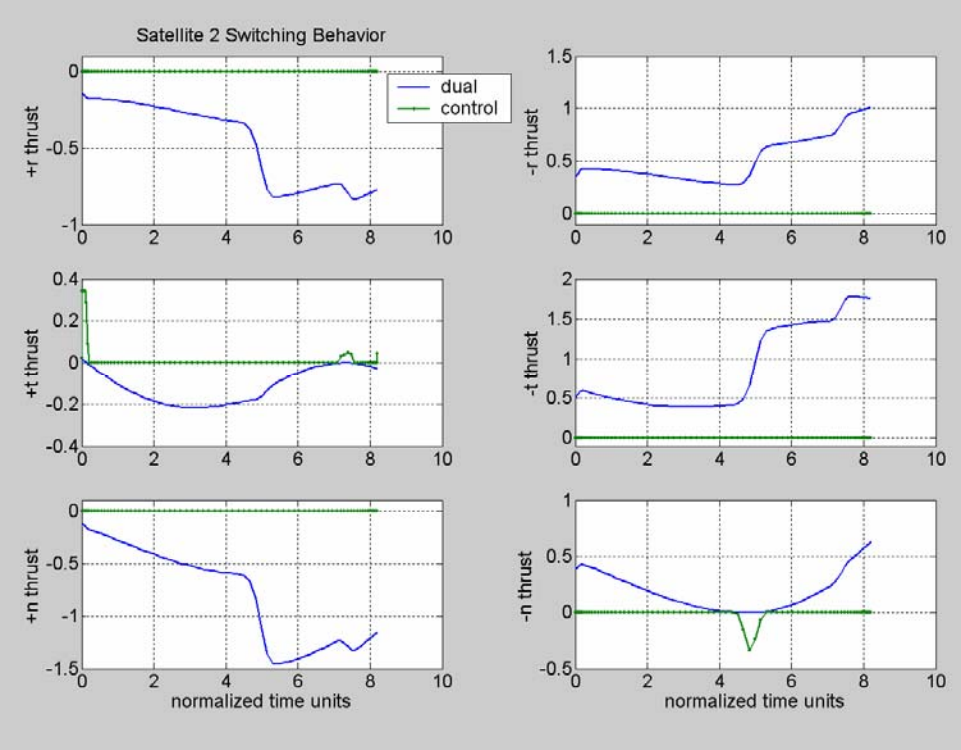

Figure 53 Switching structure for satellite 2

4. Two-Agent Model Overconstraint Issue

As performed, the two agent model appears to provide accurate prediction of optimal behavior. The individual satellites behave the same as they do would in a single satellite model, and defined inter-agent relationships appear to be maintained as desired. This scenario helps fulfill the goal of our research, and following the work performed in formulating and validating the problem seems rather anticlimactic. However, at least one point here bears visitation.

This scenario was largely symmetric, and because of this both satellites were able to finish in their final required positions at the same time. However, this is not necessarily true if "mirror image" cases are not requested for the two satellites. If concurrent solutions are possible, a feasible locally optimal solution may be found that meets the criteria required (i.e., an overconstrained solution), but is not the best or most fuel-efficient solution possible if constraints were relaxed. This is the equivalent to providing a good answer to a bad question.

As an example, a scenario was run requesting satellite 1 to perform an inclination change only (maintaining the initial orbital radius), and satellite 2 to perform a Hohmann transfer. All constraining end conditions were maintained similar to the double inclination case. Phasing of the two satellites within their respective final orbits was requested to be the same (200°), however since satellite 2 terminates in a higher orbit, it requires a greater amount of time to get there. Performance of this maneuvering is shown as Figure 54, and all tests for feasibility and optimality are met (but not shown for brevity).

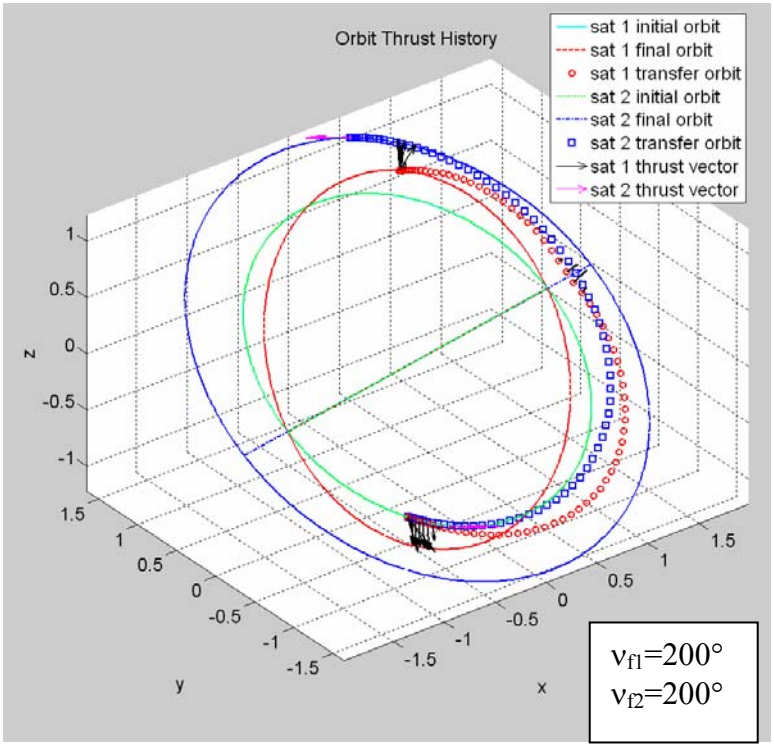

Figure 54 Multi-agent maneuver involving time constraint difficulty. Note satellite 1 orbit raise to loiter.

It can be observed that with the discussed overconstraint present, the optimal solution resulted in satellite 1 raising its orbit some to in effect "loiter" and allow satellite 2 time to reach its final position, at which time satellite 1 returns to its lower orbit to reach its final position at the same time. This does not match what intuitively makes sense to us, whereby satellite 1 would remain at the same altitude throughout the maneuver and change inclination at the node, much like the inclination change validation case discussed in chapter V. The demonstrated maneuver appears comparatively

wasteful of fuel, and is referred to it as a "false positive", however it needs to be noted that the requirement that both satellites reach their final locations at the same time drives this result, and that this is in fact the optimal solution meeting these requirements (again, a great answer to a bad question).

A solution to this issue is to constrain only one of the vehicles to a final achieved position, leaving the other to reach all orbital conditions required except for phasing. Instead, the second agent is allowed to phase itself in its orbit wherever it can while achieving all other conditions, including orbit and required operating distance with respect to satellite 1. In this way, a kind of "master/slave" relationship between the vehicles is implied, whereby satellite 1 dictates to some degree the final positioning of the constellation. But even this is not enough to avoid all problems, for some care must be taken in this case to allow enough time for satellite 2 to perform its necessary maneuvering, or else another less fuel efficient maneuver may occur. For example, using the same model (sat 1: inclination change; sat 2: Hohmann transfer) if satellite 1 is again allowed a phase change of 200° to perform its inclination change, and satellite 2 is to perform a Hohmann transfer, it can be observed that enough time is still not being allowed for this transfer to occur, and therefore another solution to the problem will be found which is less fuel efficient (but meeting the conditions requested) (Figure 55). This is because a Hohmann transfer must undergo a 180° in-plane phase shift in addition to a radial change, which requires more time to execute than does satellite 1's maneuver. Since final position is tied to satellite 1 (the "master") reaching 200°, and in this time satellite 2 only shifts 163.4˚, satellite 2 must expend additional fuel at both ends of the transfer to reach its proper orbit within the allotted time. We can fix this discrepancy by either setting a larger phase change for satellite 1 which allows satellite 2 to complete a 180° maneuver (Figure 56), or by setting the vehicle with the longer execution time as the master vehicle (Figure 57). The net fuel consumed is the same for both cases.

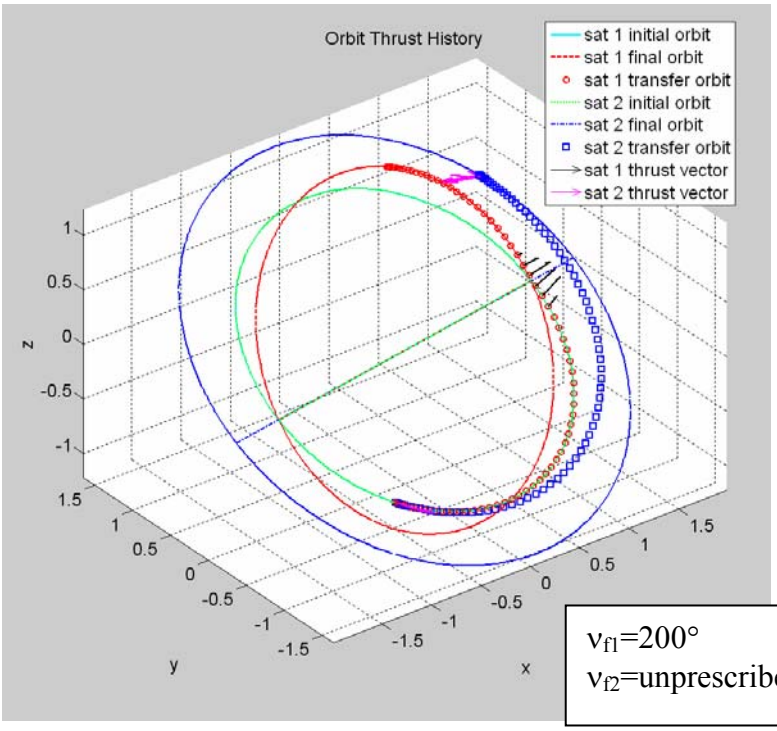

Figure 55 ***Satellite 2 (slave) not provided adequate time to perform Hohmann transfer, resulting in radial thrusting to meet final orbit***

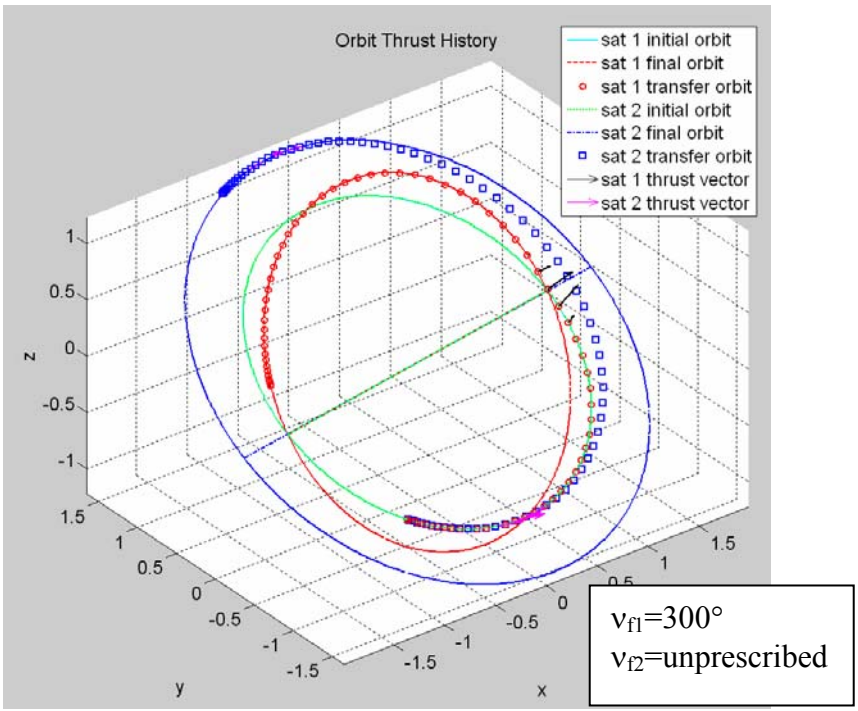

Figure 56 ***Satellite 1 (master) given longer execution time to facilitate Hohmann transfer by satellite 2***

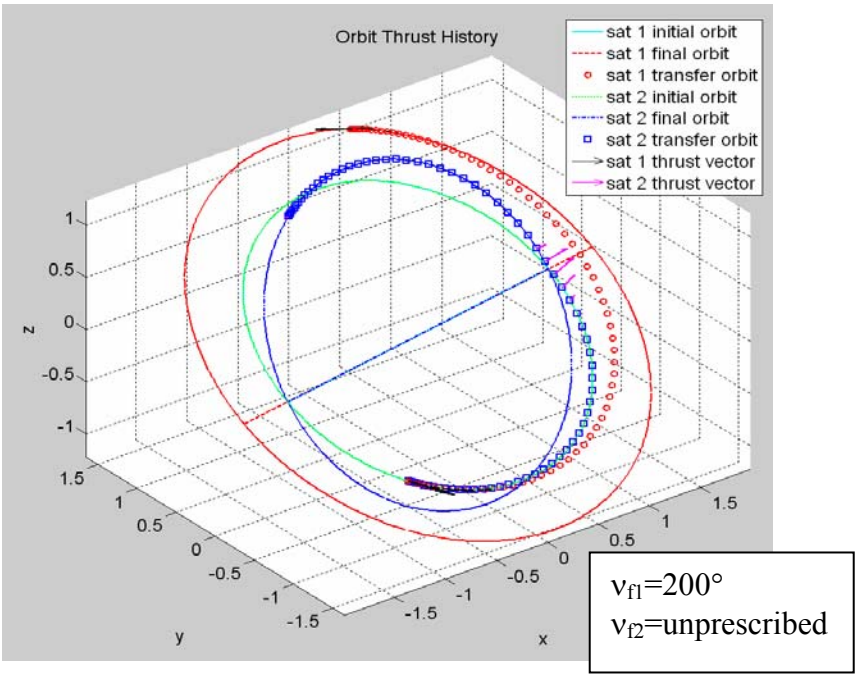

Figure 57 Satellite 1 (master, performing Hohmann transfer) sets constellation execution time, allowing adequate time for transfer and for satellite 2 inclination change. Note: satellite 1&2 designations switched from previous examples

5. Two-Agent Model Conclusions

The two-agent model appears to predict optimal control behavior as expected. Model performance meets all tests for feasibility and optimality previously used during validation, and results of individual agents within the multi-agent construct appear to behave the same as similar single agent validations. Moreover, by observing the behavior of the Hamiltonian for the entire model, we can conclude that the model as a whole is behaving in an optimal manner. Some care and consideration had to be paid to some slight behavioral differences between a single-agent model and a two-agent model, and the two agent model is more sensitive to how data is input due to time based relationships between the agents. However, once addressed the two-agent model appears to perform as expected.

The performance exhibited by this model in a scenario with a somewhat expected outcome provides proof that this model can be run for any number of scenarios, and using the Minimum Principle as a guide optimal control can be predicted with confidence. A

complex three dimensional two-agent scenario is shown as Figure 58, that meets all tests for feasibility and optimality using the methods outlined throughout this thesis.

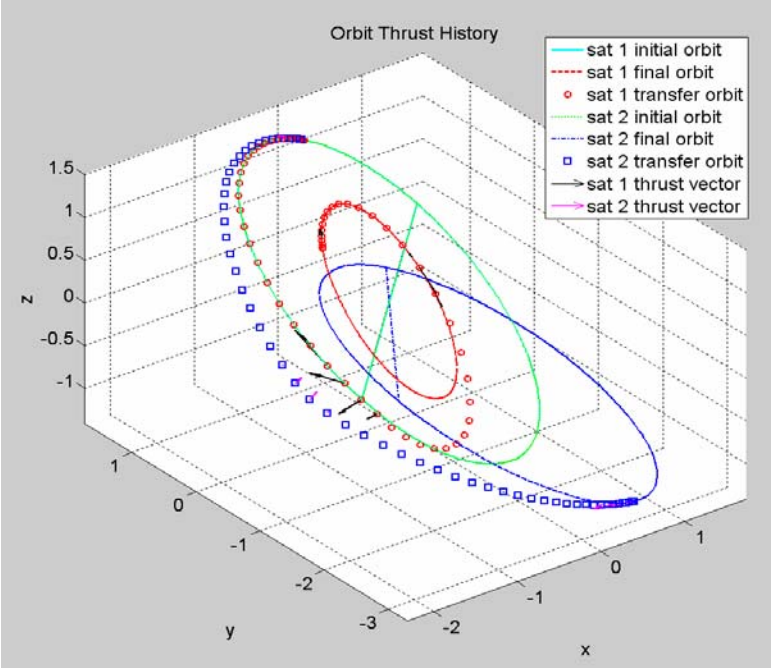

Figure 58 Complex two-agent scenario

C. CONCLUSIONS

The proof of concept for a two-agent model is a critical step in proving full multi-agent optimization capability, for the replication process for three or more agents is essentially the same as the replication process from one agent to two. Given the methodology of replication for the two agent model, there is no reason that a greater number of agents can not be similarly modeled. At the present time, it is believed that the only limitation on the number of agents possible for simultaneous optimization involves processing power, which continues to improve with time.

VII. CONCLUSIONS AND FUTURE WORK

A. CONCLUSIONS

Based on the research performed in support of this thesis, the tools and methods for multi-agent control optimization have been successfully proven. By carefully defining a set of dynamic equations for a single agent model, and thoroughly validating these equations as a foundation for the overall predictive model, it has been conclusively shown that optimizing control for multiple agents is as simple as replicating the successful single agent model.

The key to solving these problems is adherence to Pontryagin's Maximum Principle, and as has been shown time and again throughout this thesis, fulfilling the necessary conditions of this principle provides convincing evidence that optimal solutions to a given problem can be achieved. In truth, this research offers but one small application of this theory, and its real beauty is that it can be extended to a virtually limitless number of problems, the only requirement being the ability to be mathematically described by dynamic equations.

The portability of the process through replication provides an easy avenue to provide simultaneous control of as many agents as desired within available processing limitations, and there is little doubt that the methods used here can be used toward this end. Further, as processing limitations continue to deplete through the continued fulfillment of Moore's Law, larger and larger problems will be made possible, and solutions will be achievable at ever faster rates. Just within the research span of this thesis, a new release of MATLAB™ brought about observed solution times that were two to three times faster than the previous version of the software. When compared to similar DIDO related optimization projects of only three to four years ago, generally speaking solution times have progressed from measurement in hours to measurement in minutes. This will only continue to improve, enabling the tackling of more and more complex problems using these methods.

The model and the tools currently have some limitations specific to the studied orbital problem that have not been discussed in any detail thus far. They will be captured in the following sections.

B. MODEL ISSUES

1. Limitation on Number of Variables

As was touched upon in chapter V of this thesis, the underlying number of computations inherent in the model can be envisioned as a directly linear function of the number of discrete points in time (i.e., nodes) chosen for any given scenario (equation (5.3)). The number of nodes chosen can be simply equated as a measure of achievable resolution in the problem solution, and this has been illustrated to some degree in the discussion on bang-bang control.

All of the scenarios that have been demonstrated through this thesis have involved a small number of orbits, usually less than one. Combining this with a reasonably large number of nodes has provided a fairly high resolution through the orbital path, which has resulted in getting a good picture of the necessary controls to achieve a desired result. A problem starts to rear its head, however, as the number of orbits is increased for a maneuver. This can be illustrated by first envisioning a 100 node solution for a maneuver that is constrained to less than one orbit: here 100 points can describe the maneuvers within the one orbit span adequately for most purposes. Now suppose the maneuver span is opened up to include potentially 25 orbits using the same 100 nodes spread across the span. Now only four points on average can be considered per orbit[7]. If a significant number of thrust points are required (in a continuous sense), then much of this detail will be lost in the result.

An obvious solution to this problem is to continue to increase the number of nodes to as high a resolution as possible, perhaps only at the expense of computation time. However, the computation engine used within the model appears to suffer for high

[7] This is not precisely true, since the mathematical workings of the engine does not spread the nodes linearly across the span. Instead, higher nodal concentrations tend to cluster around the endpoints of the span, which can be easily seen in any of the plots used throughout the validation and multi-agent sections of the thesis.

numbers of nodes (on the order of 150 and greater). Although this engine is in theory unlimited, it involves computations of large matrices which begin to exhibit greater problems of ill-conditioning. This presents a fundamental problem for higher numbers of orbits which require large numbers of nodes for good resolution, especially since a great number of orbital problems are spread over large timeframes for increased fuel efficiency. For these cases, the only current workaround is to be able to divide the problem into discrete legs which can be independently run. However, help appears to be on the way.

The fundamental drawback in the engine appears to originate with the SNOPT algorithms around which the DIDO optimization tool is wrapped. The makers of SNOPT appear on the verge of delivering a new version which is much more highly capable, reportedly to the point of managing variables in the millions vs. the thousands currently. If this happens, it will render this issue moot, and we can again fall back to complaining about processing speed.

2. True Retrograde Orbit

Despite the promise of zero singularities by using the equinoctial orbital elements, the model does not work for an absolute retrograde orbit (i.e.- inclination of 180˚) as of the writing of this thesis. Mathematically, the issue is understood as has been touched upon in discussion of the "retrograde factor" earlier in this thesis, however as a relatively late addition to this research, full coding issues throughout the many files, functions, and subroutines of the otherwise operating model were never fully resolved for this case. This problem begins to manifest itself greater as inclination approaches 180˚, and only significantly beyond even 179˚. For this reason, the difficulty is considered a coding issue and left largely as a footnote at this point, for it is believed solvable with some significant debugging time, however only useful for a very limited number of realistic cases and perhaps as an academic exercise. A great number of other cases ranging from 0˚ to greater than 179˚ have been performed with no difficulty. Perhaps this is a major reason why the subject is completely ignored in many texts, as the vast majority of cases are performed without the added mathematical complexity, no matter how seemingly minor.

3. Scaling and Tolerance

As was noted in several places in this thesis, it is believed that there exist some issues of scaling and tolerance that are unresolved as of this writing. The scaling issues appear to manifest in the control duals in minimum fuel problems, and perhaps this coupled with behavior beginning to approach impulsive behavior [Lawden (1963)] along with internal zero-tolerance settings provides results which are not completely explained at this point. It is suggested that this be investigated further in future work on this topic.

C. FUTURE WORK

1. Extension to *N* Agents

The most obvious continuation of this work should involve proof and characterization of performance for greater numbers of satellites. It is believed at this point that this exercise should be fairly painless, however no words can substitute for actually performing the task to show that this is true. Some unanticipated issues arose with the jump from one to two agents, and some of these issues (such as master/slave relationships and collision avoidance issues) become more complicated with the addition of agents. The variable limitation issue discussed above will likely play some factor in the number of agents achievable until worked out.

2. Scaling Investigation

There appear to be issues which manifest in some scenarios run in the model where the switching structure does not appear to exhibit clean bang-bang behavior as expected, but rather appears to peak at relatively low number of nodes and "chatter" at a high number of nodes. These scenarios exhibit control costates which remain relatively close to zero through the duration of the control chattering, lending to the belief that an issue of scaling or tolerance may exist within the model. Certain scenarios, such as the minimum time scenario run in this research, do not exhibit this phenomenon, while most of the minimum fuel scenarios did to some extent. An investigation into this behavior should be continued

3. Increased Model Fidelity

The model in its current form is ideal in the sense that it does not consider perturbation or drag effects on long term orbit. Since the thrust of this thesis was aimed at injections of multiple satellites spawned from a single launch vehicle, and it is believed that these effects are very minor in a relatively frequent thrusting environment, they were not concentrated on during the proof of concept phase of this research. However, now that the concept has been proven, addition of these effects is necessary, particularly if this model is to be extended to other ideas.

4. Sensitivity Analysis

A characterization of the model's sensitivity to various inputs vs. its optimality signatures should be performed in order to offer a better understanding of effects that the questions have on the answers. Such an analysis would be useful in helping the operator determine how to best provide inputs which ensure that optimal solutions are provided in the most time efficient manner.

5. Extension to Constellation / Formation Control

The model has been built to be as generic as possible, and throughout its development an end goal of realistic long term orbit simulation was envisioned. Although the concept of trajectory insertion provided a relevant issue on which to concentrate effort, ideas and problems of formation flying are becoming more and more widespread in the literature. It is believed that these tools and methods can be adapted for use in this regime, and therefore maximum and minimum operating distances between agents have been accounted for in this work with this end in mind. It is believed that this area offers perhaps the most significant long term extension of this work, and the prospects in this field are exciting. However, the issues mentioned in the fidelity discussion above will very likely have to be worked in concert for a truly useful tool to be achieved.

6. Proportional Fuel Expenditure

If formation modeling is attempted, great consideration should be given to ensuring that fuel burn vehicle to vehicle is performed in order to ensure proportional fuel consumption occurs. This will help to ensure that all vehicles in the constellation deplete their fuel load at the same time, and making sure that the constellation mission remains intact for as long as possible. This model accounts for the possibility of different vehicle masses and fuel loads across all agents, so installation of this type of feature should merely be application of additional path constraints or a similar means of employment.

7. Interface to Graphical Visualizer and GUI Input

Although never accomplished, an interface to some graphical visualization tool, such as AGI's Satellite Toolkit® would be a very useful addition to this tool. Additionally, a long term objective should be made to make this tool as user friendly and transparent to the operator as possible. Some kind of graphical user interface could easily be envisioned which removes the user's need to understand the inner workings of this model, instead concerning him or herself with only inputs and outputs and not so much on how to feed the model.

LIST OF REFERENCES

Bate, R.R., Mueller, D.B., and White, J.E., *Fundamentals of Astrodynamics,* New York: Dover Publishing, Inc., 1971

Battin, R.H., *An Introduction to the Mathematics and Methods of Astrodynamics, Revised Edition,* New York: AIAA, 1999

Betts, J.T., *Practical Methods for Optimal Control using Nonlinear Programming*, Society for Industrial and Applied Mathematics, 2001

Broucke, R.A., and Cefola, P.J., "On the Equinoctial Orbit Elements", *Celestial Mechanics 5*, 1972

Bryson, A.E., *Dynamic Optimization*, Menlo Park: Addison Wesley Longman, Inc., 1999

Bryson, A.E., and Ho, Y.C., *Applied Optimal Control,* Washington D.C.: Hemisphere Publishing Corp., 1975

Chobotov, V.A. (ed.), *Orbital Mechanics, Third Edition*, New York: AIAA, 2002

Coverstone, V.L., and Prussing, J.E., "Technique for Escape from Geosynchronous Transfer Orbit Using a Solar Sail", *AIAA Journal of Guidance Control and Dynamics*, Vol. 26, No. 4, 2003

Danielson, D.A., Sagovac, C.P., Neta, B., and Early, L.W., *Semianalytic Satellite Theory*, NPS-MA-95-002, Naval Postgraduate School, Monterey, CA, 1995

Fleming, A., *Real-Time Optimal Slew Maneuver Design and Control*, Naval Postgraduate School, Monterey, CA, 2004

Josselyn, S.B., *Optimization of Low Thrust Trajectories with Terminal Aerocapture*, Naval Postgraduate School, Monterey, CA, 2003

Kechichian, J.A., "Equinoctial Orbit Elements: Application to Optimal Transfer Problems", in *AAS/AIAA Astrodynamics Specialist Conference*, AIAA 90-2976-C, Portland, OR, Aug. 1990

Kechichian, J.A., "Trajectory Optimization with a Modified Set of Equinoctial Orbit Elements", in *AAS/AIAA Astrodynamics Specialist Conference*, AAS 91-524, Durango, CO, Aug. 1991

King, J.T., *A Framework for Designing Optimal Spacecraft Formations,* Naval Postgraduate School, Monterey, CA, 2002

Kopp, R.E., "Pontryagin Maximum Principle", in *Optimization Techniques*, George Leitman, ed., New York: Academic Press, Inc., 1962

Lawden, D.F., "Optimal Transfer Via Tangential Ellipses", *British Interplanetary Society Journal* 11, No. 6., 1952

Lawden, D.F., "Impulsive Transfer between Elliptical Orbits", in *Optimization Techniques*, George Leitman, ed., New York: Academic Press, Inc., 1962

Lawden, D.F., *Optimal Trajectories for Space Navigation,* London: Butterworth & Co. (Publishers) Ltd., 1963

Moyer, H.G., and Pinkham, G., "Several Trajectory Optimization Techniques", in *Computing Methods in Optimization Problems,* A.V. Balakrishnan and L.W. Neustadt, ed., New York: Academic Press, 1964

Ross, I.M., Fahroo, F., *User's Manual for DIDO 2003: A MATLAB™ Application Package for Dynamic Optimization*, Naval Postgraduate School, Monterey, CA, 2002

Ross, I.M., "How to Find Minimum-Fuel Controllers", *Proceedings of the AIAA Guidance, Navagation, and Control Conference*, AIAA Paper No. 2004-5346, Providence, RI, August 2004

Shaffer, P.J., *Optimal Trajectory Reconfiguration and Retargeting for the X-33 Reusable Launch Vehicle* , Naval Postgraduate School, Monterey, CA, 2004

Stevens, R.E., *Design of Optimal Cyclers Using Solar Sails,* Naval Postgraduate School, Monterey, CA, 2002

Sutton, G.P., and Biblarz, O., *Rocket Propulsion Elements, Seventh Edition*, New York: John Wiley & Sons, 2001

Vallado, D.A., *Fundamentals of Astrodynamics and Applications*, El Segundo: Microcosm Press, 2001

INITIAL DISTRIBUTION LIST

1. Defense Technical Information Center
   Ft. Belvoir, Virginia

2. Dudley Knox Library
   Naval Postgraduate School
   Monterey, California

3. LCDR Jeff King
   SPAWAR Space Field Activity
   Falls Church, Virginia

4. ENS Jay Chaplin
   SPAWAR Space Field Activity
   Falls Church, Virginia